CHAPTER ONE

1.0 INTRODUCTION

Polyhydroxyalkanoates (PHA) are compounds for the intracellular carbon storage of many microorganism species. PHA is produced by micro-organisms as a reserve material in response to imbalanced growth conditions; where a suitable carbon source is present in excess while one or more nutrients are limiting e.g. nitrogen, oxygen, phosphorus, etc. (Braunegg *et al.*, 1998).

In 1926, Lemoigne first discovered poly-3-hydroxybutyrate (PHB), a member of the PHA family, in *Bacillus megaterium*. Since this discovery, many other PHA discoveries have generated excitement on the potential of utilizing PHA in household, industrial, medical, and other applications. Some PHA have been developed for various applications, including bioplastics for packaging, medical implant materials, biofuels and fine chemicals (Philip *et al.*, 2007; Qu *et al.*, 2005). PHA is made by microorganisms and can be easily digested by them. Some studies have shown that PHA is readily degraded by a variety of microorganisms when placed in a natural ecosystem, such as soil or aqueous environment (Boyandin *et al.*, 2012; Mergaert *et al.*, 1996; Mukai *et al.*, 1993), thus demonstrating that PHA is a bio-based, biodegradable family of polymers with no known toxicity. It biodegrades completely into oligomers and monomers and subsequently into CO_2 and water. Many PHA types exhibit thermal and mechanical properties that are similar to petroleum-based plastics, such as polypropylene (Budde *et al.*, 2011; Sudesh *et al.*, 2000; Yang *et al.*, 2012). It has a huge potential as an alternative to synthetic plastics for numerous applications, particularly in view of its biodegradability.

PHA can be divided into two classes, which are the short-chain-length PHA (scl-PHA), where the monomer contains four or five carbon atoms, and the medium chain-length PHAs (mcl-PHA) that contain monomers with carbon chain lengths ranging from

6 to 18. In the family of PHA particularly mcl-PHAs are getting much attention recently. Mcl-PHAs, such as poly 3-hydroxyoctanoate P(3HO), poly 3-hydroxyhexanoate P(3HHx) and their copolymers, are being intensively studied for applications as, surgical sutures, matrices for drug delivery and scaffold for tissue engineering (Philip *et al.*, 2007; Wang, Zhioxiong *et al.*, 2003; Wang, Zhixiong *et al.*, 2003; Xue *et al.*, 2003).

A number of bacteria are reported to accumulate mcl-PHA. Among them are the fluorescent *Pseudomonads,* belonging to rRNA homology group 1 (Huisman, GJALT W *et al.*, 1989). Species such as *Pseudomonas putida*, *Pseudomonas aeruginosa* and *Pseudomonas oleovorans* are well-known for their mcl-PHA accumulation (Ballistreri *et al.*, 2001; Eggink *et al.*, 1992; Lageveen *et al.*, 1988). The first discovery of mcl-PHA was in 1983 when *P. oleovorans* was grown with n-octane as carbon source (De Smet *et al.*, 1983). The ability to utilize different carbon substrates, especially renewable carbon sources, for producing mcl-PHAs is a major advantage for the *Pseudomonas* species. For instance, mcl-PHA can be produced from inexpensive renewable resources, such as palm kernel oil (Tan *et al.*, 1997), soy molases (Solaiman *et al.*, 2006) *etc*. The chemical structure of the carbon substrate fed to the bacteria determines the monomeric composition of mcl-PHA (Lageveen *et al.*, 1988). To date more than 150 units of mcl-PHA monomers have been produced by culturing various *Pseudomonas* strains in many different carbon sources (Do Young Kim *et al.*, 2007). In this study, a simple fermentation experiment was conducted to study the mcl-PHA production with high 3-hydroxyoctanoate monomer content by newly discovered *P. putida* Bet001, isolated from palm oil mill effluent (POME) (Gumel, A. M. *et al.*, 2012)

Much attentions has been given to low cost PHA synthesis by mean of genetic engineering and use of cheap and renewable carbon sources. However, studies on efficient PHA extraction and recovery are rare compared to its upstream processes, i.e.

fermentation/production. To make PHA production more economical and sustainable, downstream processing should be given as much attention as upstream processing. The most practical way to reduce the cost of PHA isolation is to optimize the extraction process with respect to minimum time and solvent requirements. Efficient mass transfer in the extraction system is required to achieve this goal. Ultrasound irradiation is an excellent and convenient technique to improve mass transfer processes in fluids, and thus, a practical approach towards enhancing the PHA extraction. It is a very useful contrivance in highly viscous and immiscible liquids system (Isayev *et al.*, 2003; Monnier *et al.*, 1999). The viscosity of a liquid plays an important role for the maximum impact of cavitation bubble collapse in ultrasound irradiation. A low viscous liquid, such a solvents used in the primary extraction of mcl-PHA, leads to less impact from cavitation bubble collapse. Hence, addition of marginal non-solvent could help in increasing the viscosity of the extraction solvent. Marginal non-solvent is a substance, which is a non-solvent by itself, but it does not weaken the solvating power of a solvent, when mixed with a solvent, and becomes capable of dissolving the solute (Noda, 1998). However, at high concentration, it can be a precipitant. To the best of my knowledge, the application of ultrasound irradiation for PHA extraction is scarcely studied. In this study mcl-PHA extraction from bacterial biomass suspended in solvent/marginal non-solvent and irradiated by ultrasonic waves were investigated.

The use of ultrasonic irradiation has been investigated as an enabling technology in physical and chemical processing applications. In the field of polymer chemistry, there are many aspects that have been studied in relation to this technology. For instance, ultrasound has been used as a tool to extract biopolymer from biomass (Ying *et al.*, 2011), synthesizing polymeric material (Price, 1996), mixing highly viscous polymer solution (Goyat *et al.*, 2011) *etc.* Researchers have applied this technology to sonochemical and enzymatic synthesis of biopolyesters (Gumel, *et al*., 2012a; Gumel, *et*

al., 2012b). However, there are scarce literature available on the stability and degradation characteristics of the biopolyesters dissolved in solvent, particularly mcl-PHA, when exposed to low frequency, high energy ultrasonic irradiation. It is important to investigate these aspects, since the application of ultrasound to the general field of biopolymer is gaining importance. In view of this, the present study was undertaken to investigate the effects of ultrasound irradiation on the stability of medium-chain-length poly-3-hydroxyalkanoates (mcl-PHA) dissolved in an organic solvent. In addition, the changes in key thermal and chemical properties of the sonicated mcl-PHA were analyzed with respect to non-sonicated samples (control). The data were interpreted to describe the behavior of mcl-PHA under exposure to different levels of sonication intensity and frequency. Moreover, a plausible mechanism for an ultrasonic-mediated degradation of mcl-PHA was proposed.

Monomeric composition of PHA contributes an important role towards its thermal and mechanical properties of PHA. PHA with high 3-hydroxybutyrate monomer usually exhibit a stiff, brittle and highly crystalline structure. In contrast, PHA with C6-C16 carbon atom monomers is a thermoelastomer with low or no crystallinity and has high elongation to break (Koning, 1995). A copolymer consisting of monomers of different chain lengths, such as poly(hydroxybutyrate-*co*-hydroxyhexanoate) P(HB-*co*-HHx), exhibits pliability and flexibility on film (Sudesh *et al.*, 2000). The monomer composition determines the structure of a polymer, which will then affect the film formation process. Science of film formation let us know the process of crystallization that affects the PHA film properties and morphology. If a polymer has a highly stereoregular structure with little branching, it can easily assemble in crystalline form. Polymer having this property is called a ‘semicrystalline polymer’. PHB is an example. However, monomers with more branched structure lead to coilings, which interwines, thus lowering the local order of polymer chains, resulting in low crystallization

tendency. Instead of a crystal an amorphous state is formed, which resembles a glass (Stevens, 1990), that can be defined as a frozen liquid. Polymers, like mcl-PHA, having this property are called elastomer polymers (Fig. 1.1). Unfavourable aging can lead to britillity of PHA films due to film crystallization. Britility is caused by the formation of "voids" that weaken the mechanical strength of a film (Schultz, 1984). Polymer blending is a widely used method to improve the thermal properties of polymeric materials at lower costs. Hence in this study, blends of scl/mcl-PHA with different compositions were prepared by casting of polymer solution. Thermal properties of the blends were studied by using DSC and TGA. The blends morphology were studied by using FESEM and XRD.

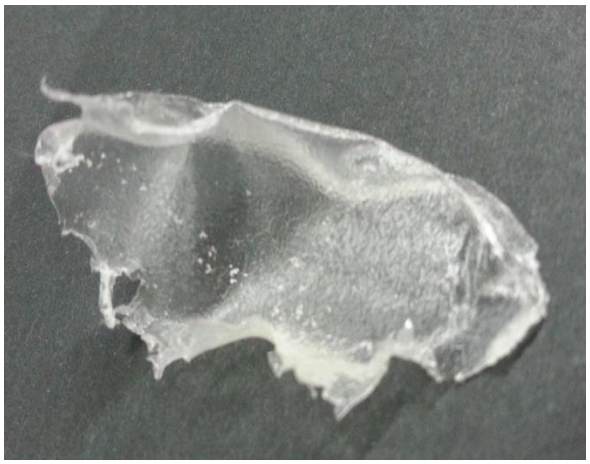

Figure 1.1: Film of mcl-PHA.

The objectives of this study are:

1) To determine the effect of different fatty acids as sole carbon and energy source on the PHA monomer composition produced by wild strain *P. putida* Bet001*;*
2) To study ultrasound-assisted PHA extraction from dried bacterial biomass and its yield;
3) To analyse the stability and degradation of mcl-PHA in organic solvent exposed to ultrasonic irradiation;
4) To study the film morphology of neat PHA and scl/mcl-PHA blends.

CHAPTER TWO

2.0 LITERATURE REVIEW

2.1 History of polyhydroxyalkanoate (PHA)

2.1.1 (1888-2001)

1888 is the year that polyhydroxyalkanoates (PHA) was first observed by Beijerinck (Braunegg, Gerhart *et al.*, 1998). The observation was reported as a lipid – like granules in *Azotobacter chroococcum.* It was known as poly (3 – hydroxybutyric acid) or PHB when its chemical composition was reported in 1927, which was later found as one of the many classes of PHA present in nature. In 1927, Lemoigne first discovered polyhydroxybutyrate (PHB), a member of the PHA family, in *Bacillus megaterium.* Despite the fact that the potential PHB as biodegradable thermoplastic was realised much earlier, this promising polymer remained as academic interest only, solely at their physiological significance as microbiological substance, until late 1980's.

Then there were two factors that put PHA in the highlight, the world oil crisis in the early 1970s and growing interest in biodegradability and sustainability in the 1980s and early 1990s. Rising price of crude oil since 1980 had given PHA the large attention to be the possible substitute to all petroleum – based plastic. However, the petroleum price did not increase significantly, resulting in the closure of many PHA related projects in some companies. Some of the companies are shown in the Table 2.1.

Table 2.1: World wide PHA production and researching companies.

Company	Types of PHA	Period	Applications
ICI, UK	PHBV	1980s to 1990s	Packaging
Mitsubishi, Japan	PHB	1990s	Packaging
Monsanto, USA	PHB, PHbV	1990s	Raw material
Chemie Linz, Austria	PHB	1980s	Packaging and drug delivery

btF, Austria	PHB	1990s	Packaging and drug delivery
Tepha, USA	Several PHA	1990s to present	Medical bio - implants

(Chen, G.-Q., 2009)

2.1.2 (2001-2013)

Right after 2001, the petroleum price began a sharp increase. In middle of 2008, the price of $140 per barrel was reached. This is the time that has promoted the development of plastics that may be independent of petroleum such as PHA and polylactic acid (PLA). However, since PLA has been available in large quantity, its application research is ahead of PHA's. Typically, PLA is cheaper and PHA is more expensive. This due to high cost in PHA production which include the microbial fermentation and its recovery processes.

Despite the fact that PLA has been substantially produced, PHA still overcome PLA in several things such as wide variation in monomer structure (at least 150 different monomers) and verstile properties from brittle, flexible to elastic. Therefore, research on PHA is still very much ongoing. Over the past years, PHA as polymeric material has been developed into several applications in various fields such as medical, medical implant biomaterial, healthy food additives, plastic processing, packaging industry and many more (Table 2.2).

To make PHA comparable to PLA in mass production, many scientists all around the world have put a lot of efforts in studying the PHA production *via* microbial fermentation. PHA production involve strain development, shake flask optimization, lab and pilot fermentor studies then industrial scale up. Factors like bacterial growth rate, PHA percentage in cell dry weight, substrate to product transformation efficiency, price of substrate and a covenient and cheap method of PHA recovery influence significantly the efficiency of microbial PHA production.

Within this era, a lot has been achieved in microbial PHA production, especially in large scale production. For example the development of industrial strain that are capable of growing in low intensity aeration and producing high content of PHA within a reasonable period of time. Recombinant *Escherichia coli* is one of example that has been commonly employed for PHA production due to its convenience in genetic manipulation, fast rowth, high final cell density and ability to utilize inexpensive carbon source. Furthermore, recombinant *E. coli* can anaerobically accumulate PHB to more than 50% of its cell dry weight during cultivation (Carlson *et al.*, 2005). Anaerobic PHA production is perhaps one of the most important ways to reduce PHA production cost. However, the slow growth of bacteria under anaerobic conditions must be considered. Besides that, using waste materials or waste water as media for PHA production is economically attractive. Khardenavis *et al.* (2007) studied that activated sludge generated from a combined dairy and food processing industry wastewater treatment plant has the potential to produce PHB in about 40% and more. Such study indicates the feasibility of using waste water for PHA production.

Table 2.2: PHA in various fields.

Applications	Examples
Packaging industry	All packaging material including food utensils, films, daily consumable, electronic appliances etc.
Fine chemical industry	PHA monomers are all in chiral *R*-form, and can be used as starting materials for the synthesis of antibiotics and other fine chemicals (Chen, G.-Q. *et al.*, 2005b)
Medical implants biomaterial	PHA have biocompatibility that can be developed into medical implant materials (Chen, G.-Q. *et al.*, 2005a). It can also be turned into drug controlled release matrices.

Medical	PHA monomers have therapeutic effects on Alzheimer's and Parkinson's diesease and even memory improvement (Massieu *et al.*, 2003).
Healthy food additives	PHA oligomers can be used as food supplements for obtaining ketone bodies (Martin *et al.*, 2003).
Biofuel	PHA can be methanolysed to produce combustible hydroxyalkanoates methyl ester (Gao *et al.*, 2011).

2.1.3 (2014 onwards – future)

To ensure the future development of PHA based industry to remain viable, the production cost of PHA would have to be lowered, and to find novel and high value added applications of PHA.

Exploring new and unique properties of PHA are also the current focus of research. Unusual PHA properties with functional side group such as double bonds, carboxyl group etc. are of great interest since these PHA have easily modified side group that could expand their applications.

The most potential application for PHA is bio-medical application. After all, bio-medical application seemed to be the most economically practical area for PHA application. Almost all PHA that are available in sufficent quantities like polyhydroxybutyrate (PHB), polyhydroxybutyrate-*co*-valerate (PHBV), polyhydroxybutyrate-*co*-hexanoate (PHBHHx) and polyhydroxyoctanoate (PHO) have been studied for bio-implant application.

For example, P4HB has been approved by the FDA for suture application. Shishatskaya *et al.* (2006) found that the monofilament sutures made of PHB and PHBV did not cause any *in vivo* acute vascular reaction at the site of implantation or any adverse effect for more than one year.

PHBHHx was successfully used as an osteosynthetic material for stimulating bone growth owing to its piezoelectric properties (Wang *et al.*, 2008) and for effectively repairing damaged nerves (Chen 2009). This is because PHBHHx is non-toxic and its degradation products including monomers and oligomers showed lack of immuno-stimulation properties (Cheng *et al.*, 2006; Sun *et al.*, 2007). Besides, they even stimulate the Ca^{2+} channel activation and promote regeneration of damaged tissues.

In conclusion, with successful approval of P4HB and PHBHHx as an implant biomaterial, more PHA based biomaterials are expected to go into clinical trials soon. With the diversity of PHA materials, one can expect the PHA to become a family of bioimplant materials with rich applications.

2.2 PHAs produced by *Pseudomonas* species

De Smet *et al.* (1983) observed the presence of intracellular granules consisting of PHO in *Pseudomonas oleovorans* grown in two-phase medium containing 50 % (v/v) octane. Lageveen *et al.*(1988) extended this study and the result was the accumulation of PHA containing two or more 3-hydroxy acids from single *n*-alkanes (C6-C12) as the sole carbon source. More than two types of 3-hydroxyacids were produced when *n*-alkanes from C8 to C12 were used as substrate. The greatest yield of polymer was obtained from octane and decane. The carbon chain length of the substrate determined the range of monomer units incorporated into PHA, with the 3-hydroxyacids possessing the same carbon chain length as the substrate being at least a major component of the polymer in all cases. Besides *n*-alkane group, the same pattern of 3-hydroxyacids production was observed when *n*-alkanoic acids and n-alkanol were used as the carbon sources.

The accumulation of PHA from *n*-alkanoic acids is not restricted to *P. oleovorans.* Haywood *et al.* (1989) examined various *Pseudomona*s species for growth and polyester accumulation with C6 to C10 straight chain alkanes, alcohol, alkanoic

acids as the sole carbon source. Polymer accumulation was detected *in P. aeruginosa, P. putida, P. fluorescens and P. testosteromi.* The pattern of PHA accumulation in these *Pseudomonas* species is clearly related to that in *P. oleovorans* since 3-hydroxyacids possessing the same carbon chain length as the substrate, or differing by multiples of two-carbon units, are the major monomer units found in the polymers. However no 3-hydroxybutyrate (3HB) monomer was present in the polymer.

The accumulation of PHAs containing medium-chain length (C6 to C12) 3-hydroxyacids, but not 3HB, appears to be a characteristic of the fluorescent pseudomonads, and it has been suggested that the ability to accumulate these PHAs could be taxanomic value (Huisman, G W *et al.*, 1991).

2.3 Microbial PHA extraction

2.3.1 Solvent extraction

Solvent extraction is the most extensively adopted method to remove PHA from the cell biomass. This method is also used routinely in the laboratory because of its simplicity and rapidity. Extraction of PHA with solvents such as chlorinated hydrocarbons like chloroform and 1,2-dichloromethane; or some cyclic carbonates like ethylene carbonate and 1,2-propylene carbonate are common. However, lower chain ketone such as acetone is the most frequently used solvent especially for the extraction of mcl-PHA (Jiang *et al.*, 2006).

Solvent extraction has undoubted advantages over the other extraction methods of PHA in terms of efficiency. This method is also able to remove bacterial endotoxin and causes negligible degradation to the polymers so it is possible to obtain very pure PHA with high molecular weights. Unfortunately, several other factors that could discourage the use of solvent for PHA extraction are high capital and operational cost as well as the high viscosity of the extracted polymer solution when PHA concentration

exceeds 5% (w/v). Viscosity of the solution could interfere with cell debris removal resulting in lengthy separation process.

The efficiency of solvent extraction can be enhanced by subjecting extra "driving forces" to the extraction system. These forces could be thermal or mechanical. Reflux and stirring are the common example for both, respectively. Sometimes, combination of both action is adopted to shorten the time for PHA extraction. Depending on diffusivity of PHA in solvent alone would not be sufficient to improve the efficiency of PHA extraction. The idea is to improve mass transfer of PHA between solid phase (the cells) and liquid phase (the solvent). This can be explained through these equations:

$$J_A = \frac{N_A}{a} = -\mathscr{D}_{AB} \frac{dC_A}{dy}$$

Equation 2.1: Fick's law of diffusion.

N_A = rate of mass transfer of component A

J_A = mass flux of component A

a = area across which mass transfer occures

D_{AB} = Binary diffusion coefficient or diffusivity of component A in a mixture of A and B

C_A = concentration of component A

y = distance

dC_A/D_y = concentration gradient or change in concentration of A with distance

In a single-phase systems, the rate of mass transfer due to molecular diffusion is given by Fick's law of diffusion, which states that mass flux is proportional to the concentration gradient. As indicated in equation above, mass flux is defined as the rate of mass transfer per unit area perpendicular to the direction of movement. Equation above also explained that rate of diffusion can be enhanced by increasing the area

available for mass transfer, the concentration gradient in the system, and the magnitude of the diffusion coefficient. D_{AB} is a property of materials which value can be found in handbooks. It reflects the ease with which diffusion takes place. Its value depends on both components of mixture and also on temperature.

Since the mass transfer process in PHA extraction system comprised of solid-liquid system, film theory model must be applied. The film theory is based on the idea that a fluid film or "mass transfer boundary layer" forms wherever there is contact between two phases (Figure 2.1).

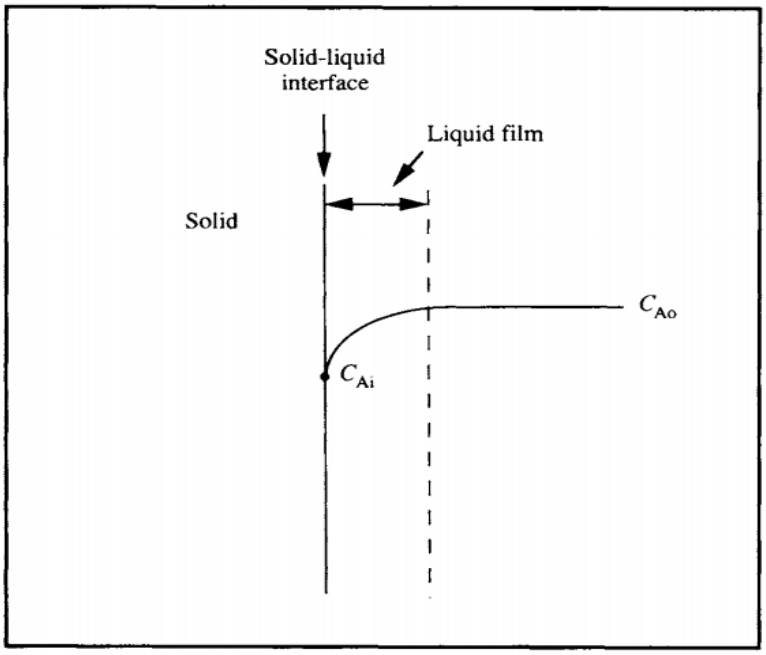

Figure 2.1: Solid-liquid interphase.

$$N_A = k_L a (C_{Ao} - C_{Ai})$$

Equation 2.2: Rate of mass transfer in solid-liquid phase system.

$\boldsymbol{k_L}$ = liquid-phase mass transfer coefficient

$\boldsymbol{a}$ = surface area

$\boldsymbol{C_{Ao}}$ = concentration of A in the bulk liquid outside the film

$\boldsymbol{C_{Ai}}$ = concentration of A at the phase boundary

Equation 2.2 is derived from equation 2.1. This derivation is necessary to accomodate the conditions found in PHA extraction.

2.3.2 Addition marginal non-solvent (co-solvent) in PHA extraction

The use of marginal non-solvent in PHA extraction can enhance the PHA recovery in large scale process (Noda, 1998). Marginal non-solvent is a substance which is a non-solvent by itself but when mixed with a solvent, it does not weaken the solvating power of a solvent and becomes capable of dissolving solute. Development of the method was aimed to find a substitute for halogenated solvents like chloroform in PHA extraction process. The recommended marginal non-solvent for PHA were preferably long chain alcohol (1-20 carbon length), alkane (1- 20 carbon), alkane, fat, neutral lipid and oil. Similar goal using different approach was studied (Kurdikar *et al.*, 2000) whereby they use PHA-poor solvent to extract PHA at high temperature. Preferred PHA-poor solvents include methanol, ethanol, *n*-propanol, *iso*-propanol, and *n*-butanol. In this study, the use of *n*-heptane (C7) and *tert*-butanol (C4) as marginal non-solvent in the ultrasound-assisted PHA extraction were tested.

2.3.3 Various methods of PHA extraction

Besides solvent extraction, there are a lot of other methods that are available for PHA recovery. For example, digestion method by using combination of enzyme and chemical (Kathiraser *et al.*, 2007), high pressure homegenization (Tamer *et al.*, 1998), aqueous two phase system (Divyashree *et al.*, 2009) and many more. However, all of them have their own advantages and disadvantages. Table 2.3 shows brief comparison between several PHA extraction methods.

Table 2.3: Various PHA recovery methods.

Recovery method	Advantages	Disadvantages	References
Digestion method: 1) Chemical 2) Enzymatic	• Native order of polymer chains in PHA granule is retained. • Mild operation conditions. • Good recovery with good quality	• Low PHA purity. • Require extra treatment to remove chemicals from waste water. • Complex process. • High cost of enzymes.	(Kathiraser *et al.*, 2007) (Kapritchkoff *et al.*, 2006)
Mechanical disruption: 1) Bead mill 2) High pressure homogenization	✓ No chemical used. ✓ Less contamination.	✓ Long processing time. ✓ Possible for thermal degradation of desired products. ✓ Formation of fine cellular debris that interfere with downstream processing.	(Tamer *et al.*, 1998) (Ghatnekar *et al.*, 2002)
Supercritical fluid (SFC)	• Simple.	• Frequent need for maintainance.	(Hejazi *et al.*, 2003)

	• Inexpensive. • Rapid. • Environmental friendly	• Difficulties in extracting polar analytes. • Difficulties in dealing with natural samples.	
Aqueous two phase system (ATPS)	✓ Short processing time. ✓ Low material cost. ✓ Low energy consumption. ✓ High yield and a relatively high capacity.	✓ Issue of reproducibility. ✓ Poor standard evaluation of efficiency ✓ Poor understanding of the mechanism.	(Divyashree *et al.*, 2009)
Cell fragility	• Simple recovery method. • Mild extraction conditions.	• Need to control cell wall softening and cell wall intergrity during cultivation.	(Wang, F. *et al.*, 1997) (Page *et al.*, 1993)

(Kunasundari *et al.*, 2011)

2.4 Ultrasound as a tool for biomass extraction

Ultrasound as an environmentally benign method that has found many interesting applications in organic chemistry. The chemical and physical effects of ultrasound arise from the implosion of cavitational bubble (Figure 2.2). The formation of cavitation bubble in liquid is due to the fluctuation of pressure caused by the ultrasound irradiation. Under constant irradiation, the cavitation bubble will keep growing to an extent where its size is not stable and eventually collapse (Brennen, 1995). When cavitation bubbles collapse near the phase boundary of two immiscible liquids or liquid – solid boundary, the resultant shock wave can provide a very efficient stirring or mixing of the layers. Besides that, the implosion also would generate an instant extreme temperature near to the boundary. Therefore, ultrasound could increase the value of liquid-phase mass transfer coefficient (k_L). Hence, ultrasound can be used to reduce mass transfer limitation in extraction process.

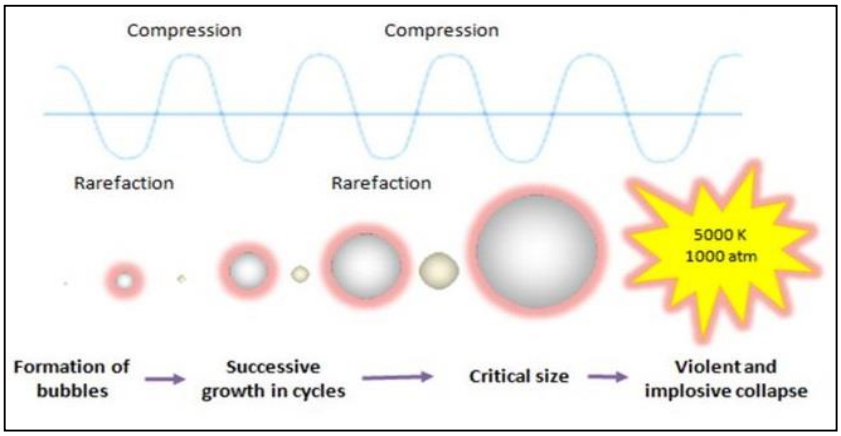

Figure 2.2: Illustration of physical growth of cavitation bubble (Kendall, 2013).

Biomass extraction by using ultrasound irradiation technique has been widely studied. For example, it has been used to extract essential polysaccharide from fruit (Zhong *et al.*, 2010) and mushroom (Chen *et al.*, 2010; Li *et al.*, 2012). However, study on PHA extraction by using this technique is never been reported. Therefore, the first step was taken in this study to investigate the application of ultrasound irradiation to PHA extraction.

2.5 RSM as a statistical method to study relationship between parameters

Response surface methodology (RSM) is a collection of mathematical and statistical techniques for designing experiments, model building , assessing the impact of factors and finding the optimum conditions of factors for desirable results. This optimization process methodology involves studying the response of statistically designed parameter combinations, estimating the coefficients by installation of a mathematical model that best fits the experimental conditions, which will then be useful to predict the outcome of a process. It can also be used to study the relationship between studied parameter by providing the interaction coefficient which indicate the significance level of the relationship. The most common designs are central composite design (CCD) and Box- Behnken design (BBD). However, Box- Behnken design, is preferably used in the optimization of chemical and physical processes because of its reasoning design and excellent outcomes (Ferreira *et al.,* 2007). In addition, a lot of biomass extraction process had utilized BBD to optimize the yield of extraction (Chen *et al.*, 2010; Dong *et al.*, 2009; Li *et al.*, 2012; Zhong *et al.*, 2010).

2.6 Stability and degradation of PHA

Behaviour of PHA stability in a specified condition is important as it can provide the knowledge on how to maintain the original properties of that polymer during physical and chemical process. Equally important, the study of PHA degradation could provide us with the method to obtain low molar mass oligomers containing reactive end groups which can be further used as building blocks for copolymerization reactions, yielding new block copolymers with improved properties.

The controlled degradation of PHAs has been discussed in many previous reports by resorting to various approaches, for instances enzymatic hydrolysis (Renard *et al.*, 2004), thermal degradation (Ariffin *et al.*, 2008), microwave–assisted degradation (Ramier *et al.*, 2012), alkaline and acid-catalyzed hydrolysis (Yu *et al.*, 2005) and etc.

The chemical structure of the resulting oligomers is very much dependent on the degradation method used. For instance, acid-catalyzed hydrolysis yields linear oligomers with a hydroxyl group at one end and a carboxyl group on the other end, along with very low proportions of cyclic structures. Alkaline conditions lead to the formation of oligomers containing a hydroxyl end group and an ester end group. As for thermal degradation, it is well established that the thermal degradation of scl-PHAs occurs almost exclusively random chain scission reaction involving a six-membered cyclic transition state, resulting in oligomers that contain an unsaturated crotonic end group. However, thermodegradation of mcl-PHA involves hydrolysis of the ester linkages that would subsequently lead to dehydration of the hydroxyl terminal groups of oligomers, producing alkenoic acids as another end product (Chan Sin *et al.*, 2010).

Nevertheless, there are scarce literature available on the stability and degradation characteristics of the biopolyesters, particularly mcl-PHA, when exposed to ultrasonic irradiation. It is important to investigate this aspects since the application of ultrasound on PHA is gaining importance. Hence, the first step was taken to investigate the effects of ultrasound irradiation on the stability and degradation of medium-chain-length poly-3-hydroxyalkanoates (mcl-PHA) dissolved in an organic solvent.

2.7 Film morphology of neat PHA and its blend

Generally, there are two morphologies that describe the characteristic of polymers i.e. amorphous and crystalline. Amorphous is a physical state characterized by almost lack of order among the molecules. For crystalline, it refers to situation whereby polymer molecules are oriented or aligned in a regular array to resemble crystal lattice packing in nonpolymeric solids. In polymer science, crystalline is always being refered as semicrystalline because polymers never achieve 100 % crystallinity. It is well established that the ultimate properties of any polymer result from combination of molecular weight and chemical structure (Deanin, 1972; Miller, 1966). Both of these

properties will influence the film formation, for instance, by evaporation of solvent from polymer solution. As the solvent evaporated off and the polymer solution become more concentrated, the cross chain linkages involving weak secondary intermolecular bonds start to become important. Eventually, the secondary intermolecular bonds grow stronger and pull the polymer chains closer to each other. If a polymer has a highly stereoregular structure with little or no branching, they may assemble themselves in crystalline form. Polymer showing this behaviour is callled semicrystalline polymer like PHB (scl-PHA). If the polymer has a branching structure they may assemble themselves by coiling and intertwined one another without having tendency toward crystallinity it is called amorphous polymer. In this state, polymer exhibits a glass behaviour (Stevens, 1990). Polymer showing this property is called elastomer polymer like mcl-PHA.

Unfavourable aging effects can lead to brittleness of PHA film due to secondary film crystallization (Alata *et al.*, 2007). Britility is cause by the formation of "voids" that weakened the mechanical strength of a film (Schultz, 1984). This matter can be overcame through polymer blending. By definition, any physical mixture of two or more different polymers or copolymers that are not linked by covalent bonds is a *polymer blend* or *polyblend*. Polymer blending is a widely used method to improve the mechanical properties of polymeric materials at lower cost. If the desired properties can be realized simply by mixing two or more existing polymer, there is an obvious pecuniary advantage. There are a lot of studies that have been reported on PHA blends, all with the same intention, to improve mechanical strength of PHA film for certain purposes (Katsumata *et al.*, 2011; Qiu *et al.*, 2003; Reis *et al.*, 2008).

CHAPTER THREE

3.0 MATERIALS AND METHODS

3.1 MATERIALS

3.1.1 Microorganisms

Two bacterial strains, i.e. *Pseudomonas putida* Bet001 and *Delftia tsuruhatensis* Bet002 were used in this study for the production of medium chain length polyhydroxyalkanoates (mcl-PHA) and short chain length polyhydroxyalkanoates (scl-PHA), respectively. The microorganisms were obtained from Bioprocess and Enzyme Technology Laboratory, Institute of Biological Science, Science Faculty, University of Malaya. They were isolated from palm oil mill effluent (POME).

3.1.2 Fatty acids

A range of different saturated fatty acids with different carbon chain length (Table 3.1) was used as carbon source for PHA production in E2 medium.

Table 3.1: List of saturated fatty acids as carbon substrate (MERCK).

Fatty acids (Systematic name / Common name)	Lipid numbers
Butanoic acid / Butyric acid	C4:0
Pentanoic acid / Valeric acid	C5:0
Hexanoic acid / Caproic acid	C6:0
Octanoic acid / Caprylic acid	C8:0
Decanoic acid / Capric acid	C10:0
Dodecanoic acid / Lauric acid	C12:0
Tetradecanoic acid / Myristic acid	C14:0
Hexadecanoic acid / Palmitic acid	C16:0

3.1.3 Media

PHA production was carried out in a two-stage culture system. Hence, two different media formula were used to culture the bacteria. Rich medium (Table 3.2) and E2 medium (Table 3.3) were formulated for cell-growth and PHA-accumulation phase, respectively. Rich medium formula was also used to prepare slant agar culture with the addition of 1.2 % (w/v) agar technical (OXOID).

Table 3.2: Rich medium.

Components	**Mass (g) per liter of distilled water**
Nutrient broth (MERCK)	8.0
Yeast extract	10.0
Ammonium sulphate	5.0

Table 3.3: E2 medium.

Components	**Mass (g) per liter of distilled water**
Ammonia solution 25% (MERCK)	(See **A** below)
Saturated fatty acids (Table 3.1)	10.0
K_2HPO_4	5.73
KH_2PO_4	3.7
Minerals solutions	**Volume (ml) per liter of distilled water**
$MgSO_4$ (0.1M)	10.0
Trace elements (MT) (See **B**)	1.0

(Lageveen *et al.*, 1988)

(A) 0.08 gram of NH_3 was needed in the PHA-accumulation culture system. Hence, 0.35 ml of 25 % ammonia solution (NH_4OH) per liter of distilled water was used as nitrogen source in E2 medium.

(B) The composition of MT solution is listed as below.

Table 3.4: MT solution composition.

Components	Mass (g) in 500 mL of 1N HCl
$FeSO_4.7H_2O$	1.39
$MnCl_2.4H_2O$	0.99
$CoSO_4.7H_2O$	1.41
$CaCl_2.2H_2O$	0.74
$CuCl_2.2H_2O$	0.08
$ZnSO_4.7H_2O$	0.14

(Lageveen *et al.*, 1988)

3.1.4 Shaker-incubator setup

Shake- flask bacterial cultivations were carried out using Hotech Model 721 orbital shaker and Hotech model 624 low-temp incubators from Hotech Instruments Corp. (Taiwan). For cell-growth and PHA-accumulation phase, the cultures were incubated at 25 °C ± 0.2 and 30 °C ± 0.2, respectively. However, rotating speed for both cultivations was fixed at 200 rpm.

3.1.5 Sterilizer

Tomy SS-325 autoclave (Japan) was used for sterilization. Temperature and pressure were set up at 121 °C and 103 kPa respectively, for 15 minutes.

3.1.6 Spectrophotometer

Spectrophotometric analysis was performed using Jasco V-630 spectrophotometer equipped with Jasco EHC-716 temperature controller (Japan).

3.1.7 Microscope

Microscopic observation was performed using Motic BA200 light microscope (U.S.A) with oil immersion lens equipped with 3.0 Megapixel moticam 2300 digital camera.

3.1.8 Centrifugation

Centrifugation was carried out using Thermo-Line MLX-210 mini centrifuges (China), Hettich Zentrifugen EBA 20S bench-top centrifuge (Germany) and Thermo Scientific Sorval RC-5C Plus ultracentrifuge (U.S.A) for liquid volumes of 1.0, 10.0 and 50.0 ml respectively.

3.1.9 Water bath ultrasonicator

Extraction experiments were done in batch system immersed in ultrasonic bath Elmasonic P 30H (Germany) except for solvent reflux extraction. Ultrasonic degradation experiments were also done using the same equipment.

3.1.10 Rotary evaporator

Filtrate of polymer solution was concentrated by using Yamato RE 300 rotary evaporator (Japan).

3.1.11 Analytical instruments

i. Gas chromatography (GC)

PHA quantification and monomeric identification were performed using Thermo Scientific Trace GC Ultra equipped with fused silica capillary column (30m x 0.32mm ID) (Thermo scientific TG-5MS) and flame ionization detector with splitless injection. Helium (2.734 ml min^{-1}) was used as a carrier gas. The temperatures of the injector and detector were set at 200 °C and 280 °C, respectively. The oven ramping temperatures were programmed from 50 to 280 °C at 10 °C min^{-1}.

ii. ^{1}H-nuclear magenetic resonance (^{1}H-NMR)

Proton NMR (^{1}H-NMR) was used to study chemical structure of mcl-PHA samples. ^{1}H-NMR spectroscopy was recorded on JEOL JNM-LA 400 FTNMR spectrometer at 400 MHz, 25 °C. The spectra was recorded using a solution of PHA-$CDCl_3$ at a concentration of 2.0 mg ml^{-1}. Tetramethylsilane (TMS) was used as internal reference.

iii. Fourier transform infrared spectroscopy (FTIR)

FTIR analysis was conducted with a Perkin-Elmer FTIR RX spectrometer. The PHA samples (control and ultrasound treated) were casted on the NaCl FTIR cells as thin film. The spectra were recorded between 4000 and 600 cm^{-1}, with 4 cm^{-1} resolution and 10 scans at room temperature.

iv. Thermogravimetric analysis (TGA)

Thermal behaviour of control and ultrasound-treated mcl-PHA were characterized using Thermogravimetric Analysis (TGA) (Perkin-Elmer). TGA was used to determine the initial degradation temperatures (T_d) of the polymer and to study thermodegradation kinetic of mcl-PHA. For TGA analysis, about 7.0 mg sample was heated from 30 to 550 °C at 10 °C min^{-1}.

v. Differential scanning calorimetry (DSC)

Differential scanning calorimetry (DSC) (Mettler Toledo) analysis was carried out in the temperature range of -65 °C to 180 °C at a heating rate of 10 K min^{-1} under nitrogen atmosphere. Glass transition temperature (T_g) and melting temperature (T_m) of the polymer sample were determined as the midpoint of steep change in energy and the lowest point of melting peak in the thermogram, respectively.

vi. Gel permeation chromatography (GPC)

Gel permeation chromatography (600-GPC) was used to determine the average molecular weight and distribution of control and ultrasound-treated PHA. The GPC was equipped with a Waters Styrogel HR column. Tetrahydrofuran was used as the eluent at 40 °C at a flow rate of 1 ml min^{-1}. 1.0 ml of a 2.0 mg ml^{-1} sample solution was filtered through a 0.45 µm filter prior to injection into the machine. 100 µl of filtrate was injected for each polymer sample. The instrument was calibrated using monodisperse polystyrene (PS) standards.

vii. Field emission scanning electron microscopy (FESEM)

Surface of neat and blended PHA films were observed under field emission scanning electron microsope (Quanta FEG 450, edx-Oxford) in low vacuum atmosphere operated at an acceleration rate of 3-5 kV. For PHA blend, the image was observed at boundary of opaque and non-opaque region.

viii. X-ray diffraction (XRD)

Crystallinity of PHA film samples were studied using a PANalytical EMPYREAN (Holland). A 20-min scan was run on each sample with the X-ray settings held at 40 kV and 40 mA. The scan range was from 10° to 70° 2-theta.

3.1.12 Analytical chemicals

i. Staining dyes

a) Safranine solution

0.25 mL of safranine (BDH) was mixed with 10.0 mL of ethyl alcohol (95%v/v) and 100.0 mL distilled water.

b) Sudan Black B solution

0.3 gram powdered Sudan Black B (Sigma Chemical) was dissolved in 100.0 mL of 70 % (v/v) ethyl alcohol.

ii. Acidified methanol

This solution was prepared for PHA methanolysis. 85 ml of cold methanol and 15 ml of concentrated sulphuric acid were mixed together and stored properly at 4°C.

iii. 3-hydroxyalkanoic methyl ester standards

Solution of methylated 3-hydroxyalkanoate monomers standards were prepared for polyhydroxyalkanoate (PHA) monomer quantification using gas chromatography technique. All of them were prepared in 10,000 part per million (PPM) of initial stock concentration using dichloromethane as the solvent (Table 3.5).

Table 3.5: PHA monomer standards.

Standards	Supplier
Methyl 3-hydroxybutyrate	Aldrich (Germany)
Methyl 3-hydroxyvalerate	Aldrich (Switzerland)
Methyl 3-hydroxyhexanoate	SAFC (U.S.A)
Methyl 3-hydroxyoctanoate	LARODAN (Sweden)
Methyl 3-hydroxydecanoate	LARODAN (Sweden)
Methyl 3-hydroxydodecanoate	LARODAN (Sweden)
Methyl 3-hydroxytetradecanoate	LARODAN (Sweden)
Methyl 3-hydroxyhexadecanoate	LARODAN (Sweden)

3.2 METHODS

3.2.1 Preparation of stock culture

Two bacterial strains used in this study i.e. *P. putida* Bet001 and *D. tsuruhatensis* Bet002 were stored at -20°C in a glycerol solution (Table 3.6). The stock was prepared by mixing 0.5 ml of rich medium, freshly cultured with *P. putida* and *D. tsuruhatensis*, with 1.5 ml of glycerol solution in an eppendorf tube. Several stocks were made to ensure the availability of these strains throughout this study.

Table 3.6: Composition of glycerol solution.

Components	Percentage (v/v)
Glycerol (100%)	65.0
$MgSO_4.7H_2O$ (1 M)	10.0
Tris base (1 M)	2.5
Distilled water	22.5

3.2.2 Bacterial cells maintenance

Cells were maintained on solidified rich medium (Table 3.2) agar slant at 4 °C. Once a month, the whole slant was sub-cultured into a fresh rich medium in a shake flask. After 36 hours of incubation at 30 °C, a loopful of this fresh culture was streaked onto nutrient agar plates to obtain single colonies and to detect for any possible contamination of the culture. Each single colonies obtained were observed under light microscope for cell morphology observation. Then a selected single colony was transferred onto each of a number of fresh rich medium agar slants which were then stored at 4 °C.

3.2.3 Media preparation

Rich medium was prepared by mixing all the individual components (Table 3.2) and fully dissolved them in distilled water. More distilled water was added up to the pre-determined volume prior to steam sterilization.

E2 medium was prepared by mixing two separate solutions. First solution is phosphate buffer which was prepared by dissolving two different phosphate salts in distilled water. Its pH was adjusted to 7.0 ± 0.03 before putting it in autoclave for steam sterilization. Second solution is fatty acid solution which was prepared by dissolving it in a low concentration of sterilized NaOH solution. It was prepared in this manner to reduce any possible evaporation of short – chain fatty acids because of the high temperature. Then its pH was adjusted to 7.0 ± 0.03 using H_2SO_4 solution to neutralize any excess NaOH. Both of these two solutions was aseptically mixed up to the total volume of the culture. Sterile solution of ammonia, trace elements and MgSO4 were added prior to the start of cultivation. This procedure was taken to avoid any precipation of E2 medium components due to the high temperature and pressure during the steam sterilization.

3.2.4 Standard calibration curve of *P. putida* biomass

A standard curve representing a range amount of dried weight of *P. putida* biomass to its corresponding optical density (OD) at 600 nm was calibrated as it is particularly useful for quick estimation of total biomass in culture. The calibration was done as follows:

Bacteria were grown in 100.0 ml of rich medium in baffled shake-flask for 24 hours at 30 °C. Five centrifuge tubes of 10.0 ml of the culture were spun down at 5000 rpm for 10 minutes. After decanting the medium supernatant, the cells pellet was rinsed with 0.9 % (w/v) of saline solution and then re-centrifuged. This step is repeated three times before the cells pellet was dried in an oven at 75 °C untill constant weight. The

total weight of biomass in 50.0 ml of the rich medium culture is the result of summation of cell pellets in the five centrifuge tubes. This value would then be divided by the respective dilution factor of the subsequent step.

Another 50.0 ml culture was spun down at 10,000 rpm for 10 minutes in centrifuge tube to remove the medium supernatant. Cells pellet was then rinsed with saline solution and re-centrifuged three times before re-suspended in 50.0 ml of 0.9 % (w/v) saline solution. 1.0 ml of this suspension was diluted accordingly so that a range of OD at 600 nm less than 1.0 unit was obtained. Linear calibration points would be chosen. These calibration points were recorded in triplicate each. The standard deviation within the replicates did not exceed ± 0.02 unit OD. The standard calibration is shown in Appendix C. The biomass concentration was calculated based on the relationship

$$y = 2.6 \times 10^3 x + 0.03$$

where y is the OD reading at 600 nm and x is the calculated biomass weight (g).

3.2.5 Growth profile of *P. putida*

Growth profile of *P. putida* in rich medium was determined to estimate the harvesting time of the culture. Plotting the growth profile was done as described below:

The whole slant of P.putida culture was used to inoculate 200 ml of rich medium in a baffled shake-flask which was then incubated at 30 °C. This slant culture had been incubated for 24 hours at 30 °C. Every four hours interval, a triplicate of 1 ml of the culture was pipetted out which was then centrifuged to obtain cells pellet. The cells pellet was rinsed with saline solution and re-centrifuged three times before resuspended in 1.0 ml of 0.9 % saline solution (w/v). Then, the suspension was diluted with saline solution up to 20 dilution factor before its optical density (OD) was taken with same concentration of saline solution as a blank. Estimated amount of biomass concentration was determined by interpolating the OD of that diluted suspension with the biomass

standard calibration curve. Fermentation was carried out untill 48 hours. Experiments were performed in triplicate. The growth profile is shown in Appendix D.

3.2.6 Standard calibration of methyl 3-hydroxyalkanoate standards and their respective retention time

A linear standard calibration for each methyl 3-hydroxyalkanoate standards was made for PHA quantification. The methyl 3-hydroxyalkanoate standards were diluted accordingly to 200, 300, 400, 500 ppm concentration from the 10,000 ppm initial stocks. For each dilutions, 0.02 % (v/v) of 10,000 ppm methyl benzoate solution was added as internal marker. All these mixtures were prepared with dichloromethane as the solvent in 1 ml volume. This monomer standard solutions were carefully prepared as the analyte peak area from the gas chromatogram would be used as the analytical parameter. A 1.0 μL portion of this mixture was then automatically injected into the GC by using autosampler to obtain the standard chromatogram. The injection mode was splitless.

Standard calibration for each methyl ester standards was established by calibrating the peak area to the increasing amount of analyte injected into the GC. These standard calibrations are shown in Appendix E.

The linear calibration of the average retention time to the increasing carbon atom number of methyl 3-hydroxyalkanoate standards is shown in Appendix F. It was found that each individual standard tested in the whole studies fell within the linear range. To show that the fatty acids used in this study did not interfere with the quantitative analysis of PHA, GC analysis of each methylated fatty acids was carried out and none of them fell within this linear range.

3.2.7 Medium chain length polyhydroxyalkanoates (mcl-PHA) production

Two-stage culture system was used to produce mcl-PHA using *P. putida*. Setup for culture system and media preparation were explained in sections 3.1.4 and 3.2.3 respectively. General method is explained as below:

For the cell-growth phase, the whole slant of *P. putida* culture was used to inoculate rich medium which was then incubated for 24 hours. After 24 hours of cultivation, cells were aseptically harvested by centrifugation at 4 °C. Then, they were aseptically transferred into E2 medium for PHA-accumulation phase. The medium was supplemented with 1.0 % (w/v) of fatty acid and 0.035 % (v/v) of ammonia solution as carbon and nitrogen source, respectively. The initial cell concentration for each E2 medium cultivation was 0.003 g/ml. This cultivation was carried out for 24 hours at 30 °C before the cells were harvested again by centrifugation at 4°C.

3.2.8 Effect of different fatty acids on mcl-PHA accumulation by *P. putida*

In this experiment, different fatty acids as listed in section 3.1.2 were used as carbon source to study their effects on the yield of biomass and PHA as well as PHA content in the cells. Cultivations were carried out in 100 ml baffled shake-flask. Procedure for this experiment is similar as described in section 3.2.7. PHA detection, biomass harvesting, extraction, quantification and identification were done as explained in sections 3.2.9 – 3.2.14.

3.2.9 *P. putida* cells staining

Sudan Black B and Safranine were used for staining in this study to qualitatively examine intracellular PHA accumulation. Sudan Black B is a special stain that would dye any lipid-like inclusion inside the cells (Burdon, 1946). Accumlated PHA can be viewed as a dark, discrete spot under light microscope. Counterstaining with safranine solution is necessary to highlight the shape of the synthesizing cells so that any contamination can be detected.

Cell suspension in distilled water was smeared on a glass slide. Then, the glass slide was heated to fix the cell suspension. After the suspension had dried, it was flooded with Sudan Black B solution for 5 minutes at room temperature. The excess stain was drained off with distilled water before the heat-fixed cells were counterstained with safranine solution for 15 seconds at room temperature. It was then drained off and the glass side was blotted and air-dried before examining it under the light microscope with oil immersion lens.

3.2.10 Biomass harvesting and removal of fatty acid residue

After 24 hours incubation in E2 medium, cells were harvested by centrifugation at 12000 ×*g* (Thermo Scientific Sorval RC-5C Plus ultracentrifuge) and 4 °C. The pellets were rinsed two times with 0.9 % saline solution and then oven dried at 70 ˚C until constant weight. Residual fatty acid was removed by biomass dissolution in *n*-heptane to prevent it from being co-extracted with the PHA. This was done by stirring 10.0 g of dried cells in 100 ml heptane at 25 ± 1 °C. This step was repeated several times. After 4 hours, cells were filtered out from the *n*-heptane and dried in oven at 70 °C until constant weight.

3.2.11 Solvent extraction and purification of PHA

For PHA extraction, 1.0 g of dried cells were refluxed in chloroform (100 ml) for 4 hours at 70°C ± 2.0. Then, the mixture was filtered through a Whatman filter paper No. 1. The filtered dried cells were collected back to undergo another 2 cycles of solvent reflux with 50.0 ml of chloroform for 4 hours. This is to ensure all the PHA inside the cells have been extracted out as much as possible. Filtrate from the 3 cycles were collected together and concentrated by using rotary evaporator until the volume reached 10.0 ml.

For PHA purification, concentrated polymer solution was mixed with cold methanol at 1: 7 ratio in a thick glass tube to allow the precipitation of PHA. After 30 minutes, the precipitated PHA was recovered by centrifugation at 1920 x*g* for 10 minutes. The solvent mixture was then decanted leaving the precipitated PHA at the bottom of the tube. Further purification was carried out by re-dissolving the PHAs in a small amount of solvent and reprecipitating them in excess methanol. A highly purified PHA can be obtained by repeating this step several times. Subsequently, the PHA film obtained was air-dried until constant weight.

3.2.12 PHA methanolysis

PHA was derivatized into detectable volatile compounds by methanolysis (Braunegg, G *et al.*, 1978) prior to GC analysis. PHA (0.05 g) was dissolved with 3.0 ml of filtered dichloromethane in a screw-cap tube sealed with PTFE tape. Then 3.0 ml of acidified methanol (containing 15 % (v/v) of concentrated sulphuric acid) was added to the polymer solution. Methanolysis was conducted at 100 °C for 140 minutes in Wisetherm HB-48 heating block with intermittent shaking to accelerate the depolymerization process. After that, the mixture was cooled down to room temperature and 3.0 ml of distilled water was added. After vigorous vortexing, the mixture was allowed to separate into two immiscible layers. Finally, the organic phase at the bottom was carefully recovered and transferred into a screw-cap small vial containing a small amount of sodium sulphate anhydrous. This step is to remove any trapped moisture in the organic phase during phase separation. A portion of this organic phase was diluted with dichloromethane (if necessary) which would then be analysed using gas chromatography.

To determine PHA content in cells, similar method was applied using dried cells. Different amounts of dried cells used at the beigining of the methanolysis process were 10.0, 30.0 and 50.0 mg.

3.2.13 PHA quantification and monomers identification

Gas chromatography (GC) was employed to perform the PHA quatification and its monomer identification. The retention time and the quantity indicated in the gas chromatogram were interpolated to standard calibration of methyl esters of 3-hydroxyalkanoates shown in Appendix E. Total polymer weight was obtained by adding up all the individual monomers present. PHA content was calculated as shown below:

PHA content (%) = [PHA weight (mg) / Total dried biomass (mg)] X 100

Eq. (3.1)

3.2.14 Ultrasound-assisted PHA extraction

All extraction experiments were done in batch system immersed in ultrasonic bath (Elmasonic P 30H) except for solvent reflux extraction. Extraction temperature was fixed at 25 ± 0.2°C. About 35.0 g of dried biomass was collected and ground, then sieved using U.S.A standard sieve series (25.0 and 50.0 μm). Consequently, the sieved biomass powder was suspended in an extraction medium and subjected to ultrasonication at specified frequency, power and time. All extractions were carried out as mentioned except stated otherwise.

3.2.14.1 Screening experiments

Preliminary experiments were conducted in screw-cap tube (18.0 cm long and 1.3 cm internal diameter). About 50.0 mg of dried biomass was charged to each tube. Chloroform and acetone were used as solvents in the experiments. Each solvent was varied into five different volumes i.e. 5, 7, 9, 11 and 13 ml. PHA was extracted using solvent reflux for four (4) hours.

For time range and ultrasonic frequency variables, dried biomass in five different volumes of selected solvent (5, 7, 9, 11 and 13 ml) were subjected to 37 kHz

and 80 kHz frequency, for 5, 10, 15, and 20 minutes at constant ultrasonic power output (60 %).

For marginal non-solvent variable, *tert*-butanol and *n*-heptane were tested. Total volume of extraction medium was fixed at 10.0 ml. The ratio of solvent:marginal non-solvent, was varied at 7.5:2.5, 5.0:5.0 and 2.5:7.5 (vol/vol)). Power output of sonication (60 %) and the selected frequency and time from previous experiments were used as fixed parameters in these experiments. All experiments were carried out in triplicate.

3.2.14.2 Box-Behnken optimization

Optimization of three selected independent variables *viz*: ultrasonic output power, time, and solvent percentage of extraction medium was studied using Box-Behnken design (BBD). Percentage of extracted PHA was used as the response variable. The range of uncoded independent variables and their levels were presented in Table 3.7. For this experimental design, the frequency was held constant at 37 kHz while acetone and *n*-heptane were selected as solvent and marginal nonsolvent respectively. About 80 ml of extraction medium was poured into 100 ml conical flask fitted with a cooling condenser. About 0.4 g of dried biomass was immersed in the extraction medium and subjected to the extraction process.

Table 3.7: The experimental points in the Box-Behnken design.

Independent variables	**Levels**		
	Lowest	**Middle**	**Highest**
Ultrasonic power output (%) (X_1)	30	60	90
Acetone percentage (X_2)	50	75	100
Extraction time (min) (X_3)	5	10	15

3.2.15 Calculation of dissipation energy

The calorimetric analysis of the ultrasonic power, *P* was determined according to equation below (Koda *et al.*, 2003).

$$P = m \text{ x } c_p \text{ x } \Delta T / \Delta t \quad \textbf{Eq.} (3.2)$$

where *P* is power (W), *m* is the mass of the water (g), c_p is the specific heat capacity of water (4.18 Jg^{-1} K^{-1}), *T* is the temperature (K) and *t* is the sonication time (s).

The sonication-dissipitated energy, *E* (J ml^{-1}) is determined according to this equation:

$$E = P \text{ x } t / V \quad \textbf{Eq.} (3.3)$$

where *V* is the working volume (ml). Relative values of the ultrasonic power output used in this study to the value of *P* and *E* are given in Table 3.8 and 3.9 respectively.

Table 3.8: Relative ultrasonic power.

Frequency	**Power output**	**Ultrasonic power, *P* (W)**			
		5 minutes	**10 minutes**	**15 minutes**	**20 minutes**
37 kHz	**30 %**	38.4 ± 0.1	19.4 ± 0.05	13.0 ± 0.02	9.7 ± 0.02
	60 %	38.8 ± 0.1	19.5 ± 0.04	13.1 ± 0.05	9.9 ± 0.03
	90 %	39.2 ± 0.1	19.7 ± 0.03	13.2 ± 0.04	9.9 ± 0.01
80 kHz	**30 %**	38.2 ± 0.04	19.1 ± 0.02	12.8 ± 0.01	9.6 ± 0.01
	60 %	38.4 ± 0.04	19.3 ± 0.04	12.9 ± 0.01	9.7 ± 0.01
	90 %	38.4 ± 0.1	19.4 ± 0.02	13.0 ± 0.01	9.8 ± 0.01

Table 3.9: Sonication energy dissipation per unit volume as a function of irradiation time.

Frequency	Power output percentage	Dissipated energy, E (J ml^{-1})			
		5 minutes	10 minutes	15 minutes	20 minutes
37 kHz	30 %	1151 ± 3	1163 ± 3	1167 ± 2	1166 ± 3
	60 %	1163 ± 4	1169 ± 2	1179 ± 4	1182 ± 3
	90 %	1175 ± 4	1179 ± 4	1184 ± 3	1191 ± 1
80 kHz	30 %	1145 ± 1	1147 ± 1	1149 ± 1	1151 ± 1
	60 %	1151 ± 1	1156 ± 2	1161 ± 1	1166 ± 1
	90 %	1152 ± 1	1161 ± 1	1170 ± 1	1179 ± 1

3.2.16 Ultrasound-mediated degradation

About 30 mg of mcl-PHA was dissolved in 10 ml acetone in a screw-cap tube (18.0 cm long and 1.3 cm internal diameter). The polymer solution was sonicated using ultrasonic bath (Elmasonic P 30H) for 5, 10, 15 and 20 minutes with ultrasonic power output and frequency held constant at 60 % and 37 kHz, respectively. Ultrasound treatment of mcl-PHA solution was also carried out at 30 and 90 % of ultrasonic power output with time and frequency held constant at 10 minutes and 37 kHz, respectively. Following exposure to the acoustic irradiation, the polymer solution was poured into a glass petri dish and dried in vacuum oven to evaporate off the acetone. All the ultrasound-treated mcl-PHAs were analyzed with TGA, DSC, GPC, ^{1}H-NMR and FTIR. Non-ultrasonicated mcl-PHA samples were used as controls

3.2.17 Determination of thermodynamic parameters for octanoic acid derived mcl-PHA

Kissinger's method was used to study the thermodegradation kinetics of mcl-PHA through Thermogravimetric Analysis (Doyle, 1961; Erceg *et al.*, 2005; Lee *et al.*, 1997). PHA samples were analyzed by TGA at multiple heating rates of 10, 15, 20, 25 and 30 °C min^{-1}. The degradation activation energy and pre-exponential factor of the process were estimated using Kissinger expression as shown in Eq. (3.4).

$$- \ln (q/T_p^{\,2}) = E_d / RT_p - \ln (AR / E_d) \quad \textbf{Eq.} (3.4)$$

where q = heating rate (K min-1), T_p = temperature at highest degradation rate (K), R = universal gas constant (8.3143 J K-1 mol^{-1}), E_d = degradation activation energy (J mol^{-1}), A = pre-exponential factor (s^{-1}). From the linear plot of - ln (q/T^2_p) versus $1/T_p$, degradation activation energy and pre-exponential factor were calculated from the gradient and the intersection at *y*-axis, respectively. The entropy of activation (ΔS) for mcl-PHA degradation was determined using Eq. (3.5) (Nair *et al.*, 2007),

$$A = (kT_p/h)\, e^{\Delta S/R} \quad \textbf{Eq.} (3.5)$$

where A = Arrhenius parameter (s^{-1}), k = Boltzman constant (J K^{-1}), T_p = peak temperature (K), h = Planck constant (J s), ΔS = entropy of activation (J K^{-1} mol^{-1}), R = general gas constant (8.314 J K^{-1} mol^{-1}). The thermal degradation rate constant, k can be calculated from the Arrhenius equation (Eq. 3.6), for each temperature of interest.

$$k = Ae^{-Ea/RT} \quad \textbf{Eq.} (3.6)$$

The temperature at the onset (T_{onset}) and complete degradation (T_{final}) were obtained from the TGA curve using instrument software. The equations are as follows:

$$T_{onset} = 1.16q + 541 \quad \textbf{Eq.} (3.7)$$

$$T_{final} = 1.12q + 570 \quad \textbf{Eq.} (3.8)$$

3.2.18 Study of film formation of mcl-PHA blends

About 0.1 g of mcl-PHA and scl-PHA were dissolved separately with 5.0 ml dichloromethane in a glass vial. Then these polymer solution were mixed together in other glass vials with different ratio of 75:25, 50:50 and 25:75 (w/w). Subsequently, the mixtures were vortexed for two minutes. The polymer solutions were concentrated to about 0.5 ml by low heating before film casting on glass slides. PHA films formed on the glass slide were air dried for about four hours and then oven dried for overnight. These film blends were left for one month in a closed container at 25 ^{o}C to allow them to achieve equilibrium in their crystallized state before being analyzed with TGA, DSC, XRD, and FESEM.

CHAPTER 4

RESULTS AND DISCUSSIONS

4.1 *P. putida* and PHA granules

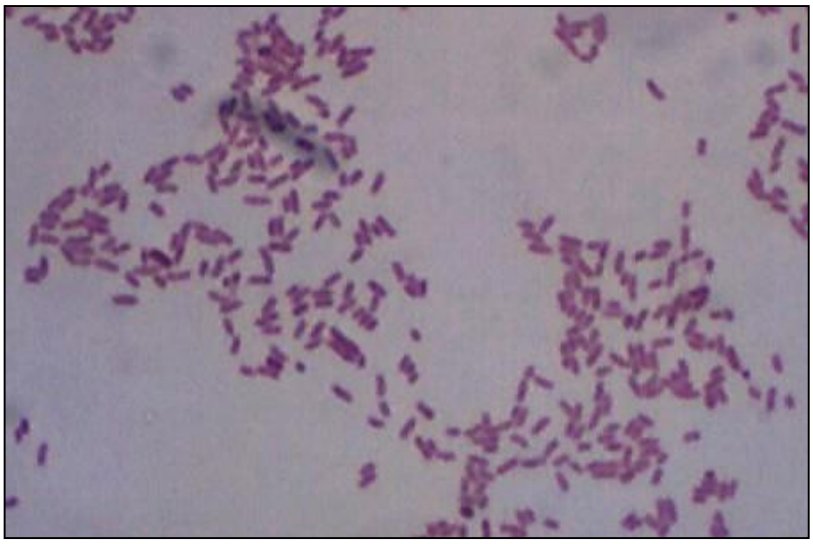

Figure: 4.1 *P. putida* cell stained with safranine solution.

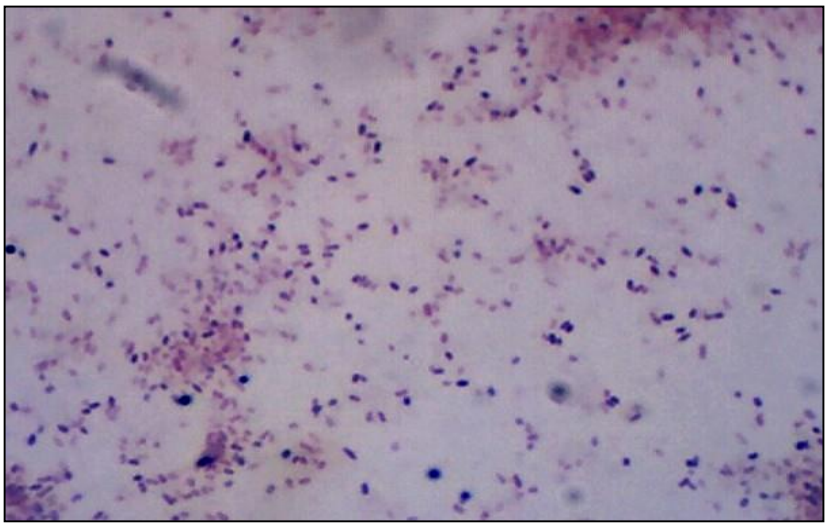

Figure 4.2: PHA granule (stained black) in *P. putida* cells.

Figure 4.1 and 4.2 showed microscopic view of *P. putida* cells under light microscope (100X). Bacterial cells, stained with safranine solution (Figure 4.1) was from rich medium after 24 hours of cultivation. Bacterial cells, double stained with safranine solution and the Sudan Black B solution (Figure 4.2) was from E2 medium after 24 hours of cultivation. Any existence of PHA inside the bacterial cells will be

stained black by Sudan Black B. Thus, PHA granules will be seen as black spots within the bacterial cells when being observed under light microscope with 100X len.

4.2 Direct cell and pure film methanolysis for PHA content determination

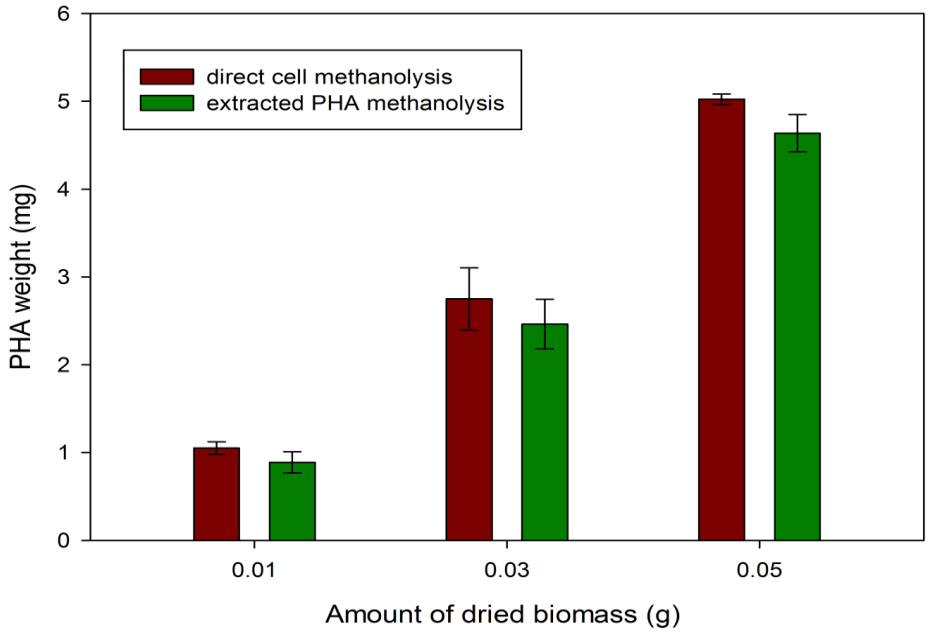

Figure 4.3: Direct cell methanolysis and extracted PHA methanolysis.

The PHA contents of the samples obtained from direct cell methanolysis was compared with samples obtained from pure PHA film methanolysis (Figure 4.3). The analysis revealed almost equal amount of PHA determined from same pool of biomass using the two independent methods. This showed that quantifying the amount of PHA by using direct cell methanolysis is not affected by non-PHA cellular materials (Huijberts, G. *et al.*, 1994). In addition, this method had been proven quantitatively reliable for direct PHA measurement from small amount dried biomass (Gross *et al.*, 1989). The slight differences in terms of PHA mass between these two methods were attributed to product loss during filtration step. However, *t*-test showed the differences at each level were not significant. This showed that direct cell methanolysis is reliable and rapid method to quantify amount of PHA in the dried biomass without having to extract out the PHA first.

4.3 Effect of different fatty acids as substrate for mcl-PHA production

4.3.1 Total biomass production (final biomass weight)

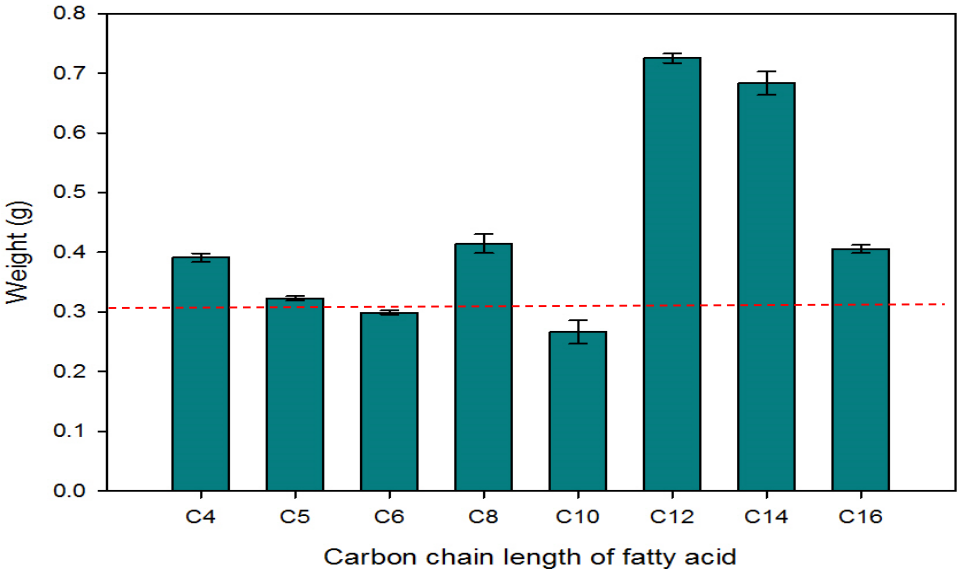

Figure 4.4: Final dried biomass weight.

Figure 4.4 showed the effect of different fatty acids towards the growth of *P. putida* during PHA – accumulation phase in E2 medium. Dotted line in the figure represents the starting amount bacterial weight that was inoculated into the E2 medium. The final biomass weight was obtained from 100.0 ml of E2 medium culture. Overall, the final biomass weight (cellular weight + PHA weight) resulted from different cultures with different fatty acids are different from each other.

From the results, shorter fatty acids (butyric acid to capric acid) used as carbon source in E2 medium were not able to promote good *P. putida* growth. Capric acid is the worst fatty acid to be used as carbon source as it caused reduction in biomass weight which is lower than initial biomass weight. However the exact reason is unknown at this stage of study. On the other hand, lauric acid produced the highest final biomass weight followed by myristic acid. The *P. putida* strain seems to prefer longer fatty acid as carbon source for growth. This probably due to the fact that longer fatty acids are major fatty acids in palm oil, which can be found abundantly from its original habitat. Therefore the strain could probably metabolize longer fatty acids efficiently. However,

palmitic acid did not promote the biomass growth as good as lauric and myristic acid. This is probably due to the solubilty issue whereby palmitic acid tend to coogulate during E2 medium culture. Therefore, the strain could not utilize the fatty acid efficiently. However, the exact reason is unknown at this stage of study.

4.3.2 PHA production

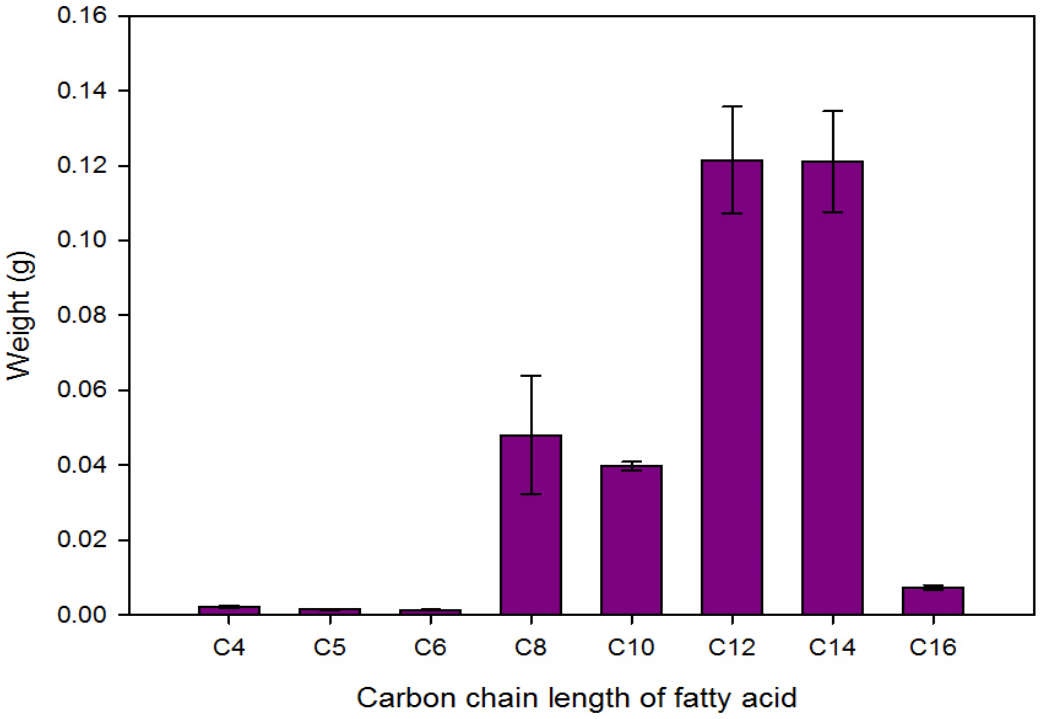

Figure 4.5: Total PHA production in 100 ml of E2 medium culture.

Figure 4.5 showed the amount of PHA (gram) obtained from 100.0 ml of E2 medium culture supplemented with different fatty acids. Of all fatty acids used in this study, only caprylic acid, capric acid, lauric acid and myristic acid were able to support PHA accumulation in reasonable amount. Lauric acid and myrsitic acid are the two best fatty acids in promoting the PHA accumulation in *P. putida.* Eventhough capric acid did not promote *P. putida* growth (Figure 4.4), it did stimulate the bacteria to accumulate PHA. However, the exact reason is unknown at this stage of study. In contrast, palmitic acid was able to promote the bacterial growth but did not support PHA accumulation very well. Low PHA production from palmitic acid can be explained as follows: as the

concentration of carbon in palmitic acid is high, there was less necessity for the cells to accumulate PHA. Instead, greater activity was directed towards cell growth.

PHA content at 0 hour of E2 medium culture is 0 % which was determined by doing direct cell methanolysis. Percentage of PHA in total dried biomass (final biomass weight) obtained from using caprylic acid as carbon source is quite low compared to lauric acid (C12) and myristic acid (C14) (Figure 4.6). However, the highest PHA content as a function of biomass increment (final biomass weight minus inoculum weight, 0.3g/100 ml) was obtained when caprylic acid was used as carbon source (Figure 4.7). It seems like caprylic acid could promote PHA accumulation more efficiently compared to lauric acid and capric acid. If the amount of inoculum is increased, caprylic acid consumption for PHA production would also be increased. Hence, less fatty acid will be wasted for cell growth.

Table 4.1 showed the monomer composition in PHA that had been produced from different fatty acids. From the results, *P. putida* is able to produce 3-hydroxydecanoate (3HD) from every single fatty acids given to it. 3-hydroxydodecanoate (3HDD) also can be produced efficiently out of all fatty acids except capric acid (decanoic acid). None of the fatty acids tested in this study including short fatty acids (butyric acid and valeric acid) are able to promote scl-monomer production (3HB and 3HV) in *P. putida.* This showed that this bacterium species does not has scl-PHA metabolic pathway and because of that, its choice of fatty acid is preferential towards the longer fatty acid for PHA synthesis.

Because of nearly homopolymer PHA (almost 90 % of 3-hydroxyoctanoate) can be produced by *P. putida* from caprylic acid, this fatty acid was selected for mass production of PHA. Homopolymer PHA will be used to conduct subsequent studies i.e extraction of PHA and scl-mcl PHA blend.

Table 4.1: 3-hydroxy monomers composition in mcl-PHA (%) as function of fatty acids substrates.

Carbon source (substrate)	3-hydroxy monomers								
	3HB (C4)	3HV (C5)	3HHx (C6)	3HO (C8)	3HD (C10)	3HDD (C12)	3HTD (C14)	3HHxD (C16)	% PHA in total biomass
Butyric acid (C4)	-	-	-	-	70	30	-	-	0.5
Valeric acid (C5)	-	-	-	-	67	33	-	-	0.4
Caproic acid (C6)	-	-	-	-	66	34	-	-	0.4
Caprylic acid (C8)	-	-	5	89	5	TC	TC	1	11.7
Capric acid (C10)	-	-	5	51	43	TC	-	1	14.9
Lauric acid (C12)	-	-	2	32	43	22	-	1	16.7
Myristic acid (C14)	-	-	2	35	42	17	2	2	17.7
Palmitic acid (C16)	-	-	-	14	56	30	-	-	1.8

(TC) = trace amount <1%), **(-)** = not found

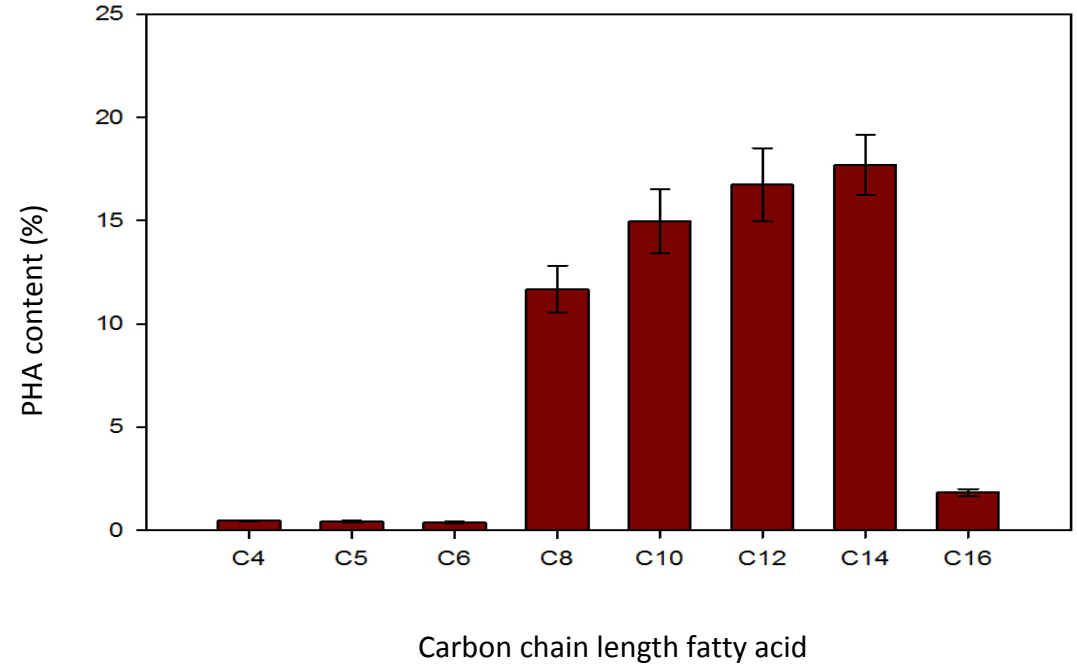

Figure 4.6: PHA content (%) in total dried biomass.

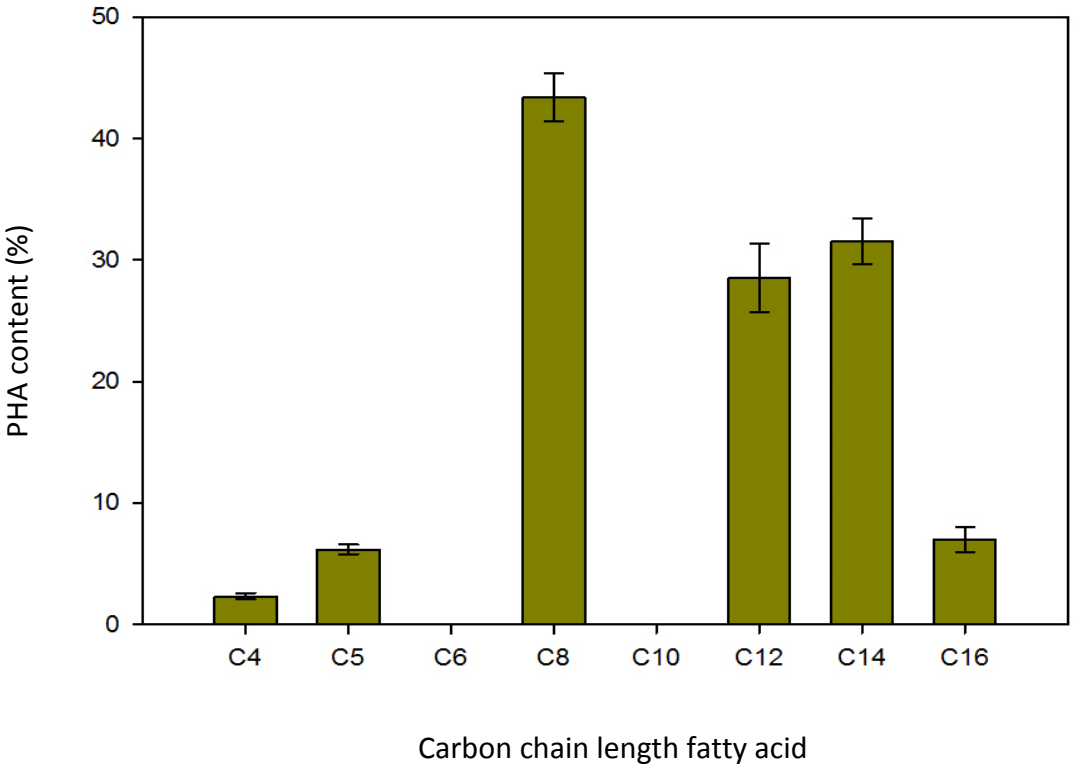

Figure 4.7: PHA content (%) as a function of biomass increment.

4.4 PHA extraction

4.4.1 Acetone vs chloroform for PHA extraction (solvent reflux)

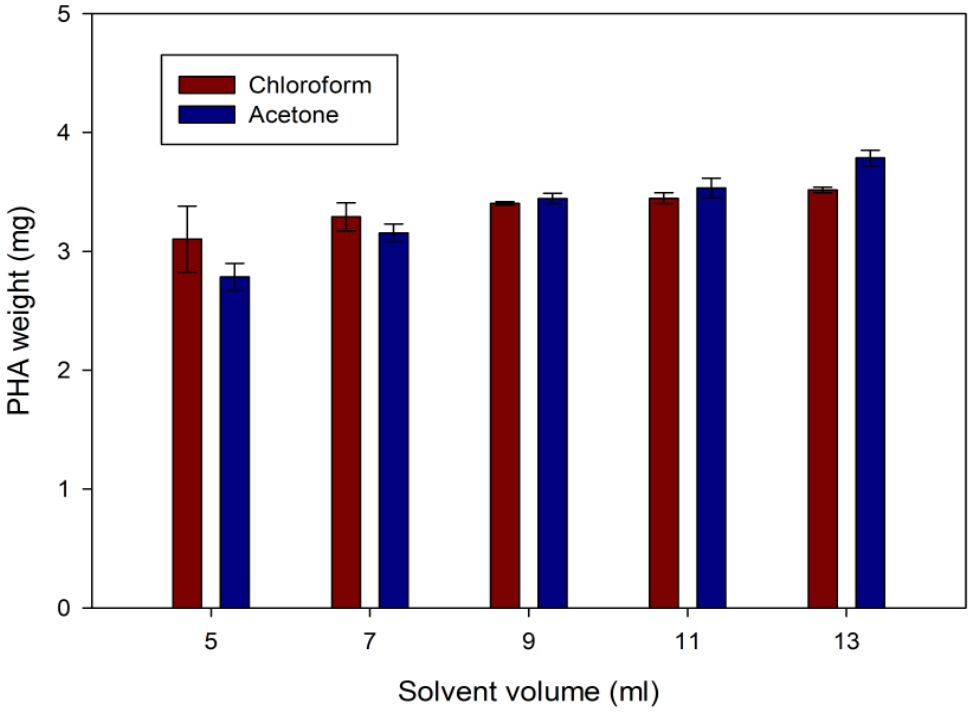

Figure 4.8: Conventional PHA extraction (solvent reflux).

The use of acetone relative to chloroform (the standard solvent) in extracting PHA out from the bacterial cells biomass was compared. From the results (Figure 4.8), acetone is shown to be comparable to chloroform in extracting the PHA from dried bacterial mass. The graph also showed that increasing the ratio of both solvent to biomass had little effect on the amount of PHA recovered. Similar observation was reported from a study (Jiang *et al.*, 2006) whereby increasing the ratio of acetone to biomass did not improve the PHA recovery when the total cell biomass contained only 10% PHA. From each different volume, similar amount of PHA content (20 – 24 %) was obtained by stirring the biomass in acetone for 24 hours. This indicated that the quantity of PHA to be extracted determined the quantity of solvent required instead of the amount of biomass. However in this study, when ultrasound irradiation was applied during acetone PHA extraction, improvement in the amount of PHA recovered from different acetone volume was observed (Figures 4.9a and b). This shows that ultrasound

irradiation could help improve the mass transfer efficiency in the extraction medium. Overall there is no significant difference between acetone and chloroform extraction as shown in Table 4.2. Therefore, acetone was selected as solvent for subsequent extraction using ultrasound.

Table 4.2: Anova table (solvent reflux of PHA extraction).

Source of Variation	DF	SS	MS	F	P
Between Groups	9	1.39×10^{-6}	1.54×10^{-7}	12.355	<0.001
Residual	10	1.25×10^{-7}	1.25×10^{-8}		
Total	19	1.51×10^{-6}			

4.4.2 Effect of time extraction on extraction yield of PHA

From the results shown in Figures 4.9 (a) and (b), it can be concluded that the most suitable time range for optimization of ultrasound-assisted PHA extraction was from 5 to 15 minutes. There was decreasing amount of extracted PHA mass from 10 to 20 minutes of extraction. Each treatment with different solvent volumes showed similar pattern. This observation could be explained as follows: sonication causes instant extreme heat production and shear forces inside the extraction medium. Thus, subjecting PHA extraction system for a long period of time would degrade the extracted polymer into chain fragments. Consequently, these fragments are easily lost during PHA purification. Hence, high molecular weight PHA mass is substantially reduced. It is believed that in ultrasonic process the polymer chain degradation occurs mainly due to the strong forces emanating from the rapid liquid flows near collapsing cavitation bubbles (Suslick *et al.*, 1990), following extremely rapid and alternate compression and expansion cycles. Macromolecules like polymer may not cope well with the drastic fluctuations. The friction generated causes strain and eventually bond rupture in the macromolecule. Unlike thermal degradation that occurs by random chain scission,

ultrasonic degradation of polymer is hypothesized to primarily occur at the main chain of the polymer (Koda *et al.*, 1994; Price *et al.*, 1993; Suslick *et al.*, 1999). Another possibility is probably because of the interuption of cellular components during PHA precipitation with methanol. Exposing the cellular biomass to the ultrasound irradiation to a longer time might disrupt more the cellular membrane which will then reduced the effciency of PHA precipitation. Thus, less PHA can be recovered from the subsequent PHA purification.

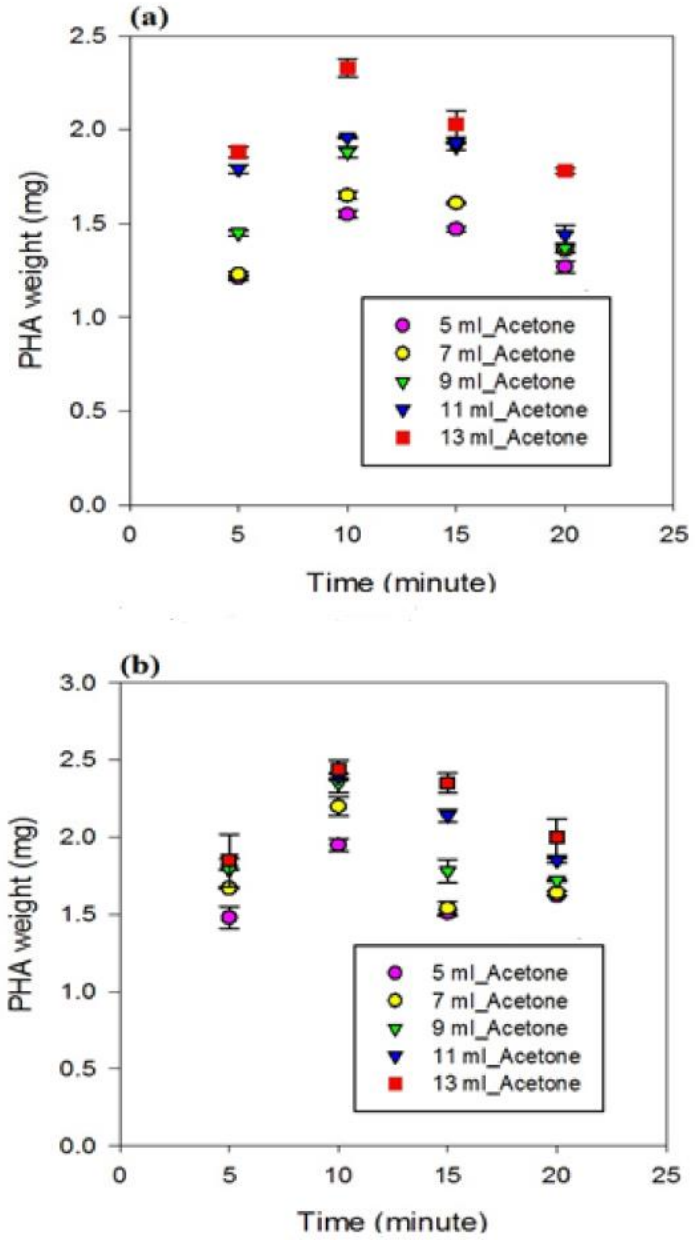

Figure 4.9: Ultrasound-assisted PHA extraction: (a) 80 kHz and (b) 37 kHz.

4.4.3 Effect of sonication frequency on PHA yield

From Figure 4.10, it is shown that 37 kHz was more efficient than 80 kHz for ultrasound-assisted PHA extraction. Hence, 37 kHz was selected for further studies. This observation is explained as follows:lower frequency of sonication can cause higher impact of cavitation bubbles implosion within the solvent than higher frequency could. As shown in Table 3.9, frequency at 37 kHz gave consistently higher dissipated energy per unit volume for all power outputs (30, 60 and 90 %) compared to similar power outputs at 80 kHz. Hence, higher temperature and shear force generated during bubble implosion enhanced the micro-streaming process of PHA from the bacterial biomass. Therefore, more PHA can be extracted out from the bacterial cells when lower sonication frequency was used.

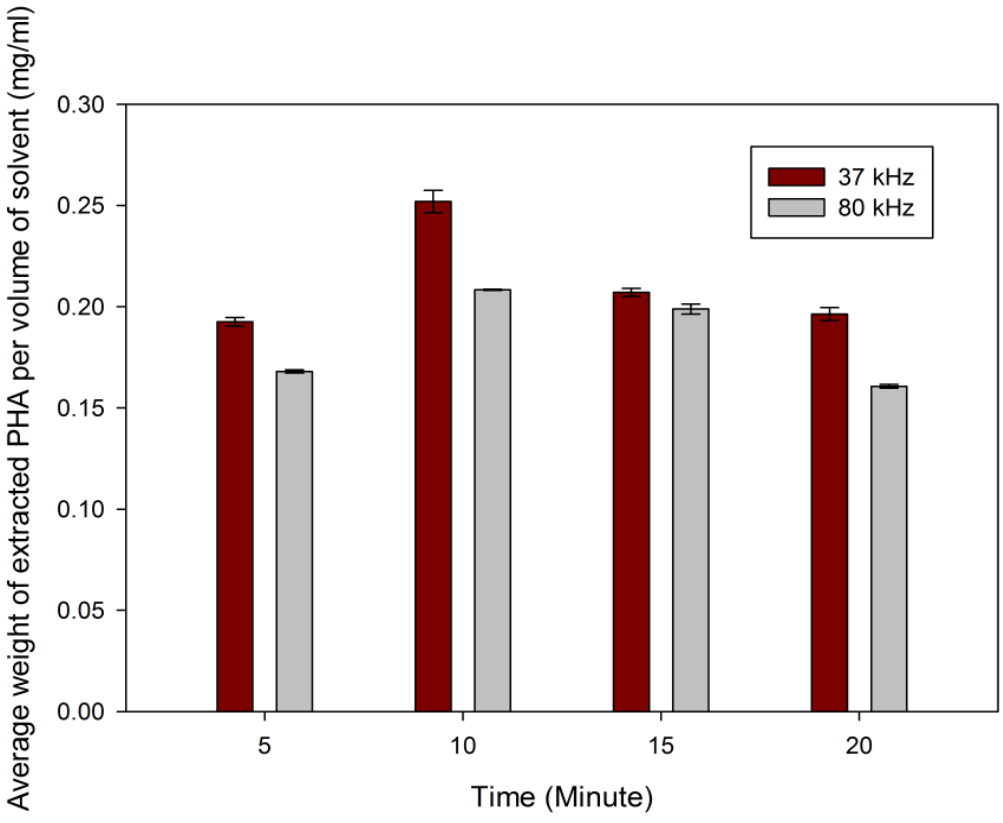

Figure 4.10: Comparison of frequency in ultrasonic PHA extraction.

4.4.4 Effect of marginal non-solvent on extraction yield of PHA

From Figure 4.11, it can be seen that the addition of *n*-heptane as marginal non-solvent in the extraction medium enhanced the extraction of PHA compared to *tert*-butanol as marginal non-solvent. This probably due to *n*-heptane ability to dissolve PHA more efficiently than *tert*-butanol. Another possibility is that *n*-heptane made the dried biomass more permeable to acetone. Consequently, acetone could easily penetrate through the cell wall and thus PHA would easily get dissolved. It may also be the combination of both. However, the amount of extracted PHA decreased as the *n*-heptane volume fraction increased more than 25 % of total extraction medium. At this point, *n*-heptane probably switched its role to be PHA precipitant instead of marginal non-solvent.

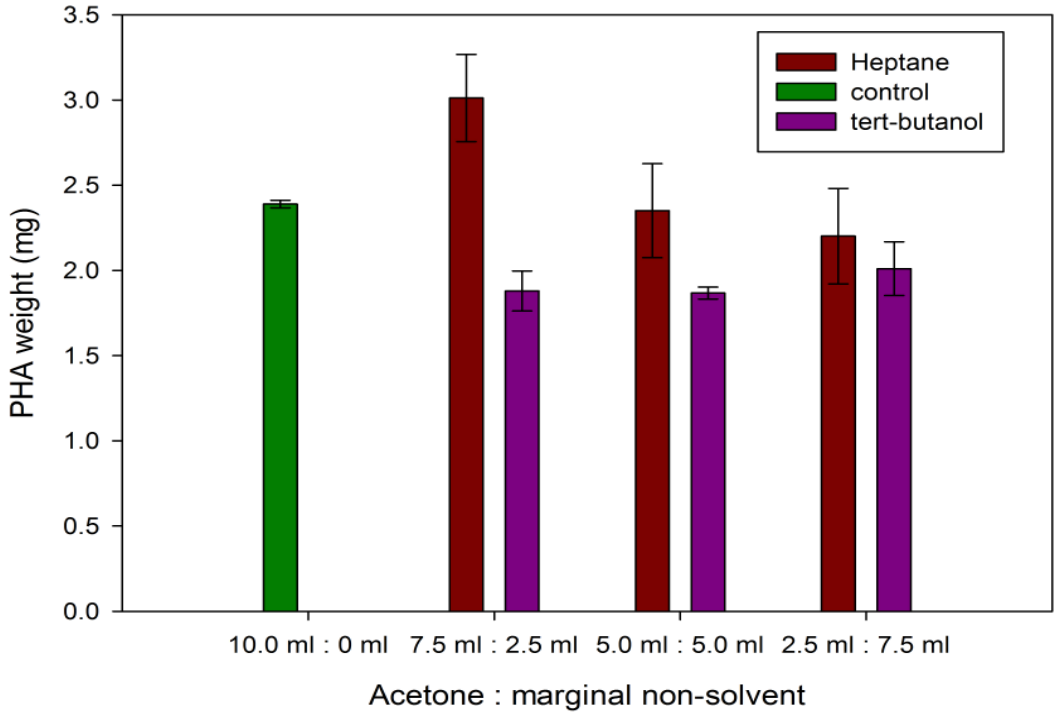

Figure 4.11: Comparison of heptane and *tert*-butanol as marginal non-solvent.

4.4.5 Optimization of the extraction parameters of mcl-PHA

4.4.5.1 Statistical analysis and model fitting

Table 4.3 shows the randomized run order for optimizing the three independent variables (including replicates) and their corresponding response variables.

By applying multiple regression analysis on the experimental data, the response variable (extraction yield of PHA) and the test variables are related by the following second-order polynomial equation:

$$Y = 32.7044 + (-0.1295\ X_1) + (0.5826\ X_2) + (-0.8250\ X_3) + (-0.0005\ X_1^2) + (-0.0093\ X_2^2) + (-0.0009\ X_3^2) + (0.0051\ X_1X_2) + (-0.0185\ X_1X_3) + (0.0191\ X_2X_3) \quad \textbf{Eq.}\ (4.1)$$

where Y is the extraction yield of PHA (%) and X_1, X_2, and X_3 are the independent variables for ultrasonic power output, acetone percentage and extraction time respectively.

Statistical testing of the model was performed in the form of analysis of variance (ANOVA). The determination coefficient (R^2 = 0.9361) indicated that only 6.39 % of the total variations were not explained by the model. The value of the adjusted determination coefficent (adjusted R^2 = 0.9163) also strongly indicated that the model utility. High F-value (F = 47.21) and low p-value (p < 0.0001) supported the significance of the model. Significance of the model was also determined by model's lack-of-fit test. The F-value and p-value for lack-of-fit were 2.44 and 0.087 respectively. This suggested that it was not significant and a 8.7% chance that noise contributed to the model prediction.

Table 4.3: Randomized runs of the design combinations and their responses.

Std Order	Run Order	Power output (%) X_1	Acetone percentage X_2	Time (minute) X_3	Extracted PHA (%)
32	1	90	75	5	39.5
17	2	90	100	10	21.9
29	3	30	100	10	15.4
20	4	30	75	15	31.0
14	5	30	50	10	37.1
21	6	90	75	15	26.4
39	7	60	75	10	32.1
36	8	60	100	5	15.6
38	9	60	100	15	17.4
25	10	60	100	15	21.7
30	11	90	100	10	19.4
6	12	90	75	5	36.6
5	13	30	75	5	35.8
34	14	90	75	15	22.2
9	15	60	50	5	36.5
15	16	90	50	10	29.3
37	17	60	50	15	27.7
13	18	60	75	10	32.0
24	19	60	50	15	30.3
18	20	30	75	5	28.6
22	21	60	50	5	36.6
4	22	90	100	10	21.6
31	23	30	75	5	32.9

27	24	30	50	10	38.2
19	25	90	75	5	37.2
33	26	30	75	15	29.5
28	27	90	50	10	35.0
23	28	60	100	5	20.5
12	29	60	100	15	19.4
26	30	60	75	10	31.8
1	31	30	50	10	38.4
16	32	30	100	10	11.1
2	33	90	50	10	27.2
35	34	60	50	5	39.3
3	35	30	100	10	13.1
8	36	90	75	15	26.2
11	37	60	50	15	30.8
7	38	30	75	15	31.4
10	39	60	100	5	17.5

4.4.5.2 Optimization of extraction conditions

3-D response surfaces and 2-D contour plots (Figure 4.12 a-f) were plotted using Minitab 16 software to study the effects of independent variables and their interactions on PHA yield. These plots showed effects of two factors on the responses while the other one factor was kept constant at middle level. Figures 4.12 (a) and (b) showed that the 2-D contour and 3-D surface plots at varying acetone-to-heptane ratio and ultrasonic power output at fixed irradiation time (10 minutes). From these, it can be seen that maximum extraction yield of PHA can be achieved when solvent percentage (acetone-to-heptane ratio) and ultrasonic power were below 55 % and 65 %, respectively. The 2-

D contour plots and 3-D response surface in Figures 4.12 (c) and (d), power output (60 %) was hold at constant value, the extraction yield of PHA decreased with irradiation time and acetone-to-heptane ratio (solvent percentage). The 2-D contour and 3-D response surface plots based on time and ultrasonic power output at constant solvent percentage (75 %) were shown in Figures 4.12 (e) and (f). Increased extraction yield of PHA could be significantly achieved with the increase in ultrasonic power output.In contrast, the extraction yield of PHA decreased with the irradiation time. Eventhough relatively high PHA extraction yield can be obtained at high ultrasonic power output, the extraction yield dropped significantly with longer irradiation time. However, at low ultrasonic power output (30 %), there was no obvious difference in PHA extraction yield with irradiation time.This indicated either PHA would be easily degraded at higher ultrasonic power output or more disruption of cellular component that will cause difficulty for subsequent purification process if the irradiation exposure time is prolonged.

The trends of PHA extraction behavior interpreted from Figure 4.12 (a-f) showed the dynamic effects of the three tested variables (solvent percentage, power output and irradiation time) on the recovery efficiency. It also allowed for the path of optimum trajectory to be assessed and determined. It was concluded that optimal extraction conditions of PHA from *P. putida* dried biomass were ultrasonic power output 30 % (equivalent to 1151 ± 3 J ml^{-1}), solvent percentage 50 %, and irradiation time 5 minutes. In addition, there were significant interactions between the different independent variables that influenced the extraction yield of PHA ($p < 0.05$).

The data presented showed the potential of ultrasound-assisted process to facilitate rapid PHA extraction from bacterial biomass with reasonably high rate of 74 × 10^{-3}g PHA g^{-1} dried biomass min^{-1}under the said optimal conditions. On the other hand, when using the conventional hot solvent extraction, the extraction rate was calculated at

3×10^{-3}g PHA g^{-1} dried biomass min^{-1}. Thus, the ultrasound-assisted extraction was at least 25 times faster than hot-solvent (4 hours) or stirring biomass at ambient temperature (24 hours) methods.

Furthermore, if repeated cycles of the high rate ultrasound-assisted extraction method were to be performed on the same batch of dried bacterial biomass, theoretically it is possible to achieve an almost complete recovery of the intracellular PHA. This opens up a way for the implementation of a high throughput process.

4.4.6 Verification of the predictive model

The predictive strength of the polynomial model was tested at the actual optimal combination plus one non-optimal combination chosen arbitrarily. Table 4.4 showed the two experimental combinations along with their predicted and experimental yields of PHA. The model was able to predict the actual outcomes satisfactorily in the ultrasound-assisted PHA extraction system.

Table 4.4: Comparison between predicted and actual responses.

Power output (%)	**Acetone percentage**	**Time (minute)**	**Extracted PHA (%)**	
			Predicted	**Actual**
30	50	5	39.7	37 ± 2
90	100	5	25.2	30 ± 2

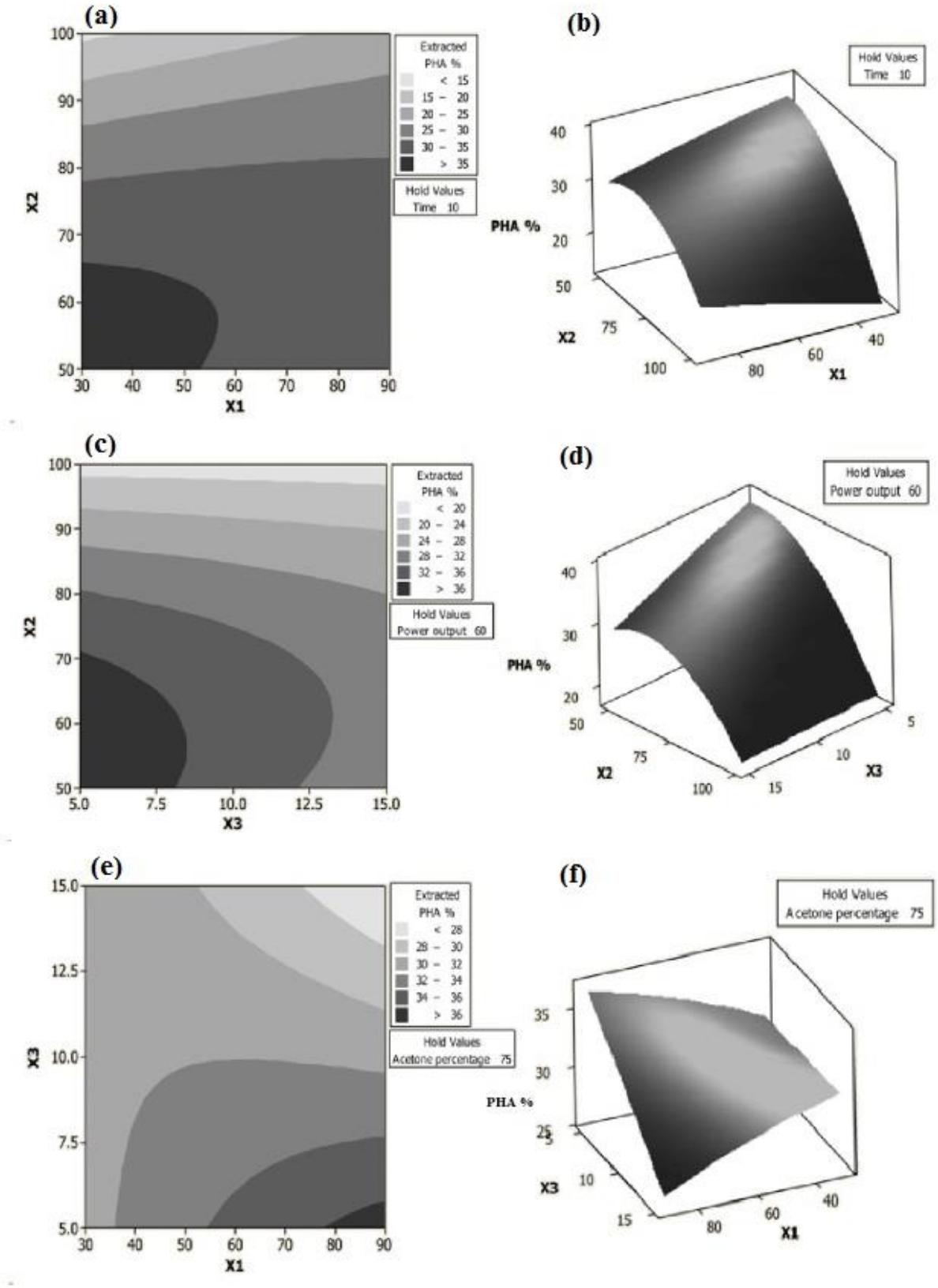

Figure 4.12: Contour and surface plots showing the effect of ultrasonic power output (X_1), acetone percentage (X_2), and extraction time (X_3) on the percentage of PHA extraction yield.

4.4.7 Characterization of ultrasound extracted mcl-PHA

4.4.7.1 Thermal properties of mcl-PHA

The glass transition temperature (T_g) and and melting point (T_m) for both control and ultrasound extracted PHA were summarized in Table 4.5. The T_m and T_g values of ultrasound treated PHA (at optimum conditions) did not vary considerably from the control PHA sample (acetone extracted without sonication). It is clear that controlled sonication did not affect significantly the thermal properties of the extracted PHA film.

4.4.7.2 Molecular weight analysis of mcl-PHA

The average molecular weights and molecular weight distribution of control and ultrasound treated PHA (at optimum conditions) were determined by GPC analysis and the results were summarized in Table 4.5. The results showed that the M_n and M_w values between control and ultrasound treated PHAs were not significantly different from each other. This further supported the applicability of ultrasound irradiation process in facilitating rapid PHA extraction from bacterial biomass.

Table 4.5: Molecular weight and thermal properties of extracted PHAs (control: non-ultrasound treated PHA in acetone/heptane 50:50).

Sample	**Molecular weight**			**Thermal property**	
	M_n (kDa)	**M_w (kDa)**	**PDI**	**T_g (°C)**	**T_m (°C)**
Control PHA	29	59	2.07	-37	51
Ultrasound treated PHA	28	59	2.11	-39	49

4.4.7.3 ^{1}H-NMR spectroscopy

Figures 4.13 (a) and (b) showed the proton NMR spectra for the control and ultrasound extracted PHA respectively. The ^{1}H-NMR spectrum of octanoic acid derived mcl-PHA produced by *P.putida* BET001 showed almost identical spectrum to the one from an earlier study (Chan Sin *et al.*, 2010) except that peaks at 1.9 and 2.4 ppm were absent. This indicated the saturation of mcl-PHA side chains. There were no unknown peaks that represent contaminants in the spectrum. Both ^{1}H-NMR spectra (control and ultrasound treated PHAs) were identical despite the decrease in peak signal intensity at 3.65 ppm. Peak 3.65 ppm was assigned to the proton of the hydroxyl groups. The observed decrease in signal intensity could probably due to the dehydration effect at the end chain of polymer when exposed to high temperature generated by the sonication bubbles implosion. The difference in the ratios a:c and b:c between the two spectra is probably due to an overlaying sharp solvent peak (e.g. water) in samples.

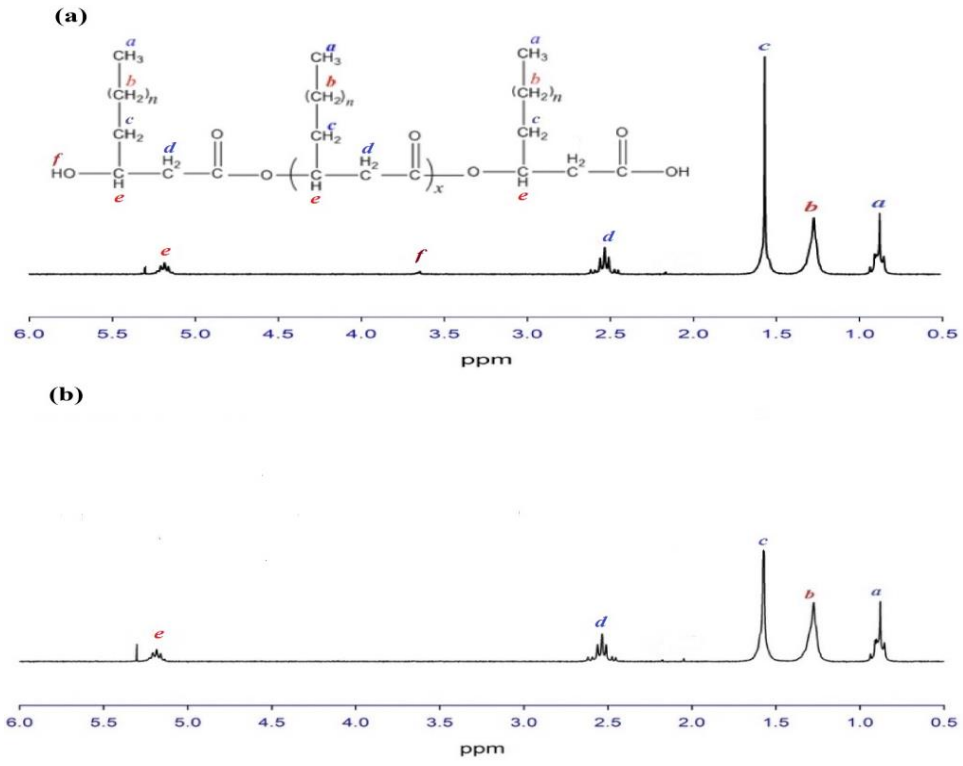

Figure: 4.13 ^{1}H-NMR spectra of (a) control and (b) ultrasound extracted PHA at optimal conditions. (control: non-ultrasound treated PHA in acetone/heptane 50:50).

4.5 Stability and degradation of mcl-PHA

4.5.1 Thermo-kinetic analysis of octanoic acid derived mcl-PHA thermodegradation

The TGA thermogram of octanoic acid derived mcl-PHA thermodegradation at different heating rates is shown in Figure 4.14 a. All thermograms showed only one-step degradation process between 250 and 340 °C. Increasing the heating rate shifted the onset temperature for maximum degradation to a higher value (Table 4.6).

The plot of -ln (q/T^2_p) versus $1/T_p$ (Figure 4.14 b) was used to determine the thermodynamic parameters for thermal degradation of mcl-PHA by Kissinger equation. The degradation activation energy, E_d and pre-exponential factor, A for octanoic acid derived mcl-PHA were 132 kJ mol^{-1} and 1.26 x $10^{10} s^{-1}$, respectively. These values were in agreement with the E_d and A for palm kernel oil derived mcl-PHA *viz*. 129 kJ mol^{-1} and 1.15 x 10^{10} s^{-1}, respectively (Sin *et al.*, 2013). A is often called the frequency factor and if the reaction is first order, it has the units s^{-1}. In this particular case, the thermal degradation of mcl-PHA can be considered as a first order reaction since the amount of degradation that takes place is proportional to the initial concentration of the mcl-PHA present.

The high E_d indicates the relative stability of octanoic acid derived mcl-PHA, which is similar to palm kernel oil derived mcl-PHA. It also indicated that degradation of these mcl-PHAs occur at relatively high temperature. This strongly points to the similarity in the thermal degradation behavior of mcl-PHA produced using carbon source consisting mainly of saturated fatty acid(s) such as octanoic acid and palm kernel oil. This is in contrast to the oleic acid derived mcl-PHA with E_d = 86 kJ mol^{-1} (Chan Sin *et al.*, 2010), where carbon source with unsaturation in the fatty acid(s) such as oleic acid produced mcl-PHA with lower thermal stability. Table 4.6 also shows the change of activation entropy (ΔS) has a negative value of -57 J K^{-1} mol^{-1} which supported the

relative stability of the octanoic acid derived mcl-PHA. Similar value of ΔS was obtained for palm kernel oil derived mcl-PHA at -58 J K^{-1} mol^{-1} (Sin *et al.*, 2013).

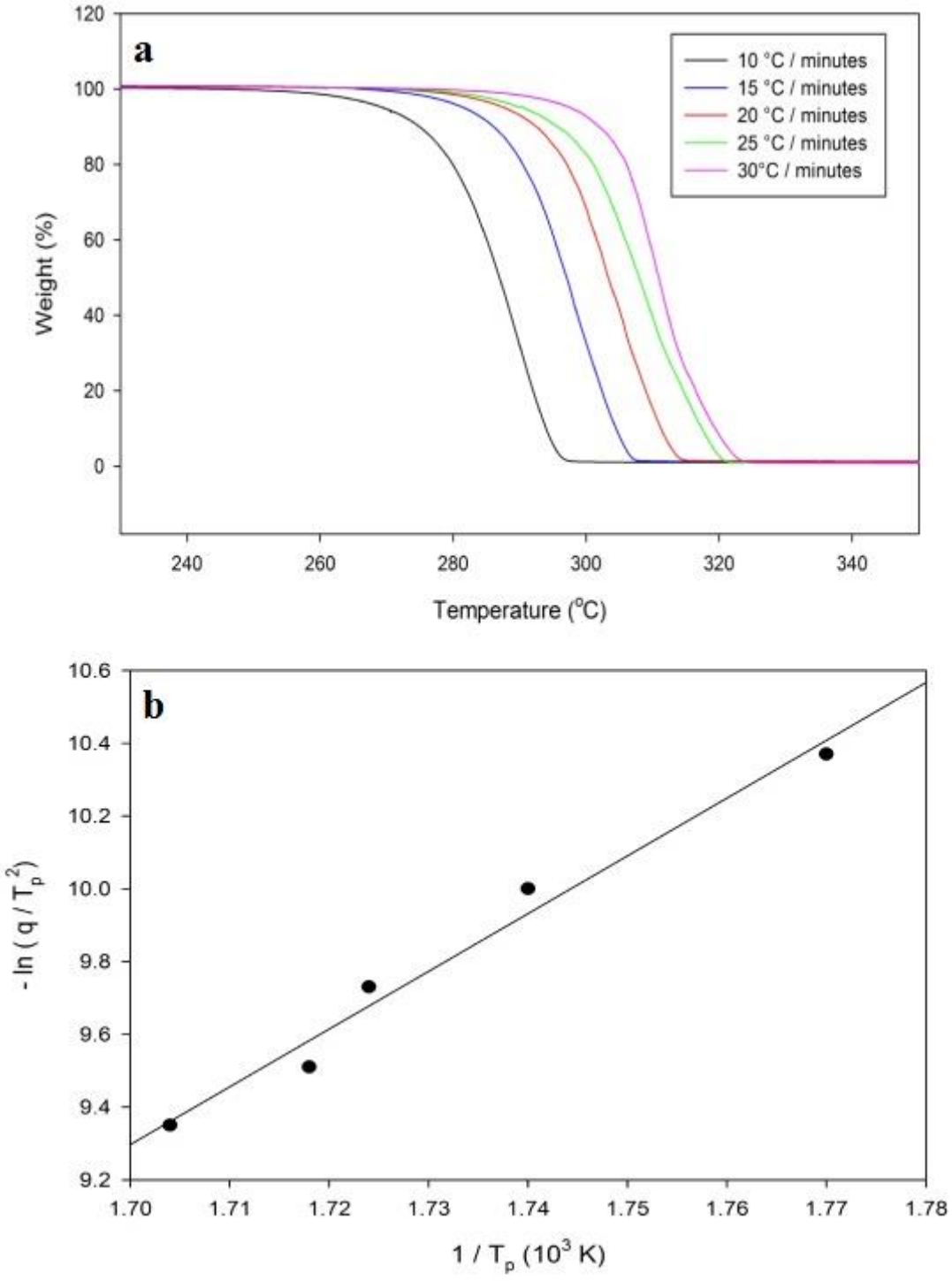

Figure 4.14: (a) Thermogram of octanoic acid derived mcl-PHA at different heating rates; (b) Kissinger plot for octanoic acid derived mcl-PHA (R^2 = 0.978).

Table 4.6: Thermodynamic parameters for thermodegradation of octanoic acid derived mcl-PHA.

q (Kmin^{-1})	T_p (K)	$e^{(-Ea/RT)}$	k (x 10^{10} s^{-1})	E_d, degradation activation energy (kJ mol^{-1})	A, pre-exponential factor (x 10^{10}s^{-1})	ΔS, entropy of activation (J K^{-1} mol^{-1})
10	565	0.972				
15	575	0.973				
20	580	0.973	1.23	132	1.26	-57
25	582	0.973				
30	587	0.973				

For degradation temperature range studied (565 to 587 K), specific degradation rate constant (k) was calculated at 1.23 x 10^{10} s^{-1} (Table 4.6). This is not surprising since the multiplier in Eq. (3.6) i.e. $e^{-Ea/RT}$ was calculated at 0.97 for all the temperatures studied (Table 4.6). This multiplier gives a probability that any given collision will result in a reaction. Hence at the calculated value of A (= 1.26 x 10^{10}s^{-1}) (Table 4.6) i.e. the total number of collisions (leading to a reaction or not) per second, the value of k, which is the number of collisions that result in a reaction per second, would be similar within the temperature range studied (Table 4.6). In other words, the increase in temperature within this range will not result in increased k nor faster thermal degradation of mcl-PHA.

Figure 4.15 showed the linear relationship between T_{onset} and T_{final} with the heating rate, q.The thermal degradation temperature can be expressed as equilibrium degradation temperature when the heating rate (q) approches zero (Li, S. D. *et al.*, 2001). Hence, from Eqs. (3.7) and (3.8), T_{onset} (0) = 541 K and T_{final} (0) = 570 K. The

progression of thermodegradation is given by $T_{final} - T_{onset} = -0.04q + 29$, which increases slowly with increasing heating rate.

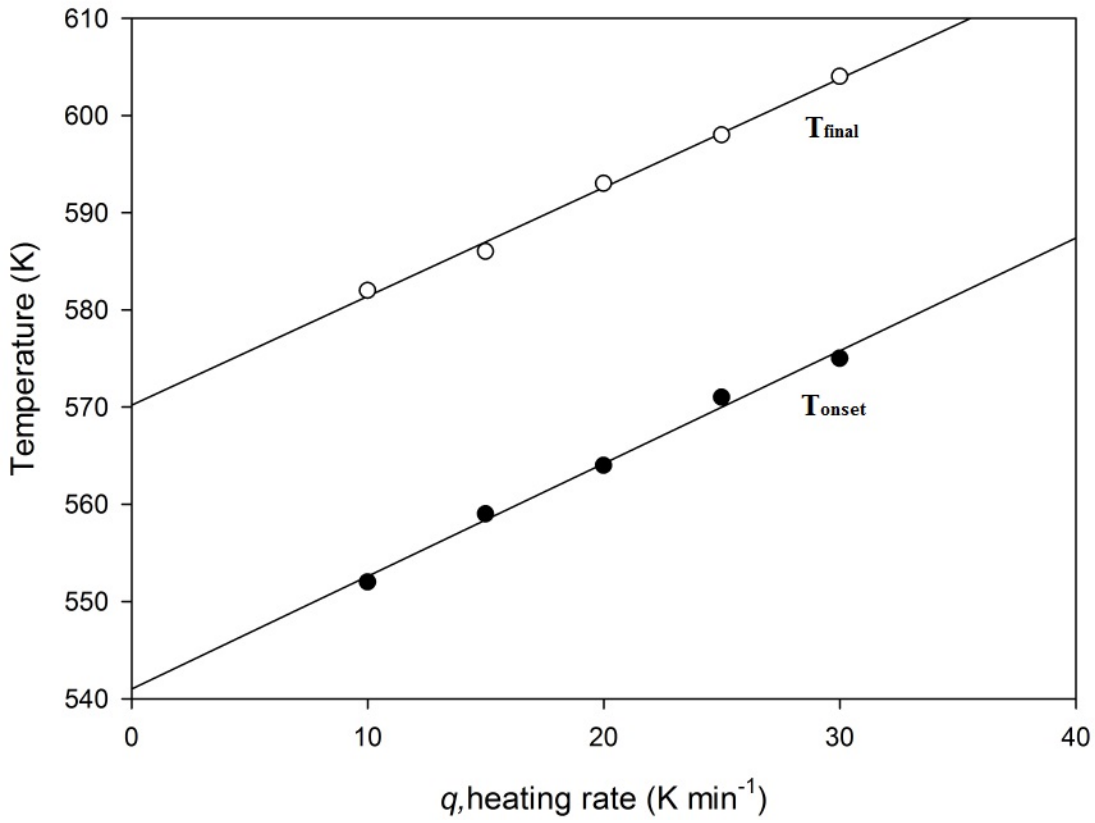

Figure 4.15: Linear relationship of T_{onset} and T_{final} with heating rate, q.

4.5.2 Thermogravimetric analysis of control and ultrasound-irradiated mcl-PHA

Figures 4.16 (a) and (b) showed the comparison of thermal stability between control PHA and those that had been exposed to ultrasound irradiation at different duration and ultrasonic power output, respectively. All mcl-PHA samples (the control and ultrasound treated samples) were thermally degraded in one-step process.

From Figure 4.16 (a), it can be seen that the duration of exposure to ultrasonic irradiation (60 % power output) showed significant effect on thermal stability of mcl-PHA. The control and 5, 10, and 15 minutes ultrasound-irradiated mcl-PHA samples started to decompose at around 250 – 280 °C, with the control registering a lower initial decomposition temperature. However, the lowest initial decomposition temperature was registered by 20 minutes ultrasound irradiated mcl-PHA, which started to decompose at

around 230 °C. A reasonable explanation could be that mcl-PHA samples exposed to ultrasound irradiation for 5, 10 and 15 minutes were only slightly degraded, leaving behind a mixture of native long polymer chains and slightly shorter polymer chains (oligomers). It is suggested that the resulting mixture is more thermally stable as they can assemble together much closer to each other. On the other hand, the 20 minutes ultrasound irradiated mcl-PHA could have been degraded much more than the rest, leaving behind higher proportion of lower molecular weight chains compared to the native long polymer chains. This resulted in a mixture that could be more easily disintegrated by heating.

In contrast to duration exposure, varying the rated ultrasonic power output (30, 60, and 90 %) at 10 minutes did not affect significantly the thermal stability of mcl-PHA (Figure 4.16 b). From Table 3.9, it is clear that at different rated percentage of ultrasonic power output (at constant frequency 37 kHz), the volumetric energy dissipated into the mcl-PHA solution was approximately similar irrespective of exposure duration. Hence, the extent of degradation subjected to the mcl-PHA solution is primarily a function of exposure duration to the acoustic energy. It is interesting to note that all ultrasound irradiated mcl-PHA samples at different ultrasonic power output (constant exposure duration 10 minutes) showed relatively higher initial decomposition temperature (around 270 – 280 °C) than the control mcl-PHA (250 °C). It is suggested that subjecting mcl-PHA sample to ultrasound irradiation resulted in a mixture of native long polymer chains and shorter degraded polymer chains, hence a more thermally stable PHA mixture was obtained as discussed earlier.

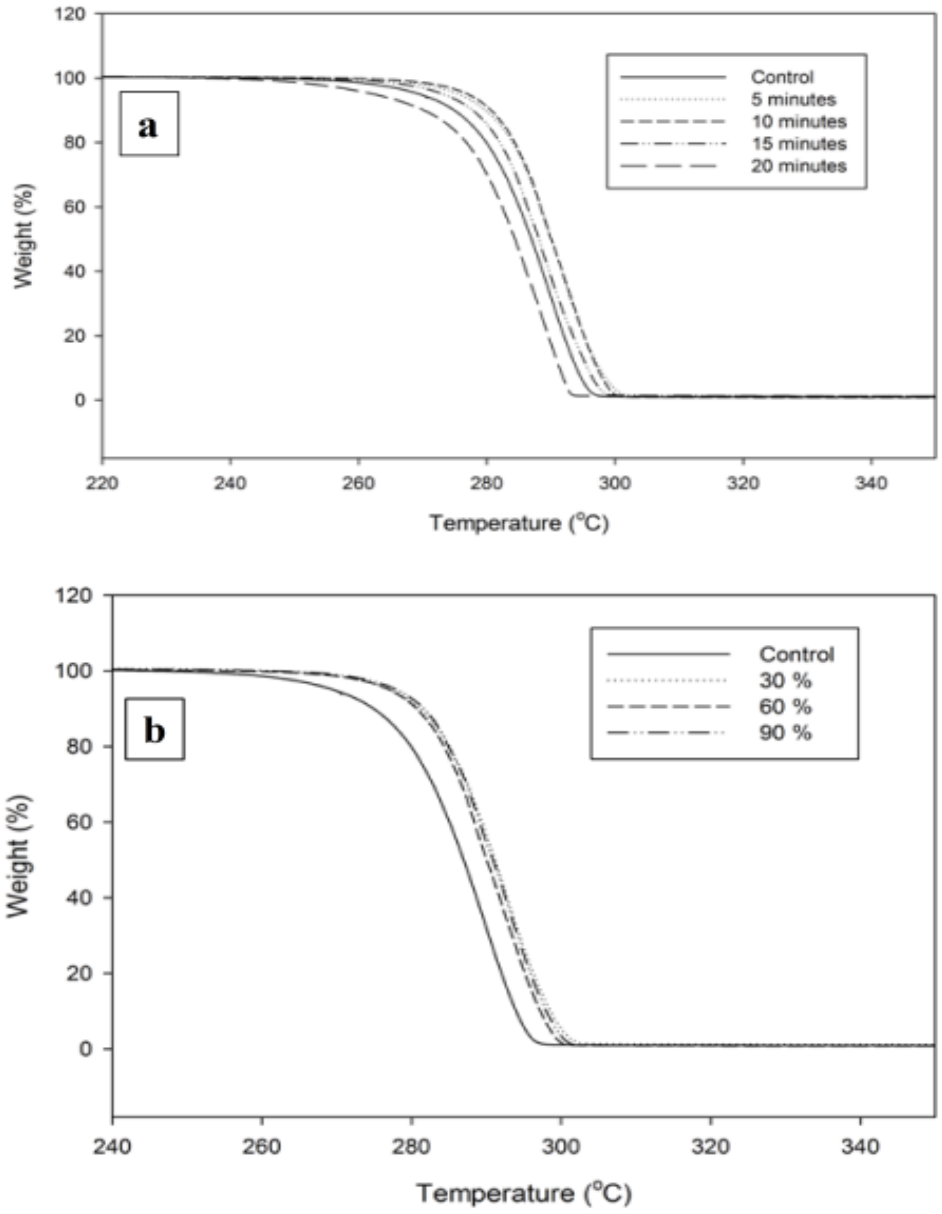

Figure 4.16: Relative thermal stability of control PHA and ultrasound irradiated mcl-PHA at different (a) exposure time and (b) ultrasonic power output.

4.5.3 Differential scanning calorimetry analysis of control and ultrasound treated mcl-PHA

Figure 4.17 shows the DSC thermograms for both control and ultrasound irradiated mcl-PHA. Glass transition (T_g) and melting temperatures (T_m) of all mcl-PHA samples can be observed from these thermograms. From Figure 4.17 (a), it is shown that there was a decrease in T_g and T_m when mcl-PHA samples were exposed to ultrasound irradiation from 5 to 20 minutes at constant 60% ultrasonic power output.

Similar trend of decrease in T_g and T_m was also be observed when ultrasonic power output was varied at constant 10 minutes of irradiation (Figure 4.17 b). In addition to generating some proportion of fragments from native mcl-PHA, subjecting the sample to ultrasound irradiation is hypothesized to promote disentanglement of the native polymer due to microstreaming effects of acoustic waves. The more streamlined, less entangled polymer mixture showed reduced hydrophobic interactions hence decreased T_g and T_m.

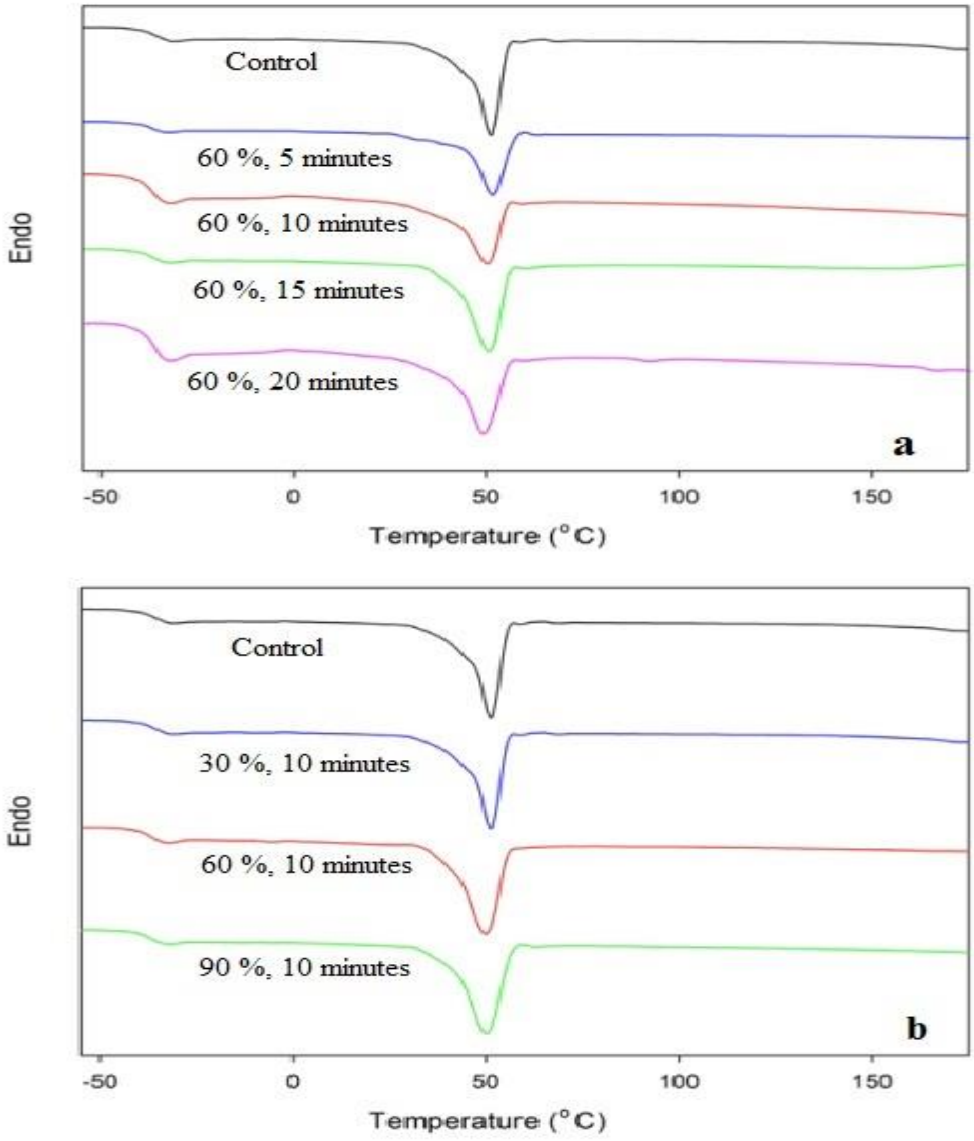

Figure 4.17: DSC thermogram of control PHA and ultrasound irradiated mcl-PHA at different (a) exposure time and (b) ultrasonic power output.

4.5.4 Molecular weight analysis of control and ultrasound irradiated mcl-PHA

The average molecular weight and molecular weight distribution of control and ultrasonic irradiated polymers were determined by GPC analysis and the results are summarized in Table 4.7. It should be pointed out here that the GPC column was calibrated using PS standards, and hence the M_n and M_w values are relative to PS. From the table, it can be seen that the values for number-averaged molecular weight (M_n), weight-averaged molecular weight (M_w), and polydispersity index (PDI) parameters of control and ultrasound irradiated mcl-PHA (5, 10, 15 and 20 minutes at constant 60 % ultrasonic power output) remained approximately constant. Similarly, constant M_n, M_w and PDI values were observed despite ultrasonic power output was varied at 30 % and 90 % with constant 10 minutes irradiation. This emphasized the earlier observation regarding the primary effect of exposure duration towards mcl-PHA upon ultrasound irradiation at constant power output.

The width of the molecular weight distribution (indicating by PDI values) remained unchanged, irrespective of the duration and/or the intensity of the sonication process. This suggests random chain scission as the likely cleavage reaction of ultrasound induced biopolyester degradation in organic solution (Reich, 1998). It is hypothesized that mcl-PHA degradation under prolonged exposure to ultrasonic irradiation occurred by random α-chain scission of the ester linkages as a result of localized intense temperature and shear force from the micro-bubbles implosion. To further elucidate the mechanism underlying the cleavage process of ultrasound-induced biopolyester degradation, following analyses of the degradation products using 400 – MHz 1H-NMR and FTIR spectroscopy were investigated.

Table 4.7: Number-average molecular weight (M_n), weight-average molecular weight (M_w) and molecular weight distribution (*PDI*) of control and ultrasound-irradiated mcl-PHA.

PHA sample	**Molecular weight**		
Ultrasound irradiated (% power output, time in minutes)	M_n **(kDa)**	M_w **(kDa)**	***PDI***
Control mcl-PHA	41	84	2.1
60 %, 5 minutes	40	80	2.0
60 %, 10 minutes	38	79	2.1
60 %, 15 minutes	40	83	2.1
60 %, 20 minutes	40	82	2.1
30 %, 10 minutes	39	80	2.1
90 %, 10 minutes	38	79	2.1

4.5.5 ^{1}H-NMR spectroscopy

Figure 4.18 shows proton NMR spectrum of the control mcl-PHA extracted by solvent diffusion (without heating). The spectrum of octanoic acid derived mcl-PHA produced by *P. putida* showed peaks at similar chemical shifts in the spectra of previous studies (Tan *et al.*, 1997). The peak *a* at 0.8 ppm and *b* at 1.2 ppm (together with peak *c* at 1.5 ppm) were assigned to the methyl and methylene group in the side chain respectively. Peak *c* was assigned to methylene group next to the main chain. The two peaks *d* and *f* at around 2.55 and 5.2 ppm represented the methylene group at the α-position and methine group at the ß-position of the ester respectively. Proton of hydroxyl group at end chain of mcl-PHA was represented by the peak *e* at around 3.65 ppm. The absence of peaks around 1.9 and 2.4 ppm which belonged to protons adjacent to double bonds indicated the saturation of octanoic acid derived mcl-PHA side chains.

The ^{1}H-NMR spectra of all ultrasound irradiated mcl-PHA (Appendices A and B) were identical to the spectrum of control PHA (Figure 4.18). Nevertheless, the intensity ratio of signal *f* (proton originated from ß methine group adjacent to ester bond) to signal *a* (proton originated from side chain methyl group) of ultrasound-irradiated mcl-PHA for 20 minutes was slightly decreased. This may indicate that some scission of ester bond had occured. Comparison of proton ratio for control and ultrasound-irradiated mcl-PHA are summarized in Table 4.8. For signal *c* (proton originated from side chain methylene group next to the main chain), the increase in ratio could probably due to contamination by solvent. However, the exact reason is unknown at this stage.

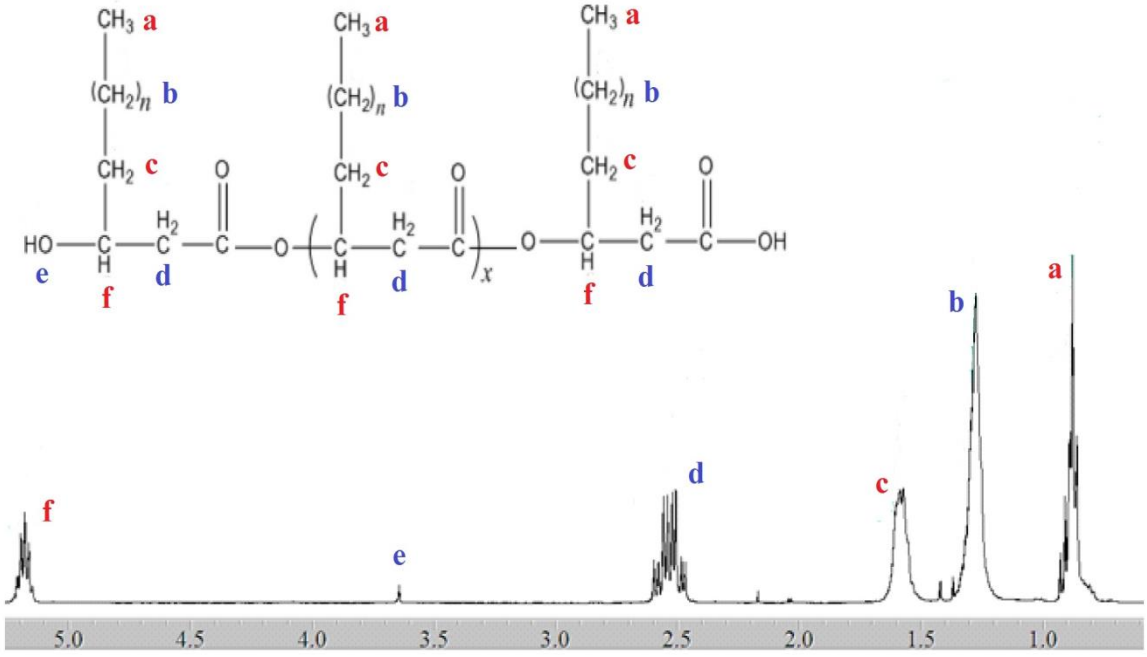

Figure 4.18 ^{1}H-NMR spectrum of octanoic acid derived mcl-PHA.

Table 4.8: Proton ratio of control and ultrasound-irradiated mcl-PHA.

	a	b	c	d	f	f / a
Control	3.2	6.0	2.8	2.0	1.0	0.31
60 %, 5 mins	3.1	5.9	4.9	2.0	1.0	0.32
60 %, 10 mins	3.1	5.9	5.7	2.0	1.0	0.32
60 %, 15 mins	3.4	6.2	7.5	2.0	1.0	0.29
60 %, 20 mins	3.6	6.4	8.4	2.0	1.0	0.27
30 %, 10 mins	3.1	5.9	5.4	2.0	1.0	0.32
90 %, 10 mins	3.1	6.2	6.4	2.0	1.0	0.32

4.5.6 FTIR spectroscopy

Figures 4.19 (a) and (b) show the FTIR spectra of the control and ultrasound irradiated mcl-PHA at different duration and ultrasonic power outputs, respectively. All spectra are practically identical, matching a previous report (Guo *et al.*, 2012). This indicated that no major changes of molecular structure when subjecting mcl-PHA samples to ultrasound irradiation at each specified condition. However, the spectrum of the ultrasound irradiated mcl-PHA after 20 min at 60 % showed one additional absorption band at 1650 cm^{-1}. This band was assigned to a C=C double bond that is conjugated to the ester carbonyl (Chan Sin *et al.*, 2010). The absorption indicates a minor, but significant degradation of the polymer upon long term exposure to ultrasonic irradiation.

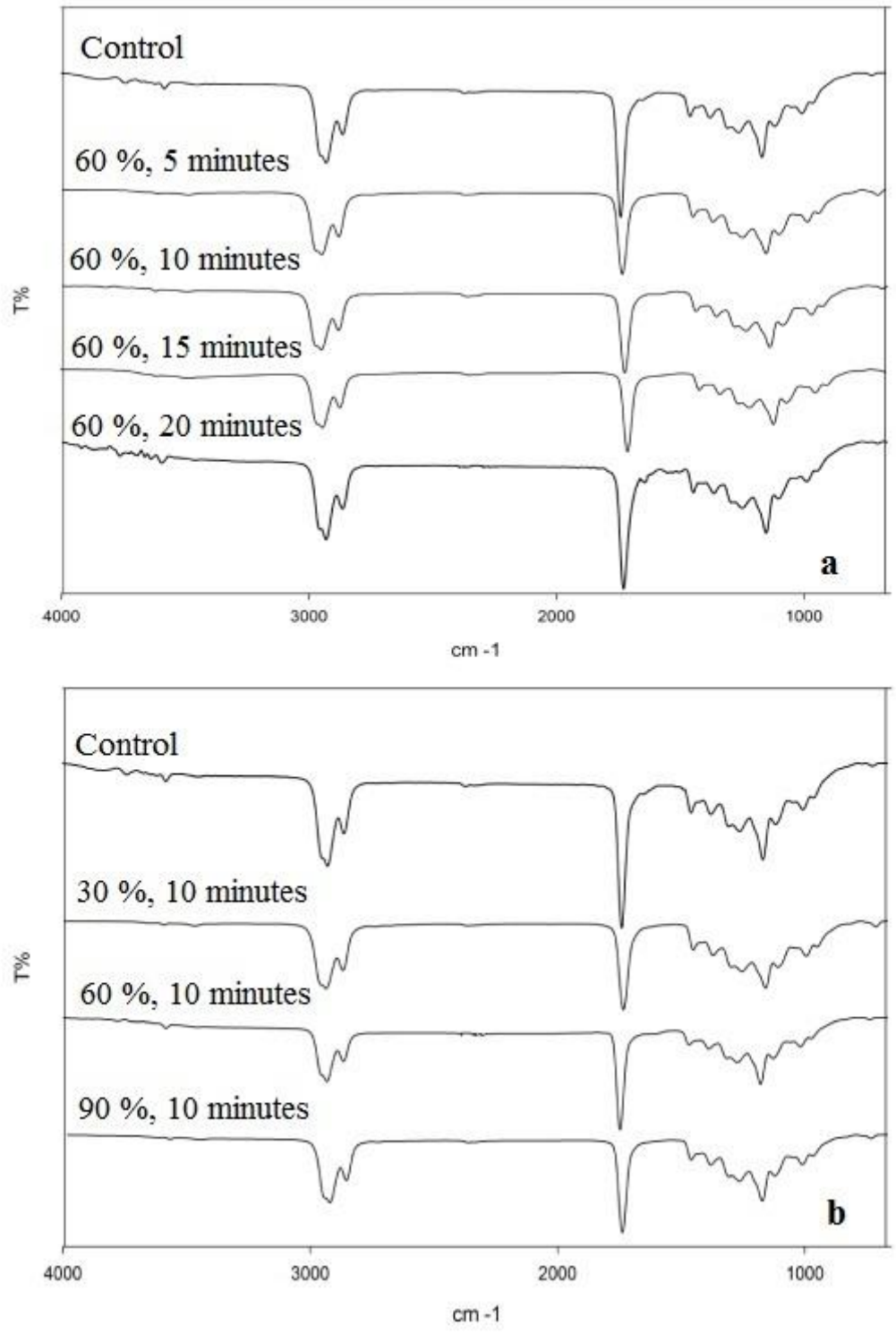

Figure 4.19: FTIR spectra of control PHA and ultrasound irradiated mcl-PHA for different (a) exposure time and (b) ultrasonic power output.

4.5.7 Mechanism of ultrasonic-mediated degradation of mcl-PHA

In this study, ultrasound irradiation is suggested to be responsible for the dehydration effects of terminal hydroxy group. A study on thermodegradation of oleic acid derived mcl-PHA (Chan Sin *et al.*, 2010), had reported that thermally degraded mcl-PHA will undergo dehydration of hydroxyl end group, producing alkenoic acid as secondary products. This effect is a consequence to the high temperature provided to the mcl-PHA oligomers. It is likely that similar effect may apply for ultrasonically degraded mcl-PHA, since they were exposed to the instant extreme high temperature resulted from implosion of cavitation bubbles in the sonicated solvent.

The ultrasonic mediated degradation process is likely to involve α-chain scission of the mcl-PHA polymer chains through eliminative ester cleavage. A proportion of the degradation products may additionally undergo dehydration of their terminal hydroxyl groups, which subsequently gives rise to more terminal unsaturation. Figure 4.20 shows the schematic diagram of the plausible chain cleavage mechanism in mcl-PHA polymers during ultrasonic mediated degradation process.

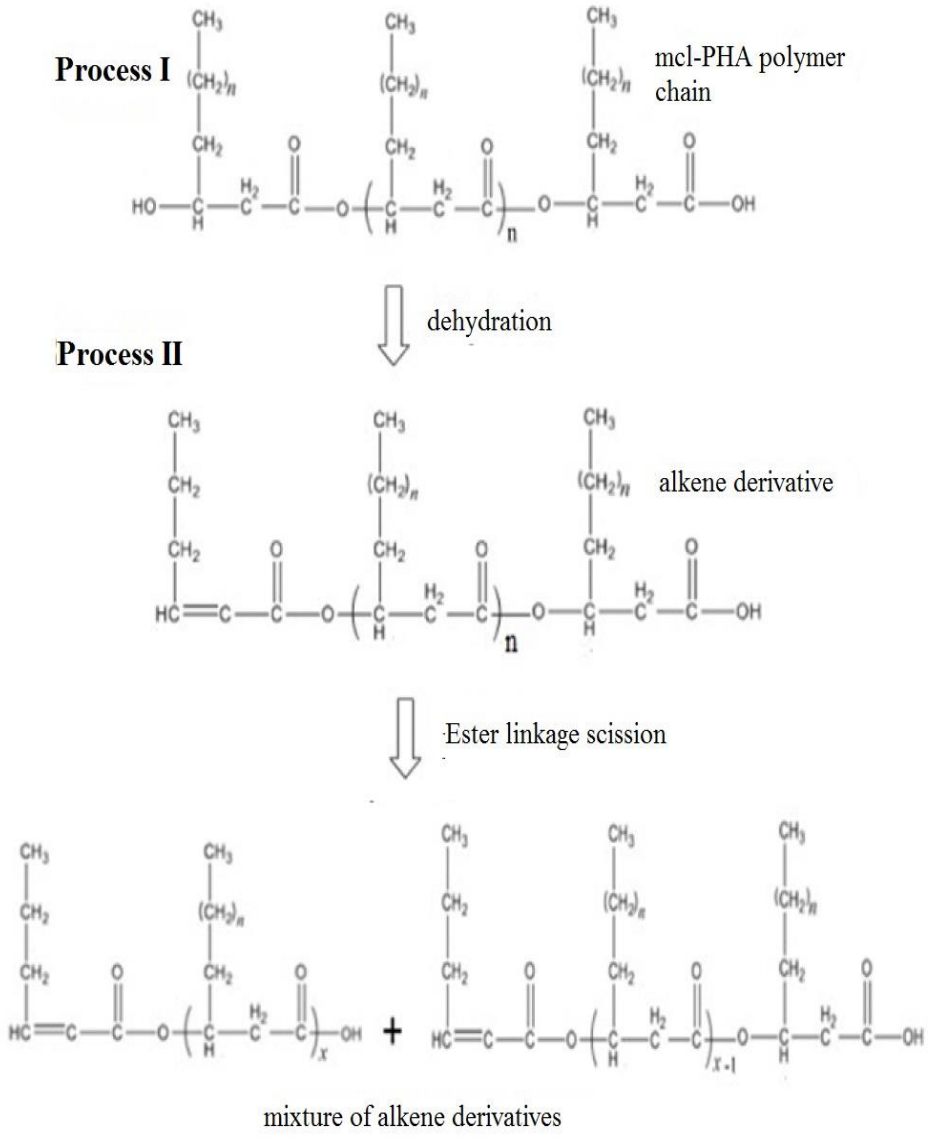

Figure 4.20: A plausible terminal hydroxyl group dehydration and main chain cleavage mechanism in mcl-PHA degradation during ultrasound irradiation. *Process I:* Plausible dehydration of hydroxyl end group. *Process II:* Random α- chain scission of the PHA ester bond.

4.6 Thermal properties and film morphology of neat PHA and its blend

4.6.1 DSC analysis of scl-mcl PHA blends

Figure 4.21 a (page 85) showed the enthalpy peak profile of neat PHAs and their blends upon heating at 10 °C min^{-1}. The T_g, T_c and T_m values obtained from the thermograms were summarized in Table 4.9.

Table 4.9: Thermal properties of scl/mcl PHA blends and neat polymers.

scl / mcl	T_g (°C)		T_c (°C)		T_m (°C)		T_{onset} (°C)	
PHA	**scl**	**mcl**	**scl**	**mcl**	**scl**	**mcl**	**scl**	**mcl**
100 / 0	0	-	34	-	162	-	219	-
25 / 75	-	-33	35	-	161	50	230	287
50 / 50	-	-38	35	-	159	51	225	292
75 / 25	-	-37	-	-	162	51	227	308
0 / 100	-	-36	-	-	-	52	-	253

Neat PHB (scl-PHA) showed an exothermic peak with a maximum at 34°C, related to the crystalline phase, while neat mcl-PHA did not show any sign of crystallization (Figure 4.21 a). This showed that, unlike PHB, octanoic acid derived mcl-PHA is not a semi-crystalline polymer. Blends containing 25 and 50 %wt of mcl-PHA also showed a main exothermic peak and a shoulder at a close temperature due to the crystallization of PHB. However, the crystallization peak of the blend with 50 % wt of mcl-PHA was relatively smaller and shifted to a slightly higher temperature (maximum at 35°C). This was probably due to the curtailment of crystallization process of the PHB by the predominant side-chain monomer (C_8) of the mcl-PHA, which domitaes the PHA with an abundance of ~ 89 %. This is also known as plasticizing effect. This effect became significant when the mcl-PHA content of the blend was

increased to 75 % wt, at which the crystallization peak almost disappears in the thermogram. All PHA blends showed an endothermic peak at around 160 °C, similar to neat PHB, indicating the melting of crystalline PHB. However, the endothermic peak of the blends are broader compared to the neat PHB. An exothermic peak close to the PHB melting peak for all blends, except 75 % wt mcl-PHA, was a strong indication of crystallization, thus indicating incomplete crystallization during the initial film formation. The heating scan for 25 % wt mcl-PHA blend showed a broad exothermic peak within the temperature range of 73 to 130 °C, probably due to residual crystallization and reorganization of PHB chains. This could be explained as follows: as the temperature increases, at 25 % wt blend the mcl-PHA side-chains were not able to fully curtail the PHB chains to order themselves in a thermodynamically favorable alignment, despite the side-chains becoming highly disorganized upon heating. Thus, PHB molecules would attempt to re-crystallize prior to them reaching the melting temperature.

Even though octanoic acid derived mcl-PHA did not show any exothermic peak for crystallization, it showed an endothermic peak at 52 °C, which indicated the existence of crystallites within the film. Unlike PHB chains that have a highly stereo-regular structure with little branching, polymer with longer side-chain monomers, like mcl-PHA, usually exhibit less tendency toward crystallization of the polymer backbone. However, due to strong intermolecular forces between the long and extended side chains, they may form crystalline domains there. From the results, octanoic acid derived mcl-PHA possesses a semicrystalline characteristic. Similar result was obtained with mcl-PHA produced by *P. putida* PGA1 grown in saponified palm kernel oil (SPKO) as sole carbon and energy source. These mcl-PHA showed a melting peak at 45 °C upon heating (Sin *et al.*, 2011). In contrast, oleic acid derived mcl-PHA did not show any evidence of crystallite melting (Chan Sin *et al.*, 2010). This was probably due to

unsaturated side chains, as the cis-configuration of natural double bonds provide "kinks" that hinder closer packing of the side chains. Similarly, homopolymers of poly-3-hydroxyhexanoate (PHHx) (Tripathi *et al.*, 2012) and poly-3-hydroxyheptanoate (PHHp) (Wang, H.-h. *et al.*, 2009) also did not exhibit a melting peak, eventhough their side chains are saturated. They are amorphous polymers, which liquify gradually over a broad temperature range above the glass transition temperature. Compared to the octanoic acid derived mcl-PHA that contained predominantly 3-hydroxyoctanoate side-chains, PHHx and PHHp consist of monomers with shorter carbon atom length side-chains. Hence, they exhibit a relatively weaker intermolecular interactions to form crystallites. This shows that side-chain crystalline behavior can be influenced by the saturation and length of hydrocarbon chains extended from the main polymer chain.

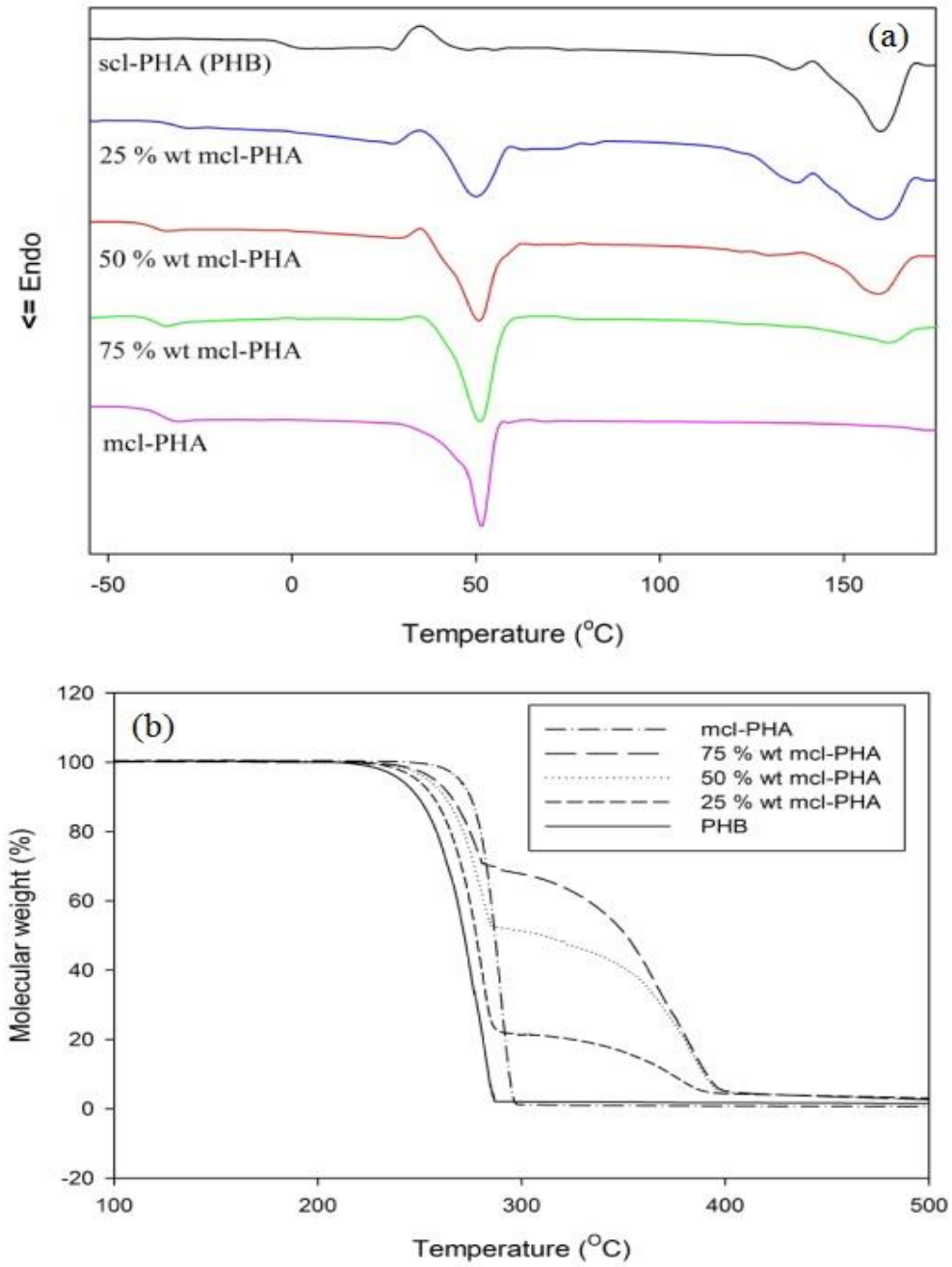

Figure 4.21: (a) DSC analysis - enthalpy peak profile of neat PHAs and their blends upon heating at 10 °C min^{-1} ; (b) Thermogravimetric curves of scl/mcl PHA blends and neat polymers.

4.6.2 Thermogravimetric analysis of scl-mcl PHA blends

From Figure 4.21 b, scl-PHA (PHB) and mcl-PHA degraded in a single stage decomposition. On the other hand, the blends showed a two-stage decomposition. The molecular weight percentage of each degradation step, determined from TGA curves was compared to the mass fraction of each polymer component in the blends. This analysis led to the conclusion that the first stage corresponds to the decomposition of scl-PHA (PHB) and the second stage to the decomposition of mcl-PHA. The temperature at the start of the degradation (T_{onset}) for each samples were summarized in Table 4.9. PHB degradation starts at 219 °C and mcl-PHA starts at 253 °C. T_{onset} of the PHB phase in the blends was significantly higher than the T_{onset} value for neat PHB. Similarly, a significant shift to higher temperature was observed for the mcl-PHA phase in the blends, in comparison with neat mcl-PHA.Thus, it can be concluded that the degradation of one blend component appears to affect the degradation behavior of the other component. This observation indicated that the existence of intermolecular interactions between scl-PHA (PHB) chains and mcl-PHA chains. Possible nature of interactions between the two different PHA chains is discussed in section 4.6.3.

4.6.3 Neat PHA and blend film morpholgy

Figure 4.22 showed the film surface morphology of scl-mcl PHA blends. From Figure 4.22 a, it is clear that the morphology of the film surfaces was affected by the scl-mcl PHA ratio. Neat scl-PHA (PHB) showed a pronounced opaqueness while neat mcl-PHA appeared as a translucent film layer. The opaqueness arose from scattering of light by the crystallites and it decreased as the mcl-PHA content was increased in the PHA blend film. This observation corresponded to the XRD analysis shown in Figure 4.23, where the peak intensity of PHB crystal decreased when the content of mcl-PHA in the blend was increased. This was attributed to reduced formation of PHB crystallites as the mcl-PHA longer side-chains would curtail the crystallization of scl-PHA.

However, XRD analysis of mcl-PHA did not show any intense peaks, which indicates the absence of crystallite in its neat film.

PHB film formed in this study was very brittle. The brittleness was suggested to be caused by the formation of voids at inter-spherulite regions as the polymer molecules undergo crystallization. From FESEM analysis, it is clear that PHB film possessed voids with 2-5 μm size (Figure 4.22 b). At the initial stage of crystallization, spherulite were formed followed by spherulite boundaries demarcating the uncrystallized amorphous material. Due to aging, the polymers in the inter-spherulite region will gradually crytallize and the density of the inter-spherulite region became reduced. This results in the formation of voids or cracks in the vicinity (Katsumata *et al.*, 2011).

Figure 4.22 c showed the FESEM image of the mcl-PHA film morphology. On the film surface, formation of white aggregates was observed.It is suggested that the melting peak obtained from DSC analysis was due to the melting of these white aggregates. Unlike PHB film which formed spherulite or crystallite from the whole main chain, mcl-PHA film is believed to form the observed white aggregates from the interactions among the long side-chains (Van der Walle *et al.*, 2001). However, this side-chain crystallization did not achieve the level of symmetrical order of a true crystal, hence the absence of evidence of exothermic peak on the DSC curve (Figure 4.21 a). This observation corresponded to the XRD analysis where there was no peak detected for mcl-PHA film indicating the absence of crystallites. Nevertheless, this aggregates act as physical cross-links to make the film stiffer unlike a gel-like structure of oleic acid derived mcl-PHA (Yasotha *et al.*, 2006). The elasticity and flexiblity of the mcl-PHA were attributed to the amorphous region of the film. This could be seen from Figure 4.22 c, where the shiny texture resembling a glass surface is thought to be the amorphous region. When stress is applied to the octanoic acid derived mcl-PHA, the

amorphous region would induce ductile deformation to accomodate the mechanical forces responsible for the shape change (Gagnon *et al.*, 1992).

Figures 4.22 (d, e and f) showed the film morphology of scl-mcl PHA blend at different ratios, as indicated. At 25 %wt of mcl-PHA content in the blend (Figure 4.22 d), no visible voids could be seen in the film. Addition of mcl-PHA might have restricted the molecular motion of PHB chains for further crystallization as the solvent was evaporated off and the polymer solution became more concentrated. However, when the blend film was heated to the melting temperatureof mcl-PHA during DSC analysis, PHB chains motion was no longer restricted and able to re-orient themselves into a crystalline morphology. Hence, the broad exothermic peak within the temperature range of 73 to 130 °C, probably indicating the further crystallization. Figure 4.22 e showed the surface morpholgy of 50 % wt mcl-PHA blend film. It can be seen that the arrangement of PHB crystallites were as if they were pushed and compressed to a narrow confined region to form a needle-like shaped crytallite. This may be due to the phase separation of the initially homegenous PHA solution to PHB and mcl-PHA rich solution phases during evaporation of the solvent. Next to the needle-like shaped region of PHB crystallite, the presence of white aggregates as observed in FESEM image of octanoic acid derived mcl-PHA film can be seen. The mcl-PHA could have been drawn to the crystallite boundary of PHB to form spherullites during film casting process. The drawing force is attributed to the interaction forces between the PHB crystallites and the mcl-PHA saturated side-chains. When the mcl-PHA was increased to 75 % wt (Figure 4.22 f), the domain size of needle-like shaped crytallites and white aggregates became narrower to about 10 μm. The frequency of occurrence of this domain became rather scarce which probably due to low concentration of PHB in the blend film.

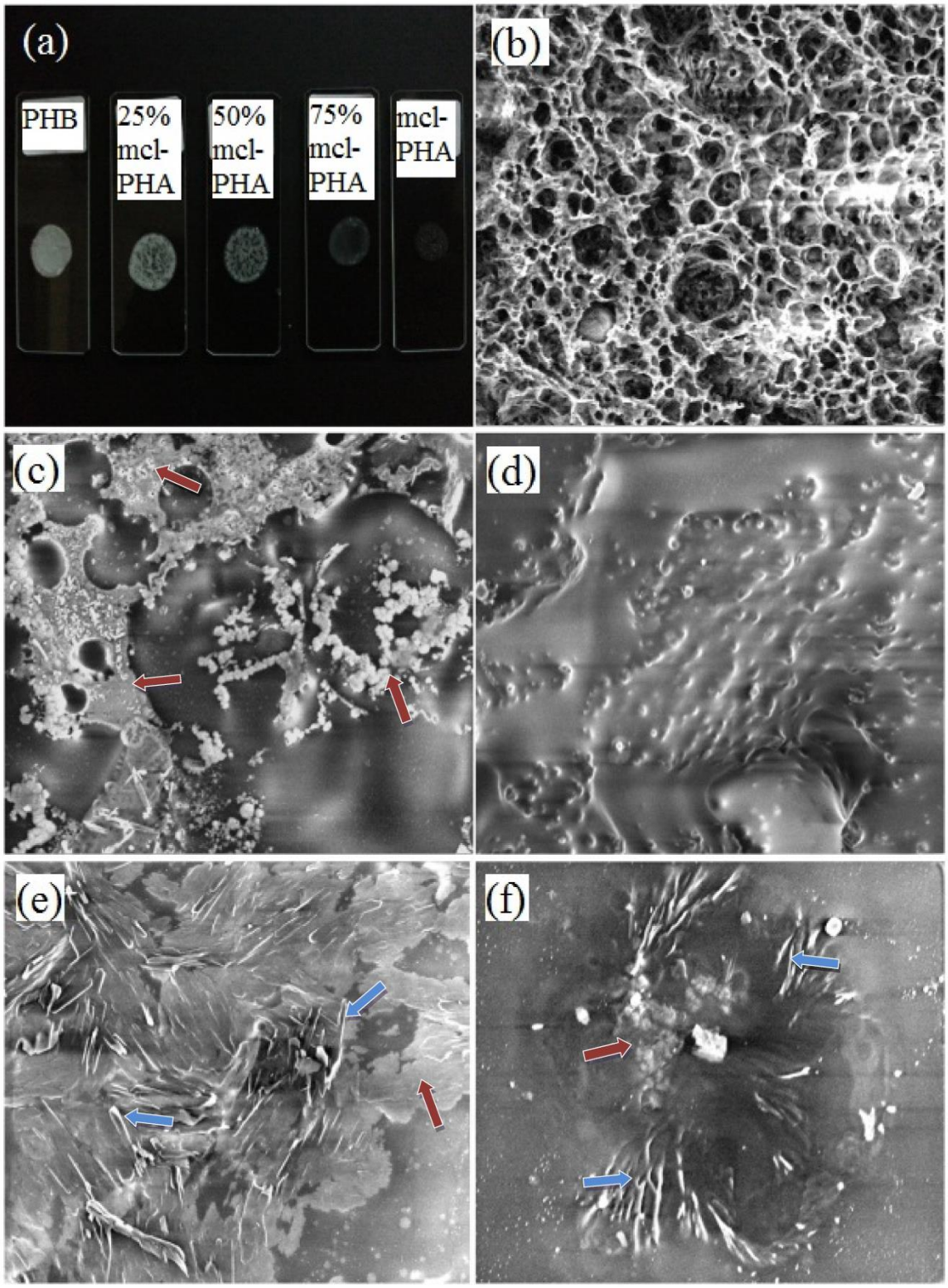

Figure 4.22: (a) Neat PHA and blend film; FESEM image of (b) neat PHB film (10000 X), (c) neat mcl-PHA film (10000 X), (d) 25 % wt mcl-PHA blend film (5000 X), (e) 50 % wt mcl-PHA blend film (5000 X) and (f) 75 % wt mcl-PHA blend film (10000 X). (red arrow: white aggregate, blue arrow: needle-like shaped crystallite).

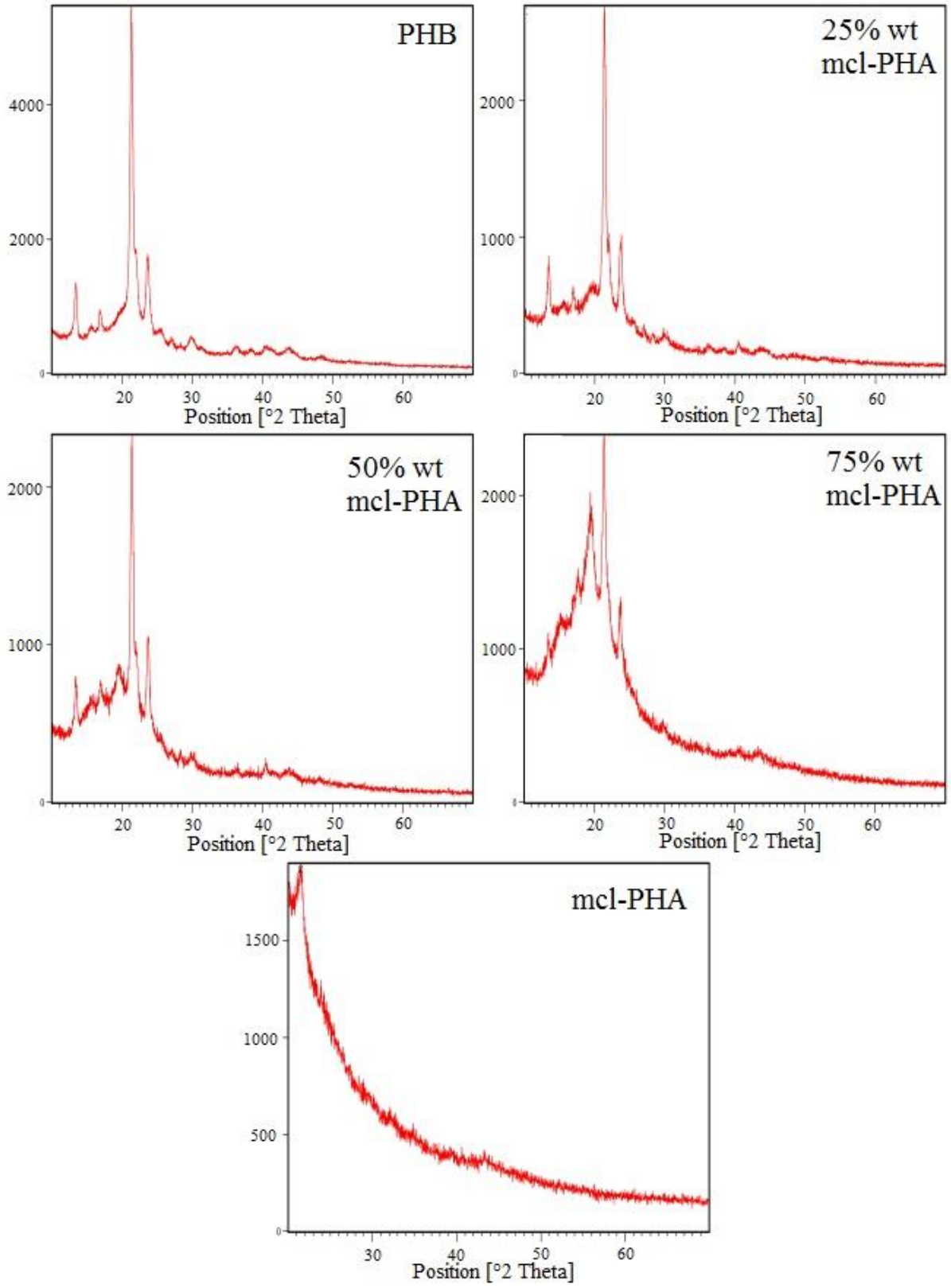

Figure 4.23: X ray diffraction (XRD) of scl/mcl PHA blends and neat polymers.

CHAPTER FIVE

5.0 CONCLUSIONS

Newly isolated *P. putida* Bet001 from palm oil mill effluent was able to produce mcl-PHA with 3-hydoxyoctanate as the major monomer from different fatty acids as carbon source. Octanoic acids (C8) was the best carbon source to obtain predominantly 3-hydroxyoctanoate based mcl- PHA.

Experimental data on ultrasound-assisted PHA extraction demonstrated the prospect of applying the technique for rapid PHA extraction in a multiphase system. The study also showed that mass transfer is the major limitation in the solvent extraction of intracellular PHA. The use of heptane as marginal non-solvent in the ultrasound-assisted system led to improved PHA extraction yields. Under optimal conditions, insignificant effects of ultrasound irradiation on post-extraction thermal properties, molecular weights and chemical structure of mcl–PHA were observed.

It can be concluded that mcl-PHA in acetone solution is quite stable (i.e. no significant degradation) when subjected to ultrasound irradiation within 1160 – 1185 J ml^{-1} power dissipation within an exposure ranging from 5 to 15 minutes. However, slightly but significant degradation of mcl-PHA was evident when the duration of exposure was prolonged to 20 minutes. It is expected that longer exposure results in a more extensive degradation mcl-PHA , consequently affecting thermal and physical properties of the mcl-PHA as well. Within a reasonable duration of exposure to ultrasound irradiation octanoic acid derived mcl-PHA, however, is quite stable. This is an important finding, since it suggests no practical limitations for the application of ultrasound technology in rapid extractions of mcl-PHA from bacterial biomass.

Degradation of the mcl-PHA was proposed to occur *via* cleavage of the ester linkages, resulting in monounsaturated polymer fragments. Extreme high temperature (and possibly extreme high shear force too) during ultrasound irradiation probably also

led to a dehydration of the terminal hydroxyl groups. This knowledge is important as it provides structural information of polymer fragments arising from ultrasound-assisted extraction of mcl-PHA, which may give rise to subsequent polymer modifications.

Mcl-PHA with 3-hydoxyoctanate as the major monomer was blended with PHB at different ratios. While the PHB/mcl-PHA blends were generally immiscible, the blend morphologies varied with the ratio. Crystallization and thermal properties of these polymer blends depend on the ratio of blend components.The macroscopic changes observed were explained and correlated with the chemical structure of both blend components. The explanation given may provide insights into the relationship between bulk behavior of the blended polymer and its chemical basis, and this could be extended to other similar blend systems.

BIBLIOGRAPHY

Alata, H., Aoyama, T., & Inoue, Y. (2007). Effect of aging on the mechanical properties of poly (3-hydroxybutyrate-co-3-hydroxyhexanoate). *Macromolecules, 40*(13), 4546-4551.

Ariffin, H., Nishida, H., Shirai, Y., & Hassan, M.A. (2008). Determination of multiple thermal degradation mechanisms of poly (3-hydroxybutyrate). *Polymer Degradation and Stability, 93*(8), 1433-1439.

Ballistreri, A., Giuffrida, M., Guglielmino, S.P., Carnazza, S., Ferreri, A., & Impallomeni, G. (2001). Biosynthesis and structural characterization of medium-chain-length poly (3-hydroxyalkanoates) produced by *Pseudomonas aeruginosa* from fatty acids. *International Journal of Biological Macromolecules, 29*(2), 107-114.

Boyandin, A.N., Prudnikova, S.V., Filipenko, M.L., Khrapov, E.A., Vasil'ev, A.D., & Volova, T.G. (2012). Biodegradation of polyhydroxyalkanoates by soil microbial communities of different structures and detection of PHA degrading microorganisms. *Applied Biochemistry and Microbiology, 48*(1), 28-36.

Braunegg, G., Lefebvre, G., & Genser, K.F. (1998). Polyhydroxyalkanoates, biopolyesters from renewable resources: Physiological and engineering aspects. *Journal of Biotechnology, 65*(2–3), 127-161.

Braunegg, G., Sonnleitner, B., & Lafferty, R. (1978). A rapid gas chromatographic method for the determination of Poly-*β*-hydroxybutyric acid in microbial biomass. *European Journal of Applied Microbiology and Biotechnology, 6*(1), 29-37.

Brennen, C.E. (1995). *Cavitation and Bubble Dynamics*: Oxford University Press.

Budde, C.F., Riedel, S.L., Willis, L.B., Rha, C., & Sinskey, A.J. (2011). Production of poly(3-hydroxybutyrate-*co*-3-hydroxyhexanoate) from plant oil by engineered *Ralstonia eutropha* strains. *Applied and Environmental Microbiology, 77*(9), 2847-2854.

Burdon, K.L. (1946). Fatty material in bacteria and fungi revealed by staining dried, fixed slide preparations. *Journal of Bacteriology, 52*(6), 665.

Carlson, R., Wlaschin, A., & Srienc, F. (2005). Kinetic studies and biochemical pathway analysis of anaerobic poly-(*r*)-3-hydroxybutyric acid synthesis in *Escherichia coli*. *Applied and Environmental Microbiology, 71*(2), 713-720.

Chan Sin, M., Gan, S.N., Mohd Annuar, M.S., & Ping Tan, I.K. (2010). Thermodegradation of medium-chain-length poly (3-hydroxyalkanoates) produced by *Pseudomonas putida* from oleic acid. *Polymer Degradation and Stability, 95*(12), 2334-2342.

Chen, G.-Q. (2009). A microbial polyhydroxyalkanoates (PHA) based bio- and materials industry. *Chemical Society Reviews, 38*(8), 2434-2446.

Chen, G.-Q., & Wu, Q. (2005a). The application of polyhydroxyalkanoates as tissue engineering materials. *Biomaterials, 26*(33), 6565-6578.

Chen, G.-Q., & Wu, Q. (2005b). Microbial production and applications of chiral hydroxyalkanoates. *Applied Microbiology and Biotechnology, 67*(5), 592-599.

Chen, X., Wang, W., Li, S., Xue, J., Fan, L., Sheng, Z., & Chen, Y. (2010). Optimization of ultrasound-assisted extraction of lingzhi polysaccharides using response surface methodology and its inhibitory effect on cervical cancer cells. *Carbohydrate Polymers, 80*(3), 944-948.

Cheng, S., Chen, G.-Q., Leski, M., Zou, B., Wang, Y., & Wu, Q. (2006). The effect of *d*,l-*β*-hydroxybutyric acid on cell death and proliferation in l929 cells. *Biomaterials, 27*(20), 3758-3765.

De Smet, M., Eggink, G., Witholt, B., Kingma, J., & Wynberg, H. (1983). Characterization of intracellular inclusions formed by *Pseudomonas oleovorans* during growth on octane. *Journal of Bacteriology, 154*(2), 870-878.

Deanin, R.D. (1972). *Polymer structure, properties, and applications*: Cahners Books.

Divyashree, M.S., Shamala, T.R., & Rastogi, N.K. (2009). Isolation of polyhydroxyalkanoate from hydrolyzed cells of *Bacillus flexus* using aqueous two-phase system containing polyethylene glycol and phosphate. *Biotechnology and Bioprocess Engineering, 14*(4), 482-489.

Do Young Kim, H.W.K., Chung, M.G., & Rhee, Y.H. (2007). Biosynthesis, modification, and biodegradation of bacterial medium-chain-length polyhydroxyalkanoates. *The Journal of Microbiology*, 87-97.

Dong, C.-H., Xie, X.-Q., Wang, X.-L., Zhan, Y., & Yao, Y.-J. (2009). Application of box-behnken design in optimisation for polysaccharides extraction from cultured mycelium of *Cordyceps sinensis*. *Food and Bioproducts Processing, 87*(2), 139-144.

Doyle, C. (1961). Kinetic analysis of thermogravimetric data. *Journal of Applied Polymer Science, 5*(15), 285-292.

Eggink, G., van der Wal, H., Huijberts, G.N., & de Waard, P. (1992). Oleic acid as a substrate for poly-3-hydroxyalkanoate formation in *Alcaligenes eutrophus* and *Pseudomonas putida*. *Industrial Crops and Products, 1*(2), 157-163.

Erceg, M., Kovačić, T., & Klarić, I. (2005). Dynamic thermogravimetric degradation of poly(3-hydroxybutyrate)/aliphatic–aromatic copolyester blends. *Polymer Degradation and Stability, 90*(1), 86-94.

Ferreira, S.C., Bruns, R., Ferreira, H., Matos, G., David, J., Brandão, G., Souza, A. (2007). Box-behnken design: An alternative for the optimization of analytical methods. *Analytica Chimica Acta, 597*(2), 179-186.

Gagnon, K., Lenz, R., Farris, R., & Fuller, R. (1992). The mechanical properties of a thermoplastic elastomer produced by the bacterium *Pseudomonas oleovorans*. *Rubber Chemistry and Technology, 65*(4), 761-777.

Gao, X., Chen, J.-C., Wu, Q., & Chen, G.-Q. (2011). Polyhydroxyalkanoates as a source of chemicals, polymers, and biofuels. *Current Opinion in Biotechnology, 22*(6), 768-774.

Ghatnekar, M.S., Pai, J.S., & Ganesh, M. (2002). Production and recovery of poly-3-hydroxybutyrate from *Methylobacterium* sp. v49. *Journal of Chemical Technology and Biotechnology, 77*(4), 444-448.

Goyat, M., Ray, S., & Ghosh, P. (2011). Innovative application of ultrasonic mixing to produce homogeneously mixed nanoparticulate-epoxy composite of improved physical properties. *Composites Part A: Applied Science and Manufacturing, 42*(10), 1421-1431.

Gross, R.A., DeMello, C., Lenz, R.W., Brandl, H., & Fuller, R.C. (1989). The biosynthesis and characterization of poly (*β*-hydroxyalkanoates) produced by *Pseudomonas oleovorans*. *Macromolecules, 22*(3), 1106-1115.

Gumel, A., Annuar, M., & Chisti, Y. (2012). Lipase catalyzed ultrasonic synthesis of poly-4-hydroxybutyrate-*co*-6-hydroxyhexanoate. *Ultrasonics Sonochemistry, 20*(3), 937-947.

Gumel, A., Annuar, M., Chisti, Y., & Heidelberg, T. (2012). Ultrasound assisted lipase catalyzed synthesis of poly-6-hydroxyhexanoate. *Ultrasonics Sonochemistry, 19*(3), 659-667.

Gumel, A.M., Annuar, M.S.M., & Heidelberg, T. (2012). Biosynthesis and characterization of polyhydroxyalkanoates copolymers produced by *Pseudomonas putida* bet001 isolated from palm oil mill effluent. *PLoS One, 7*(9), e45214.

Guo, W., Duan, J., Geng, W., Feng, J., Wang, S., & Song, C. (2012). Comparison of medium-chain-length polyhydroxyalkanoates synthases from *Pseudomonas mendocina* nk-01 with the same substrate specificity. *Microbiological Research*.

Hejazi, P., Vasheghani-Farahani, E., & Yamini, Y. (2003). Supercritical fluid disruption of *Ralstonia eutropha* for poly (*β*-hydroxybutyrate) recovery. *Biotechnology Progress, 19*(5), 1519-1523.

Huijberts, G., de Rijk, T.C., de Waard, P., & Eggink, G. (1994). 13c nuclear magnetic resonance studies of *Pseudomonas putida* fatty acid metabolic routes involved in poly (3-hydroxyalkanoate) synthesis. *Journal of Bacteriology, 176*(6), 1661-1666.

Huijberts, G.N., van der Wal, H., Wilkinson, C., & Eggink, G. (1994). Gas-chromatographic analysis of poly (3-hydroxyalkanoates) in bacteria. *Biotechnology Techniques, 8*(3), 187-192.

Huisman, G.W., de Leeuw, O., Eggink, G., & Witholt, B. (1989). Synthesis of poly-3-hydroxyalkanoates is a common feature of fluorescent pseudomonads. *Applied and Environmental Microbiology, 55*(8), 1949-1954.

Huisman, G.W., Wonink, E., Meima, R., Kazemier, B., Terpstra, P., & Witholt, B. (1991). Metabolism of poly(3-hydroxyalkanoates) (PHAs) by *Pseudomonas oleovorans.* Identification and sequences of genes and function of the encoded proteins in the synthesis and degradation of PHA. *Journal of Biological Chemistry, 266*(4), 2191-2198.

Isayev, A., & Hong, C.K. (2003). Novel ultrasonic process for in-situ copolymer formation and compatibilization of immiscible polymers. *Polymer Engineering & Science, 43*(1), 91-101.

Jiang, X., Ramsay, J.A., & Ramsay, B.A. (2006). Acetone extraction of mcl-PHA from *Pseudomonas putida* kt2440. *Journal of Microbiological Methods, 67*(2), 212-219.

Kapritchkoff, F.M., Viotti, A.P., Alli, R.C., Zuccolo, M., Pradella, J.G., Maiorano, A.E., Bonomi, A. (2006). Enzymatic recovery and purification of polyhydroxybutyrate produced by *Ralstonia eutropha*. *Journal of Biotechnology*, *122*(4), 453-462.

Kathiraser, Y., Aroua, M.K., Ramachandran, K.B., & Tan, I.K.P. (2007). Chemical characterization of medium-chain-length polyhydroxyalkanoates (PHAs) recovered by enzymatic treatment and ultrafiltration. *Journal of Chemical Technology & Biotechnology, 82*(9), 847-855.

Katsumata, K., Saito, T., Yu, F., Nakamura, N., & Inoue, Y. (2011). The toughening effect of a small amount of poly (*e*-caprolactone) on the mechanical properties of the poly (3-hydroxybutyrate-co-3-hydroxyhexanoate)/pcl blend. *Polymer Journal, 43*(5), 484-492.

Kendall, G. (2013, June 25). What is Pharmaceutical Nanoemulsion? [Blog Post] Retrieved from https://blogs.nottingham.ac.uk/malaysiaknowledgetransfer/2013/06/25/what-is-pharmaceutical-nanoemulsion/

Koda, S., Kimura, T., Kondo, T., & Mitome, H. (2003). A standard method to calibrate sonochemical efficiency of an individual reaction system. *Ultrasonics Sonochemistry, 10*(3), 149-156.

Koda, S., Mori, H., Matsumoto, K., & Nomura, H. (1994). Ultrasonic degradation of water-soluble polymers. *Polymer, 35*(1), 30-33.

Koning, G.d. (1995). Physical properties of bacterial poly ((*r*)-3-hydroxyalkanoates). *Canadian Journal of Microbiology, 41*(13), 303-309.

Kunasundari, B., & Sudesh, K. (2011). Isolation and recovery of microbial polyhydroxyalkanoates. *Express Polymer Letters, 5*, 620-634.

Kurdikar, D.L., Strauser, F.E., Solodar, A.J., & Paster, M.D. (2000). High temperature PHA extraction using PHA-poor solvents: U.S. Patent 6,087,471 (2000).

Lageveen, R.G., Huisman, G.W., Preusting, H., Ketelaar, P., Eggink, G., & Witholt, B. (1988). Formation of polyesters by *Pseudomonas oleovorans*: Effect of substrates on formation and composition of poly-(*r*)-3-hydroxyalkanoates and poly-(*r*)-3-hydroxyalkenoates. *Applied and Environmental Microbiology, 54*(12), 2924-2932.

Lee, J.Y., Choi, H.K., Shim, M.J., & Kim, S.W. (1997). Estimation of cure rate for dgeba/mda/pge-acam system by Kissinger expression. *Applied Chemistry, 1*(2), 714e717.

Li, S.D., Yu, P.H., & Cheung, M.K. (2001). Thermogravimetric analysis of poly (3-hydroxybutyrate) and poly (3-hydroxybutyrate-co-3-hydroxyvalerate). *Journal of Applied Polymer Science, 80*(12), 2237-2244.

Li, X., Wang, Z., Wang, L., Walid, E., & Zhang, H. (2012). Ultrasonic-assisted extraction of polysaccharides from *Hohenbuehelia serotina* by response surface methodology. *International Journal of Biological Macromolecules, 51*(4), 523-530.

Martin, D.P., & Williams, S.F. (2003). Medical applications of poly-4-hydroxybutyrate: A strong flexible absorbable biomaterial. *Biochemical Engineering Journal, 16*(2), 97-105.

Massieu, L., Haces, M.L., Montiel, T., & Hernández-Fonseca, K. (2003). Acetoacetate protects hippocampal neurons against glutamate-mediated neuronal damage during glycolysis inhibition. *Neuroscience, 120*(2), 365-378.

Mergaert, J., & Swings, J. (1996). Biodiversity of microorganisms that degrade bacterial and synthetic polyesters. *Journal of Industrial Microbiology, 17*(5-6), 463-469.

Miller, M.L. (1966). *The structure of polymers* (Vol. 10): Reinhold New York.

Monnier, H., Wilhelm, A.-M., & Delmas, H. (1999). Influence of ultrasound on mixing on the molecular scale for water and viscous liquids. *Ultrasonics Sonochemistry, 6*(1), 67-74.

Mukai, K., Doi, Y., Sema, Y., & Tomita, K. (1993). Substrate specificities in hydrolysis of polyhydroxyalkanoates by microbial esterases. *Biotechnology Letters, 15*(6), 601-604.

Nair, R., Thomas, G.V., & Gopinathan Nair, M. (2007). Thermogravimetric analysis of pvc/elnr blends. *Polymer Degradation and Stability, 92*(2), 189-196.

Noda, I. (1998). Solvent extraction of polyhydroxyalkanoates from biomass facilitated by the use of marginal nonsolvent: U.S. Patent 5,821,299 (1998).

Page, W.J., & Cornish, A. (1993). Growth of *Azotobacter vinelandii* uwd in fish peptone medium and simplified extraction of poly-*β*-hydroxybutyrate. *Applied and Environmental Microbiology, 59*(12), 4236-4244.

Philip, S., Keshavarz, T., & Roy, I. (2007). Polyhydroxyalkanoates: Biodegradable polymers with a range of applications. *Journal of Chemical Technology and Biotechnology, 82*(3), 233-247.

Price, G.J. (1996). Ultrasonically enhanced polymer synthesis. *Ultrasonics Sonochemistry, 3*(3), S229-S238.

Price, G.J., & Smith, P.F. (1993). Ultrasonic degradation of polymer solutions—iii. The effect of changing solvent and solution concentration. *European Polymer Journal, 29*(2), 419-424.

Qiu, Z., Ikehara, T., & Nishi, T. (2003). Poly (hydroxybutyrate)/poly (butylene succinate) blends: Miscibility and nonisothermal crystallization. *Polymer, 44*(8), 2503-2508.

Qu, X.-H., Wu, Q., Liang, J., Qu, X., Wang, S.-G., & Chen, G.-Q. (2005). Enhanced vascular-related cellular affinity on surface modified copolyesters of 3-hydroxybutyrate and 3-hydroxyhexanoate (PHBHHX). *Biomaterials, 26*(34), 6991-7001.

Ramier, J., Grande, D., Langlois, V., & Renard, E. (2012). Toward the controlled production of oligoesters by microwave-assisted degradation of poly (3-hydroxyalkanoate)s. *Polymer Degradation and Stability, 97*(3), 322-328.

Reich, G. (1998). Ultrasound-induced degradation of PLA and PLGA during microsphere processing: Influence of formulation variables. *European Journal of Pharmaceutics and Biopharmaceutics, 45*(2), 165-171.

Reis, K., Pereira, J., Smith, A., Carvalho, C., Wellner, N., & Yakimets, I. (2008). Characterization of polyhydroxybutyrate-hydroxyvalerate (PHB-HV)/maize starch blend films. *Journal of Food Engineering, 89*(4), 361-369.

Renard, E., Walls, M., Guérin, P., & Langlois, V. (2004). Hydrolytic degradation of blends of polyhydroxyalkanoates and functionalized polyhydroxyalkanoates. *Polymer Degradation and Stability, 85*(2), 779-787.

Schultz, J. (1984). Microstructural aspects of failure in semicrystalline polymers. *Polymer Engineering & Science, 24*(10), 770-785.

Shishatskaya, E.I., Khlusov, I.A., & Volova, T.G. (2006). A hybrid PHB–hydroxyapatite composite for biomedical application: Production, *in vitro* and *in vivo* investigation. *Journal of Biomaterials Science, Polymer Edition, 17*(5), 481-498.

Sin, M.C., Tan, I.K.P., Annuar, M.S.M., & Gan, S.N. (2011). Characterization of oligomeric hydroxyalkanoic acids from thermal decomposition of palm kernel oil–based biopolyester. *International Journal of Polymer Analysis and Characterization, 16*(5), 337-347.

Sin, M.C., Tan, I.K.P., Annuar, M.S.M., & Gan, S.N. (2013). Kinetics of thermodegradation of palm kernel oil derived medium-chain-length polyhydroxyalkanoates. *Journal of Applied Polymer Science, 127*(6), 4422-4425.

Solaiman, D.K., Ashby, R.D., Hotchkiss Jr, A.T., & Foglia, T.A. (2006). Biosynthesis of medium-chain-length poly (hydroxyalkanoates) from soy molasses. *Biotechnology Letters, 28*(3), 157-162.

Stevens, M.P. (1990). *Polymer chemistry* (Vol. 2): Oxford University Press New York.

Sudesh, K., Abe, H., & Doi, Y. (2000). Synthesis, structure and properties of polyhydroxyalkanoates: Biological polyesters. *Progress in Polymer Science, 25*(10), 1503-1555.

Sun, J., Dai, Z., & Chen, G. (2007). Oligomers of polyhydroxyalkanoates stimulated calcium ion channels in mammalian cells. *Biomaterials, 28*, 3896-3903.

Suslick, K.S., & Nyborg, W.L. (1990). Ultrasound: Its chemical, physical and biological effects. *The Journal of the Acoustical Society of America, 87*(2), 919-920.

Suslick, K.S., & Price, G.J. (1999). Applications of ultrasound to materials chemistry. *Annual Review of Materials Science, 29*(1), 295-326.

Tamer, I.M., Moo-Young, M., & Chisti, Y. (1998). Disruption of *Alcaligenes latus* for recovery of poly(*β*-hydroxybutyric acid): Comparison of high-pressure homogenization, bead milling, and chemically induced lysis. *Industrial & Engineering Chemistry Research, 37*(5), 1807-1814.

Tan, I., Kumar, K.S., Theanmalar, M., Gan, S., & Gordon Iii, B. (1997). Saponified palm kernel oil and its major free fatty acids as carbon substrates for the production of polyhydroxyalkanoates in *Pseudomonas putida* pga1. *Applied Microbiology and Biotechnology, 47*(3), 207-211.

Tripathi, L., Wu, L.-P., Chen, J., & Chen, G.-Q. (2012). Synthesis of diblock copolymer poly-3-hydroxybutyrate -block-poly-3-hydroxyhexanoate [PHB-b-PHHx] by a *β*-oxidation weakened *Pseudomonas putida* kt2442. *Microbial Cell Factories, 11*(1), 1-11.

Van der Walle, G., De Koning, G., Weusthuis, R., & Eggink, G. (2001). Properties, modifications and applications of biopolyesters. *Biopolyesters* (pp. 263-291): Springer.

Wang, F., & Lee, S.Y. (1997). Production of poly (3-hydroxybutyrate) by fed-batch culture of filamentation-suppressed recombinant *Escherichia coli. Applied and Environmental Microbiology, 63*(12), 4765-4769.

Wang, H.-h., Li, X.-t., & Chen, G.-Q. (2009). Production and characterization of homopolymer polyhydroxyheptanoate (P3HHp) by a *fadba* knockout mutant *Pseudomonas putida* ktoy06 derived from *P. putida* kt2442. *Process Biochemistry, 44*(1), 106-111.

Wang, Y., Bian, Y.-Z., Wu, Q., & Chen, G.-Q. (2008). Evaluation of three-dimensional scaffolds prepared from poly(3-hydroxybutyrate-*co*-3-hydroxyhexanoate) for growth of *Allogeneic chondrocytes* for cartilage repair in rabbits. *Biomaterials, 29*(19), 2858-2868.

Wang, Z., Itoh, Y., Hosaka, Y., Kobayashi, I., Nakano, Y., Maeda, I., Yag, K. (2003). Novel transdermal drug delivery system with polyhydroxyalkanoate and starburst polyamidoamine dendrimer. *Journal of Bioscience and Bioengineering, 95*(5), 541-543.

Wang, Z., Itoh, Y., Hosaka, Y., Kobayashi, I., Nakano, Y., Maeda, I., Suenobu, T. (2003). Mechanism of enhancement effect of dendrimer on transdermal drug permeation through polyhydroxyalkanoate matrix. *Journal of Bioscience and Bioengineering, 96*(6), 537-540.

Xue, L., & Greisler, H.P. (2003). Biomaterials in the development and future of vascular grafts. *Journal of Vascular Surgery, 37*(2), 472-480.

Yang, Y.H., Brigham, C.J., Song, E., Jeon, J.M., Rha, C.K., & Sinskey, A.J. (2012). Biosynthesis of poly(3-hydroxybutyrate-*co*-3-hydroxyvalerate) containing a predominant amount of 3-hydroxyvalerate by engineered *Escherichia coli* expressing propionate-coa transferase. *Journal of Applied Microbiology, 113*(4), 815-823.

Yasotha, K., Aroua, M., Ramachandran, K., & Tan, I. (2006). Recovery of medium-chain-length polyhydroxyalkanoates (PHAs) through enzymatic digestion treatments and ultrafiltration. *Biochemical Engineering Journal, 30*(3), 260-268.

Ying, Z., Han, X., & Li, J. (2011). Ultrasound-assisted extraction of polysaccharides from mulberry leaves. *Food Chemistry, 127*(3), 1273-1279.

Yu, J., Plackett, D., & Chen, L.X. (2005). Kinetics and mechanism of the monomeric products from abiotic hydrolysis of poly [(*r*)-3-hydroxybutyrate] under acidic and alkaline conditions. *Polymer Degradation and Stability, 89*(2), 289-299.

Zhong, K., & Wang, Q. (2010). Optimization of ultrasonic extraction of polysaccharides from dried longan pulp using response surface methodology. *Carbohydrate Polymers, 80*(1), 19-25.

APPENDIX A

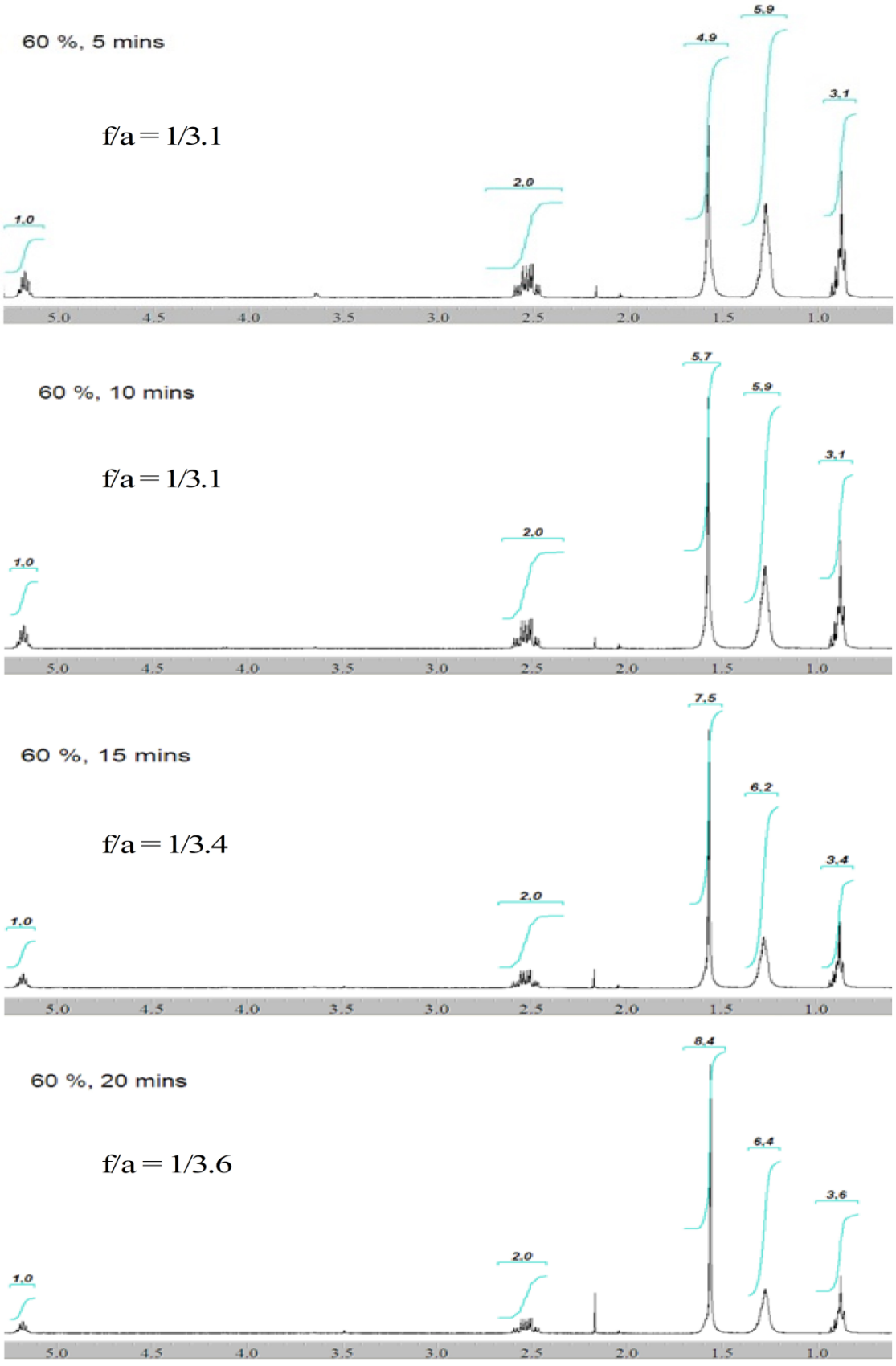
60 %, 5 mins
f/a = 1/3.1
1.0
2.0
4.9
5.9
3.1
5.0 4.5 4.0 3.5 3.0 2.5 2.0 1.5 1.0
60 %, 10 mins
f/a = 1/3.1
1.0
2.0
5.7
5.9
3.1
5.0 4.5 4.0 3.5 3.0 2.5 2.0 1.5 1.0
60 %, 15 mins
f/a = 1/3.4
1.0
2.0
7.5
6.2
3.4
5.0 4.5 4.0 3.5 3.0 2.5 2.0 1.5 1.0
60 %, 20 mins
f/a = 1/3.6
1.0
2.0
8.4
6.4
3.6
5.0 4.5 4.0 3.5 3.0 2.5 2.0 1.5 1.0

APPENDIX B

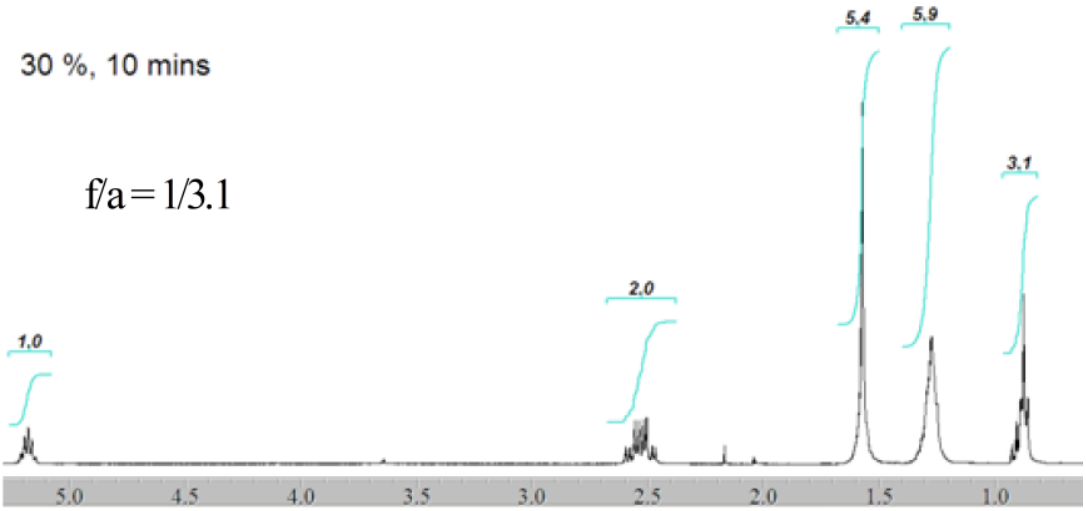
30 %, 10 mins
f/a = 1/3.1
1.0
2.0
5.4
5.9
3.1
5.0
4.5
4.0
3.5
3.0
2.5
2.0
1.5
1.0

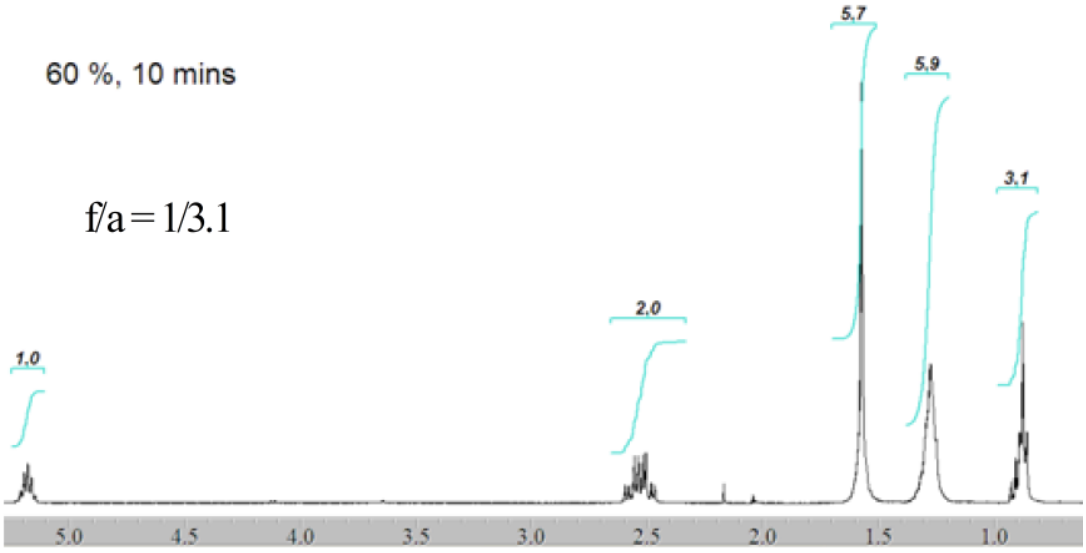
60 %, 10 mins
f/a = 1/3.1
1.0
2.0
5.7
5.9
3.1
5.0
4.5
4.0
3.5
3.0
2.5
2.0
1.5
1.0

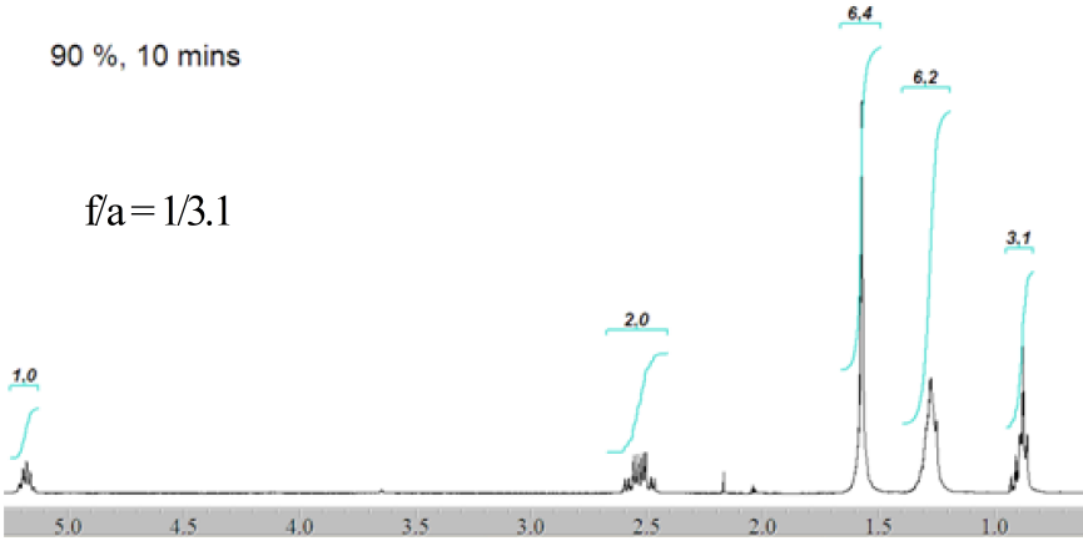
90 %, 10 mins
f/a = 1/3.1
1.0
2.0
6.4
6.2
3.1
5.0
4.5
4.0
3.5
3.0
2.5
2.0
1.5
1.0

APPENDIX C

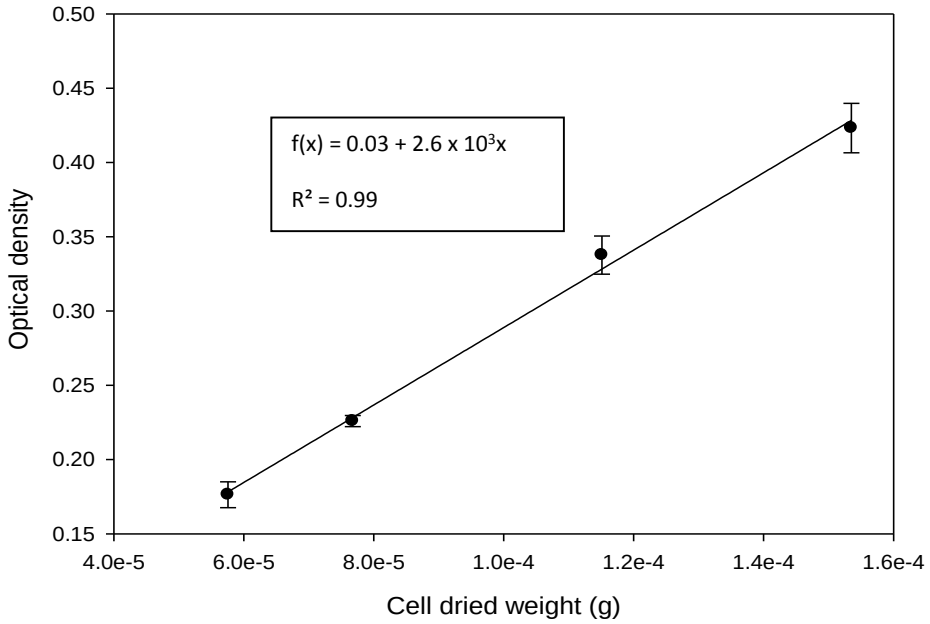
0.50
0.45
0.40
0.35
0.30
0.25
0.20
0.15
Optical density
f(x) = 0.03 + 2.6 x 10³x
R² = 0.99
4.0e-5
6.0e-5
8.0e-5
1.0e-4
1.2e-4
1.4e-4
1.6e-4
Cell dried weight (g)

APPENDIX D

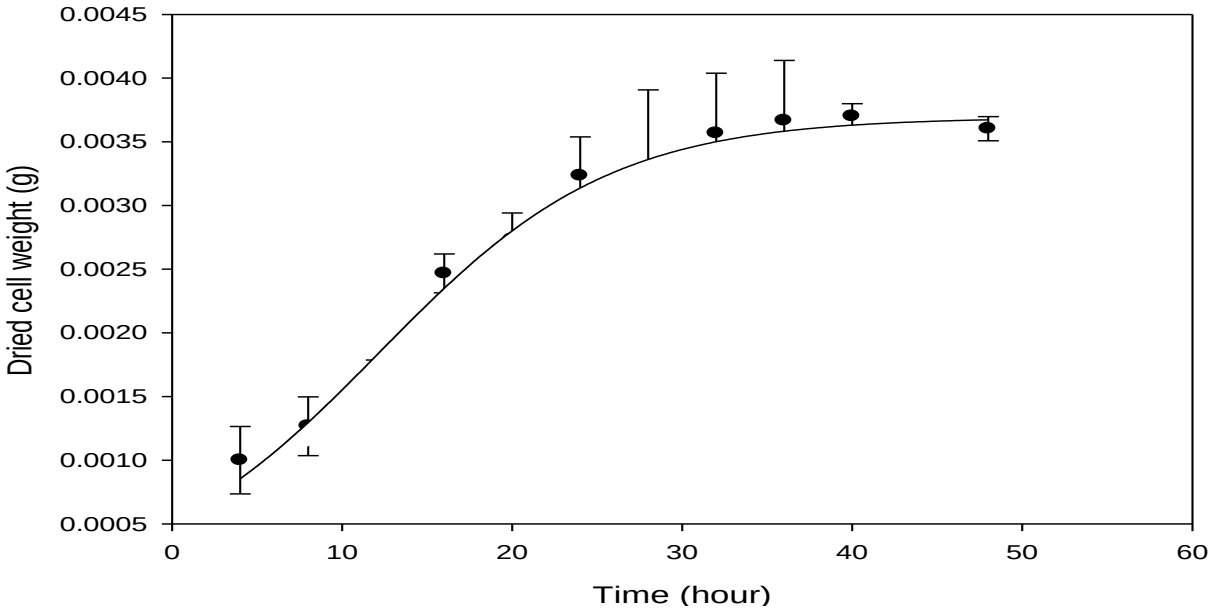
Dried cell weight (g)
0.0045
0.0040
0.0035
0.0030
0.0025
0.0020
0.0015
0.0010
0.0005
0
10
20
30
40
50
60
Time (hour)

APPENDIX E

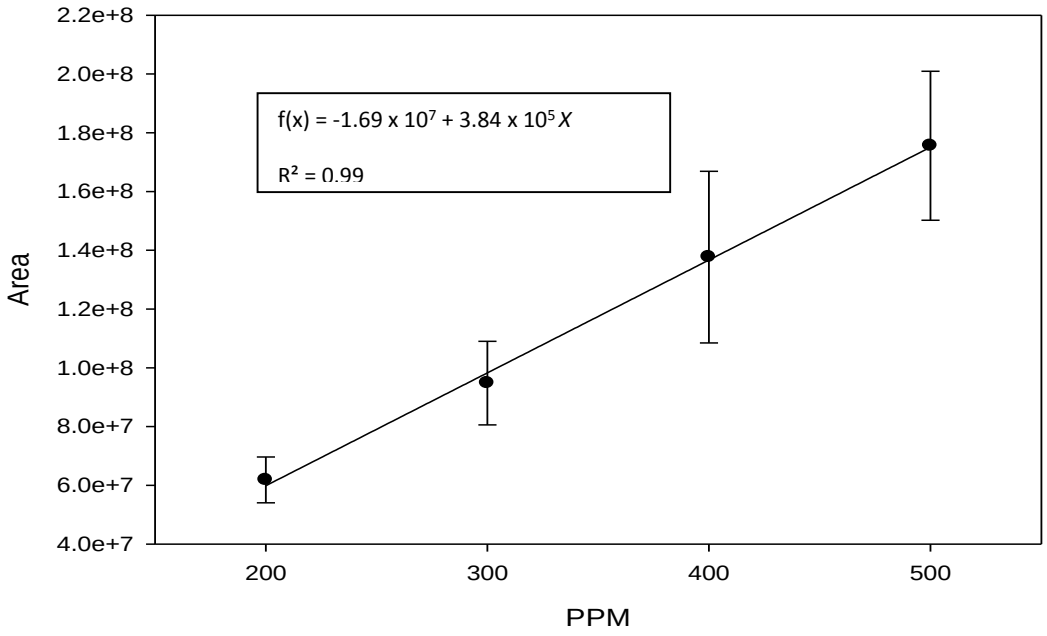

Standard curve of 3-hydroxybutyrate

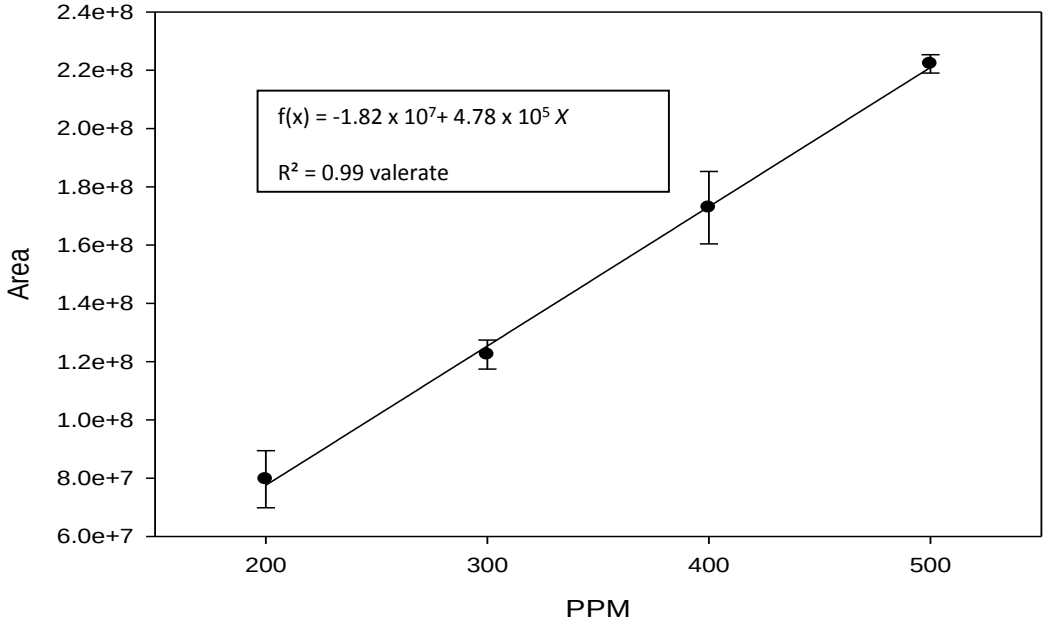

Standard curve of 3-hydroxyvalerate

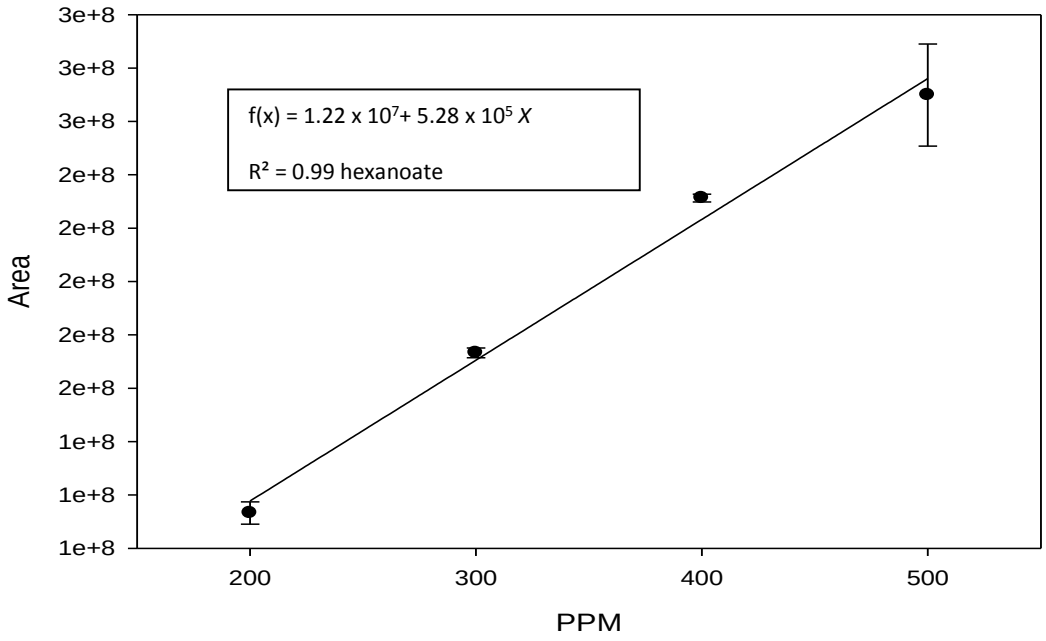

Standard curve of 3-hydroxyhexanoate

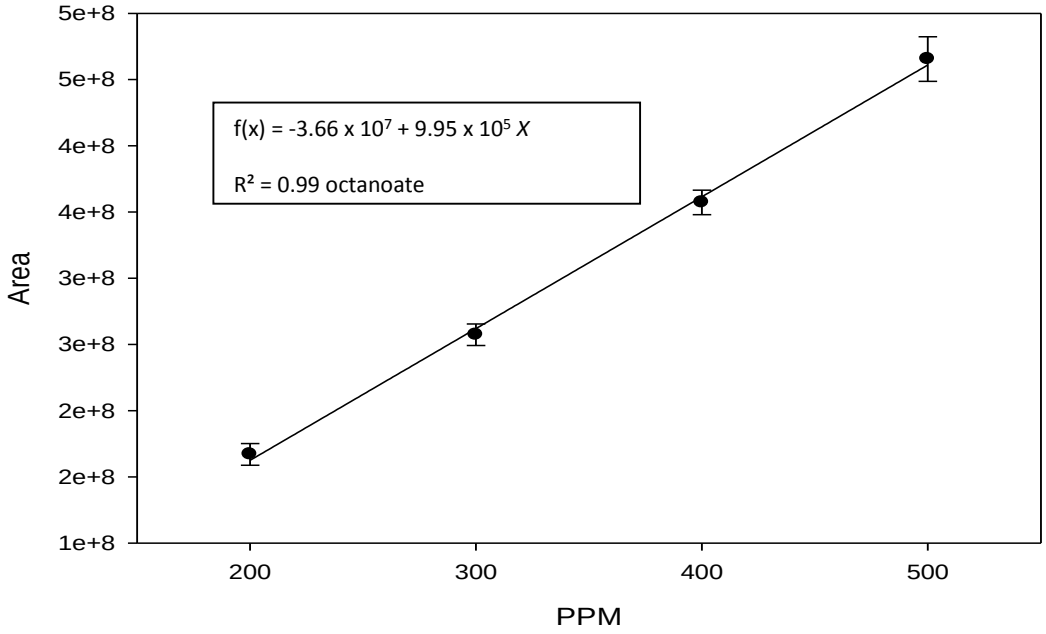

Standard curve of 3-hydroxyoctanoate

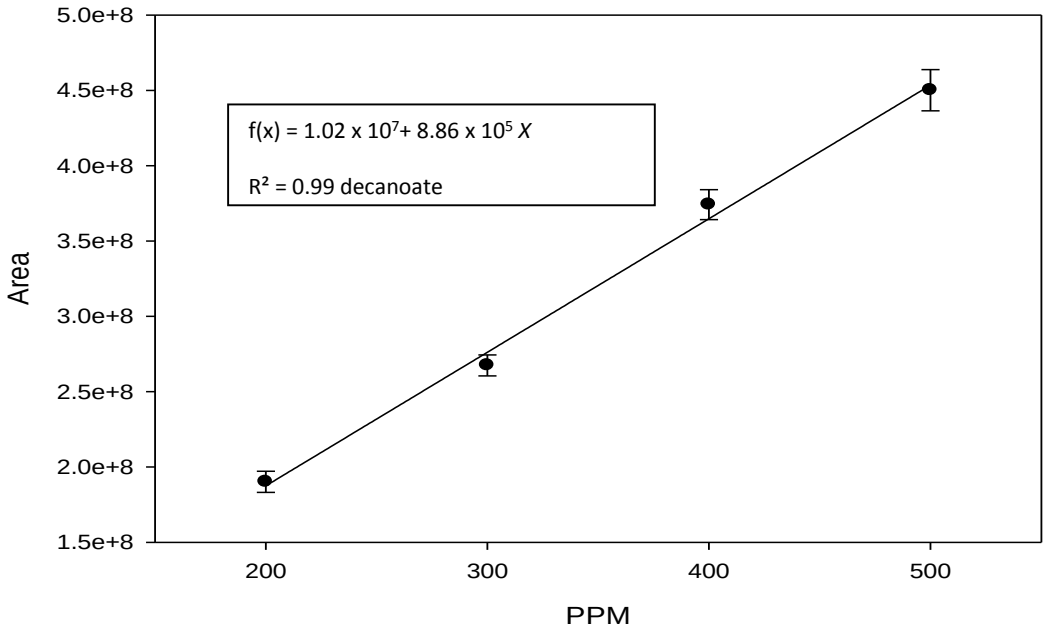

Standard curve of 3-hydroxydecanoate

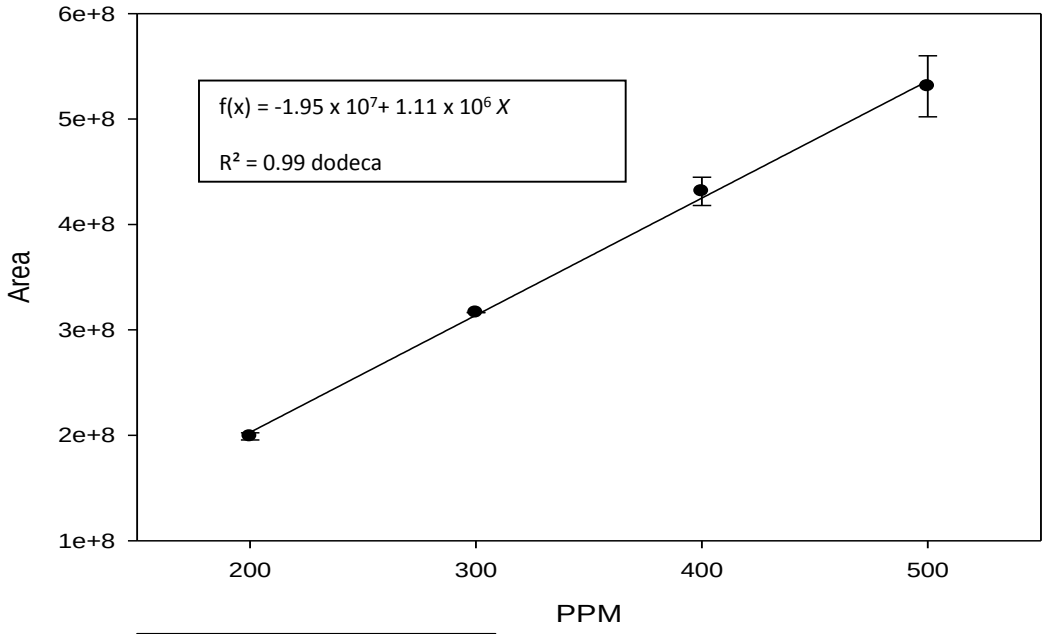

Standard curve of 3-hydroxydodecanoate

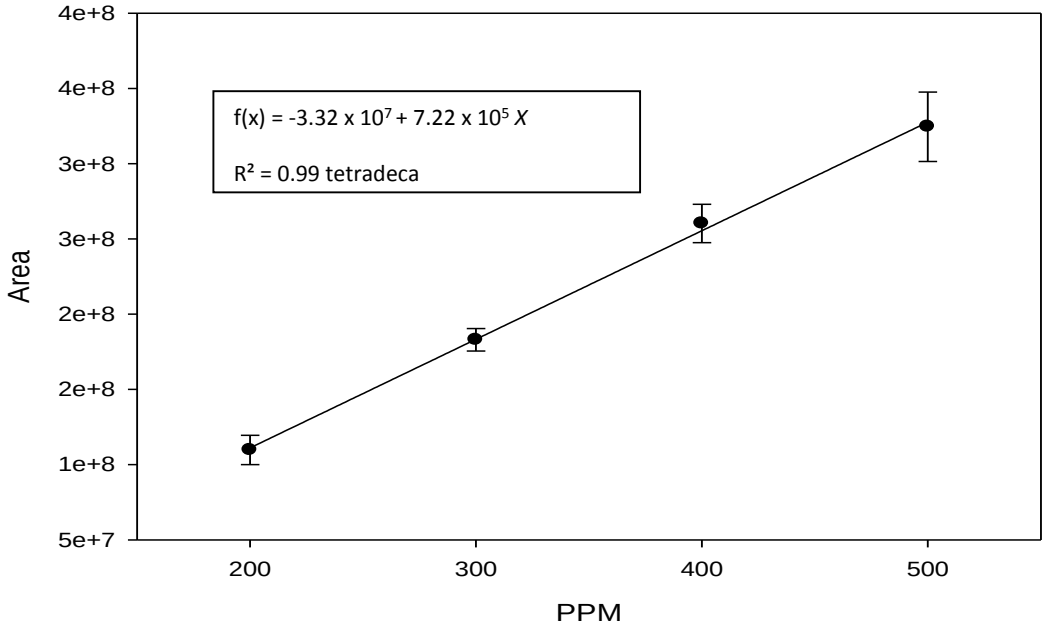

Standard curve of 3-hydroxytetradecanoate

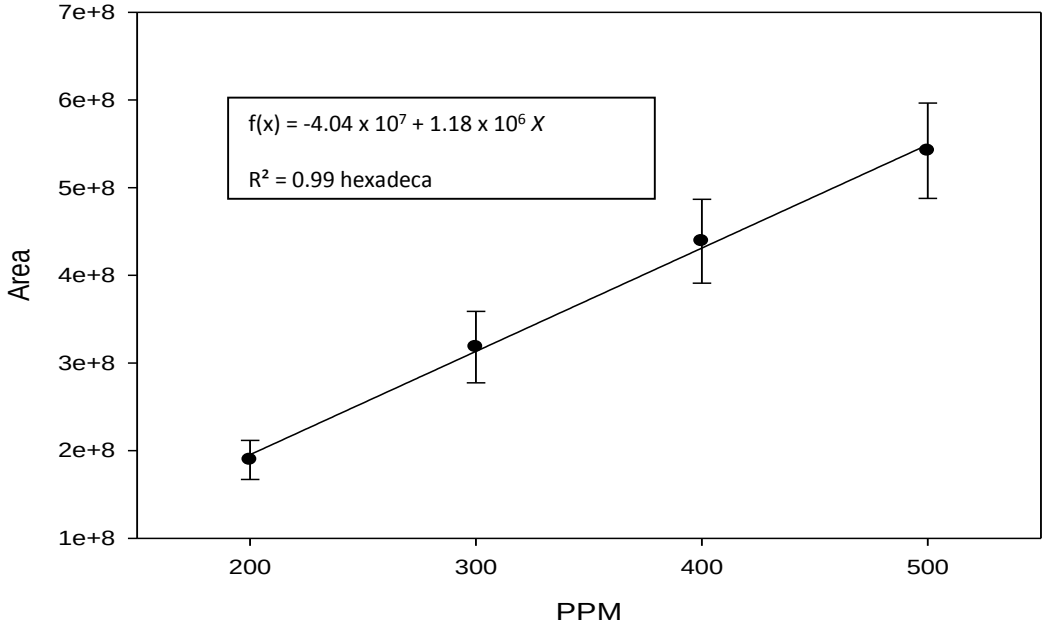

Standard curve of 3-hydroxyhexadecanoate

APPENDIX F

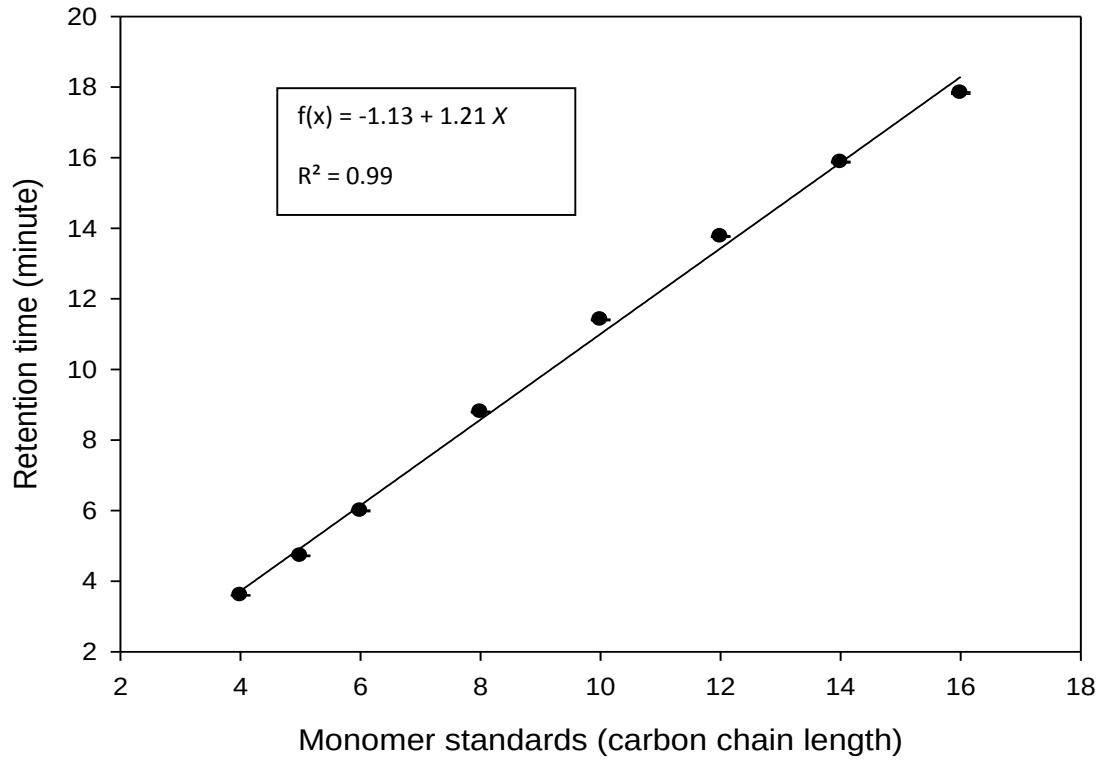
f(x) = -1.13 + 1.21 X
R² = 0.99
Retention time (minute)
Monomer standards (carbon chain length)
20
18
16
14
12
10
8
6
4
2
2
4
6
8
10
12
14
16
18